POLITECNICO DI TORINO & AALTO UNIVERSITY

MASTER'S DEGREE IN ENERGY AND NUCEAR ENGINEERING (LM-30)

Politecnico di Torino

Aalto University
School of Electrical
Engineering

MASTER'S DEGREE THESIS

DEMAND RESPONSE OF A HOUSEHOLD WITH DISTRIBUTED ENERGY RESOURCES

Supervisors

Prof. ENRICO PONS

Prof. MATTI LEHTONEN

Advisor

M.Sc. (Tech.) VERNER PÜVI

Candidate

EMANUELE BERTE'

MASTER'S DEGREE SESSION OF JULY 2024

Abstract

Due to uncontrollable renewable generation, future households have to adapt their consumption to match the production. This master's thesis explores the optimization of demand response for a prosumer equipped with distributed energy resources (DER). The research focuses on solving the energy consumption demand response problem for a household. In this study, the problem has been formulated as an optimization task. To address the problem, a Python code was written using the Pyomo optimization modeling language and the GLPK solver for MILP-type optimization problems. The prosumer, located near Helsinki, Finland, owns a villa, and the analysis spans an optimization window with hourly resolution. Local climate data, including outdoor temperature and irradiation, are incorporated to model environmental conditions affecting renewable energy production and building energy consumption. The prosumer system integrates various components, including photovoltaic (PV) panels, whose generation was calculated using measured irradiance data, an electrical energy storage system (BESS), an electric vehicle (EV) with a charging station, and a storage and heating system for domestic hot water (EWH). Additionally, a two-capacity thermal model for the building considers air conditioning through an HVAC system with an air-to-water heat pump (HP) and thermal storage (TESS). The prosumer interacts with the grid, adhering to governmental limits on energy export and import. The optimization problem aims to minimize total costs, factoring in energy prices based on market trends (Day-Ahead price) and controllable variables. After outlining the prosumer's energy model, the thesis scrutinizes results obtained by modifying input data, facilitating the identification of daily expenditure or gain based on the analyzed time periods. This analysis enhances understanding of the impact of variables on system behavior and identifies optimal strategies for energy resource management. Conducted over the course of one year (2022 price data), the analysis code is versatile and easily adaptable to obtain new analyzable results by adjusting input data. Applicable to any prosumer scenario, the code holds potential for broader community use, allowing communication among users producing and consuming energy. Consequently, this thesis significantly contributes to the field of energy optimization and the management of distributed energy resources.

Contents

List of Tables

List of Figures

Nomenclature

Abbreviations

ACP	Available Charging Power
AHEMS	Autonomous Home Energy Management System
BESS	Battery Energy Storage System
CET	Central European Time
COP	Coefficient of Performance
DA_p	Day-Ahead price
DER	Distributed Energy Resources
DHW	Domestic Hot Water
DR	Demand Response
DSO	Distribution System Operator
EVCS	Electric Vehicle Charging System
EWH	Electric Water Heater
GLPK	GNU Linear Programming Kit
HP	Heat Pump
HVAC	Heating Ventilation Air Conditioning
LMI	Load Matching Index
MILP	Mixed Integer Linear Programming
PCC	Point of Common Coupling
PU	Per-Unit system
PV	Photovoltaic
PW	Plant Water
RES	Renewable Energy Sources
SOC	State Of Charge
TESS	Thermal Energy Storage System

Indices and sets

h, H, Δh	Index, set of time slot and hourly time interval

Parameters

$P_{threshold}$	Limit importation/exportation from and to the grid $[kW]$
C_{nom}^{BESS}	BESS rated capacity $[Wh]$
P_{nom}^{BESS}	BESS rated power $[W]$
SOC_{max}^{BESS}	Maximum BESS SOC $[Wh]$
SOC_{mim}^{BESS}	Minimum BESS SOC $[Wh]$
ϵ_c^{BESS}, ϵ_d^{BESS}	BESS charge and discharge efficiencies
C_{nom}^{EV}	Rated EV battery capacity $[Wh]$
P_{nom}^{EV}	Rated EV battery power $[W]$
SOC_{in}^{EV}	Initial EV SOC $[Wh]$
SOC_{max}^{EV}	Maximum EV SOC $[Wh]$
SOC_{mim}^{EV}	Minimum EV SOC $[Wh]$
ϵ_c^{EV}, ϵ_d^{EV}	EV battery charge and discharge efficiencies
C_a	Indoor air heat capacity $[Wh/°C/m^2]$
C_m	Building mass heat capacity $[Wh/°C/m^2]$
H_e	Heat conductance: External air to indoor air $[W/°C/m^2]$
H_g	Heat conductance: Indoor air to ground $[W/°C/m^2]$
H_m	Heat conductance: Indoor air to building mass $[W/°C/m^2]$
H_x	Heat conductance: HVAC air to indoor air $[W/°C/m^2]$
H_y	Heat conductance: External air to building mass $[W/°C/m^2]$
Q_{max}^{HVAC}	Rated maximum power of HVAC unit $[W]$
$T_{a,max}$	Maximum indoor air temperature $[°C]$
$T_{a,min}$	Minimum indoor air temperature $[°C]$
T_g	Ground node temperature $[°C]$
T_x	Ventilation temperature $[°C]$

c_w	Specific heat capacity of water $[J/kg/°C]$
P_{max}^{EWH}	Maximum EWH power consumption $[W]$
T_{in}^{EWH}	Inlet temperature of cold water into the EWH $[°C]$
T_{max}^{DHW}	Maximum DHW temperature in tank $[°C]$
T_{min}^{DHW}	Minimum DHW temperature in tank $[°C]$
V^{EWH}	EWH total volume $[l]$
ϕ_T^{EWH}	Constant EWH heat loss percentage per hour [%]

P_{max}^{TESS}	Maximum power of the TES system $[kW]$
T_{max}^{TESS}	Maximum PW temperature in tank $[°C]$
T_{min}^{TESS}	Minimum PW temperature in tank $[°C]$
V^{TESS}	TESS total volume $[l]$
ϕ_T^{TESS}	Constant TESS heat loss percentage per hour [%]

G_{ref}	Reference irradiance $[Wh/m^2]$
I_{sc}	Short-circuit current of the PV cell $[A]$
$NOCT$	Normal operating cell temperature of the PV module $[°C]$
P_{max}^{PV}	Maximum power of the PV system $[W]$
P_{peak}^{PV}	Size of the PV system $[Wp]$
S	Isolation level of the PV panel $[mW/cm^2]$
T_{ref}^{PV}	Reference temperature of the PV module $[°C]$

Time-dependent binary, auxiliary variables and arrays

$b_{dch,h}^{BESS}$, $b_{ch,h}^{BESS}$	Disharging and Charging decisions of BESS at hour h
$b_{dch,h}^{EV}$, $b_{ch,h}^{EV}$	Disharging and Charging decisions of EV battery at hour h
$b_{dch,h}^{TESS}$, $b_{ch,h}^{TESS}$	Disharging and Charging decisions of TESS at hour h
b_h^a, b_h^b	Auxiliary binary variables for HVAC setup at hour h
Q_h^a, Q_h^b	Auxiliary non-negative variables for HVAC setup at hour h
w_{EV}	Binary array establishing EV connection

Time-dependent real variables

$DA_{p,h}$	Day-Ahead price at hour h $[cent/Wh]$
G_h	Irradiance at hour h $[Wh/m^2]$
P_h^{crit}	Critical load of the customer x in hour h $[W]$
$P_{exp,h}$	Power flow from building to electrical grid at hour h $[W]$
$P_{imp,h}$	Power flow from electrical grid into building at hour h $[W]$
P_h^{PV}	Power generated by PV system at hour h $[W]$
T_h^{ext}	External temperature at hour h $[°C]$
T_h^{PV}	PV cell operating temperature at hour h $[°C]$
$P_{dch,h}^{BESS}$	BESS discharging power at hour h $[W]$
$P_{ch,h}^{BESS}$	BESS charging power at hour h $[W]$
SOC_h^{BESS}	BESS SOC at hour h $[Wh]$
P_h^{ACP}	Available Charging Power at hour h $[W]$
$P_{dch,h}^{EV}$	EV discharging power at hour h $[W]$
$P_{ch,h}^{EV}$	EV charging power at hour h $[W]$
SOC_h^{EV}	EV SOC at hour h $[Wh]$
COP_h^{HP}	Variable COP of the HP at hour h
P_h^{HVAC}	HVAC power demand at hour h $[W]$
Q_h^{HVAC}	HVAC thermal demand at hour h $[W]$
$T_{a,h}$	Indoor air temperature at hour h $[°C]$
$T_{m,h}$	Temperature of building's thermal mass at hour h $[°C]$
P_h^{EWH}	EWH power consumption at hour h $[W]$
T_h^{DHW}	DHW temperature in tank at hour h $[°C]$
$V_{use,h}^{DHW}$	DHW volume used $[l/h]$
$P_{dch,h}^{TESS}$	Power released by the TESS at hour h $[W]$
$P_{ch,h}^{TESS}$	Power required by the TESS for charging at hour h $[W]$
SOC_h^{TESS}	TESS SOC at hour h $[Wh]$
T_h^{TESS}	PW temperature in tank at hour h $[°C]$

Other Parameters

---

bb_h	Storages balance at hour h $[W]$
c^{exp}	Added cost for Exported Power $[cents/kWh]$
c^{imp}	Added cost to Imported Power $[cents/kWh]$
g_h	Total generation from the RES at hour h $[W]$
l_h	Total load at hour h $[W]$

Chapter 1

Introduction

The depletion of fossil fuel reserves and the exacerbation of global warming due to the greenhouse effect have necessitated a paradigm shift in energy generation towards renewable sources. Utilizing renewable sources, such as solar, wind, hydro, and biomass, holds the promise of significantly reducing harmful gas emissions, thereby supporting a more sustainable energy generation process [1]. This shift is critical not only for environmental protection but also for enhancing energy security and reducing dependence on imported fossil fuels.

Photovoltaic (PV) systems are a cornerstone of renewable energy generation. They convert sunlight directly into electricity using semiconductor materials, typically silicon-based. These systems can be installed on rooftops or in larger-scale solar farms, making them highly versatile for both residential and commercial applications. Within the scientific community, there is an increasing interest in photovoltaic energy self-consumption by grid-connected residential systems [2]. Self-consumption involves using the generated solar power directly within the household, reducing the reliance on grid electricity and minimizing transmission losses.

Given the reduction of subsidies for photovoltaic energy in various countries, enhancing self-consumption through the integration of energy storage systems could significantly boost the profitability of photovoltaic installations and reduce the strain on distribution grids. Energy storage systems (ESS), such as batteries, allow excess energy generated during peak sunlight hours to be stored and used during periods of low or no sunlight, thus enhancing the overall efficiency and reliability of PV systems.

As renewable energy infrastructures are typically decentralized and span

vast geographical areas, research focus has shifted towards distributed generation. Distributed generation refers to electricity generation from sources that are directly connected to the distribution network or the customer side of the meter, rather than centralized power plants [3]. This approach offers several benefits, including reduced transmission losses, improved reliability, and enhanced resilience of the power grid.

The smart grid paradigm aims to harness secure bidirectional communication technologies to facilitate the flow of critical information from generators through distribution networks to end-user consumption [4]. Smart grids integrate advanced sensing, communication, and control technologies to enable real-time monitoring and management of the electricity grid. This integration allows for better demand response, improved grid stability, and the incorporation of a higher proportion of renewable energy sources.

Prosumers—customers who produce and share excess energy with the grid and other users—are integral to smart grids. Prosumers not only contribute to future smart grids but also play a pivotal role in peak demand management [5], [6]. From an economic standpoint, prosumers benefit from the implementation of autonomous, self-interested agents capable of making effective decisions regarding the use of energy sources. This ensures that demand is met at the lowest possible cost, or that profit is made by selling surplus electricity to other entities [7].

In this context, the role of advanced algorithms becomes crucial. Optimization algorithms, particularly Mixed-Integer Linear Programming (MILP), are employed to address complex decision-making processes in energy management. These algorithms can handle various constraints and objectives, such as minimizing costs, maximizing profits, or ensuring the balance between energy supply and demand. MILP is particularly suited for problems involving both continuous and discrete variables, making it ideal for modeling energy systems where binary decisions (e.g., whether to turn a device on or off) are required.

This study introduces an algorithm designed for prosumers to optimize the operation of their generation and consumption devices, aiming to maximize profits while contributing to the overall stability of the electrical grid. The algorithm accounts for generation and recharge costs, as well as anticipated levels of consumption and production, creating an operational plan that maximizes the prosumer's profitability. This work underscores the efficacy of MILP optimization techniques in the smart grid domain, formulating a minimization

problem solved using the Python programming language (Pyomo) in conjunction with the GLPK solver.

The thesis is organized as follows:

Chapter 2 conducts a comprehensive review of the state of the art, detailing existing codes and optimization algorithms in the energy sector and highlighting current limitations. This chapter provides a critical analysis of contemporary methodologies and identifies gaps in the literature. Chapter 3 introduces the methodology employed to model the Finnish grid-connected prosumer using the Pyomo optimization language in Python. This chapter begins with a geopolitical and administrative contextualization of the prosumer, followed by a detailed examination of the equations modeling various system components. Input data are meticulously researched to ensure accuracy and relevance. Chapter 4 presents the results of the identified Base Case, offering a detailed analysis of the different seasonal variations for the year 2022, which is the focal year for this analysis. The chapter includes graphs illustrating the behavior of various system components, accompanied by in-depth commentary and result analysis. The objective is to understand the impact of Finland's highly variable climate on the optimization outcomes. Chapter 5 explores scenarios different from the Base Case by considering various prosumer configurations. This includes modifying the sizes of the photovoltaic (PV) system and the energy storage system (BESS) to assess how different configurations affect user benefits. A comprehensive comparative analysis is conducted across different scenarios to determine optimal configurations under various conditions. Chapter 6 concludes the study and suggests directions for future research. This chapter synthesizes the findings, underscores the contributions to the field, and proposes potential areas for further investigation to enhance the optimization of prosumer operations and smart grid management.

By thoroughly exploring these topics, this thesis aims to contribute significantly to the understanding and optimization of prosumer operations in smart grids, leveraging advanced optimization techniques to promote sustainable and efficient energy management practices.

Chapter 2

State of the Art

2.1 Overview

In recent years, the term "*prosumer*" has emerged in the power system lexicon. A prosumer is a consumer who, due to advancements in technology and attractive feed-in tariffs for renewable energy-based power plants, installs micro-generation systems (typically a few kilowatts) to meet their energy needs and sell surplus electricity to the market, thereby also becoming a producer [8].

The model in this thesis is based on a Finnish rural house equipped with both thermal and electrical storage systems. It incorporates common generation systems, particularly photovoltaics (PVs), and electric vehicles (EVs), which are becoming increasingly prevalent. In the context of Finnish households, energy consumption typically includes heating for living spaces and domestic water, as well as electricity for household appliances. It also involves the use of natural gas and liquid gas for cooking, and wood and electricity for heating saunas [9]. This model, along with the challenges it presents, aligns well with the concept of optimization in the energy sector.

Optimization algorithms are becoming crucial for addressing complex issues in specific sectors like the electricity market. In the context of a prosumer-grid system, these algorithms are essential for efficiently managing electricity generation, consumption, and distribution. By applying optimization techniques, stakeholders can enhance resource allocation, optimize energy trading strategies, and balance supply-demand dynamics within the prosumer-grid framework.

These algorithms are particularly valuable for determining the optimal configuration of energy resources for prosumers, taking into account factors

like renewable energy sources, storage capacities, and demand patterns. Additionally, optimization algorithms enable dynamic pricing mechanisms, allowing prosumers to make informed decisions based on real-time market conditions. Integrating these algorithms into the prosumer-grid system promotes a more resilient and adaptive electricity market, ensuring efficient resource utilization and fostering sustainable energy practices.

The expansion of distributed generation from renewable sources is critical for decarbonizing the economy, mitigating global warming, and reducing external energy dependence in countries lacking indigenous fossil resources. However, this transition presents unique challenges. Large-scale electricity storage for later use remains a significant hurdle. Traditionally, electricity production is aligned with real-time demand, leading to the underutilization of expensive power plants designed to meet peak demands that occur sporadically throughout the year. This practice increases maintenance and management costs, affects tariffs, and raises expenses for consumers. The electrification of various sectors, such as transportation, requires widespread implementation of chargers, including fast and ultra-fast chargers. Comfort requirements in buildings increase air conditioning loads. Consumers now play a more active role in managing their own energy resources, becoming prosumers who should globally optimize exchanges with the grid, load management, local microgeneration (especially rooftop PVs), and storage resources (static batteries and electric vehicles). The traditional grid paradigm of "supply follows the load" is evolving towards smart grids that facilitate "load follows the supply" operations, supported by widespread deployment of sensing and control equipment, especially in the distribution network, including smart meters at customer residences that enable bidirectional communication with the grid. This technological infrastructure, along with the vast amount of data it allows to collect, enables more efficient network management [10].

Demand Response (DR) emerges as a solution to these challenges, allowing for the postponement of investments in new capital-intensive capacities and providing a means to manage the transition until such capacities are fully operational. Additionally, DR helps reduce consumers' electricity bills by offering economic incentives for using electricity during times when prices are lower than the marginal generation cost. According to the Agency for the Cooperation of Energy Regulators (ACER), "Demand Response" fundamentally involves changes in electricity consumption by customers (individually or collectively) in

response to a market signal such as a change in electricity prices or a financial incentive to increase, decrease, or shift the timing of their electricity consumption [11]. Demand response can be categorized into two types: incentive-based and price-based. The former is suitable for large industrial and commercial customers, while the latter is popular among residential customers.

In this context, all tariff components (energy, power, network usage) can become time-differentiated based on wholesale market price variability, renewable energy availability, and network conditions (e.g., congestion in distribution transformers), inducing appropriate changes in consumption patterns. Therefore, demand response programs play a key role in the energy transition, offering potential benefits to multiple stakeholders. These programs involve time-differentiated tariffs that can exhibit significant variations, prompting consumers to adjust operating hours to achieve bill savings without compromising comfort. Incentive-based programs include schemes such as direct load control, interruptible load contracts, refunds during peak hours, emergency offer/return programs, and capacity and ancillary service markets. Consumers can reduce their electricity bills by adapting consumption patterns, leveraging the integrated optimization of all energy resources based on their flexibility in providing required energy services (lighting, hot water, electric mobility, etc.). Retailers can profit by offering a portfolio of time-differentiated tariffs to distinct consumer segments, exploiting the difference between wholesale and retail prices. Aggregators can develop new business models to provide demand response capacity as a service to the grid. Network operators can avoid power peaks, reducing losses and deferring expensive network upgrades. Generators can avoid operating costly and less environmentally friendly peak units.

Recently, there has been growing attention on energy consumption scheduling algorithms for demand response by residential customers, who constitute approximately 40% of the total demand.

In one study, a game theory-based approach [12] was employed to schedule a group of residential customers with the aim of reducing the peak-to-average ratio and individual bills. Another study [13] utilized real-time price forecasting on the responsive tariff to decide on demand response in subsequent hours, reducing appliance waiting times. Other approaches, such as the use of genetic algorithms and particle swarm optimization, have been proposed to develop demand response algorithms for residential customers. To address peak rebound issues, measures like imposing maximum hourly load constraints and

random scheduling among customers have been suggested. The residential load scheduling problem has been formulated in various ways, including as an Integer Linear Programming (ILP) problem, Mixed-Integer Linear Programming (MILP) problem, and Mixed-Integer Nonlinear Programming (MINLP) problem [14], [15], [16]. The importance of demand optimization in conjunction with energy storage devices such as batteries has been emphasized [17]. Finally, parallel load optimization approaches have been proposed for aggregated customer loads in the presence of renewable generation or customer-owned assets [11].

The literature presents a wide range of simulation and optimization models dedicated to demand response. Authors, such as those in [18], [19], [20], [21], and others, provide comprehensive reviews, highlighting perspectives in the field and presenting optimization models with various approaches regarding the physical modeling of appliances. Common themes include cost and discomfort assessment, with minimization of functional objectives and consideration of consumer flexibility.

In particular, MILP optimization methods have become increasingly relevant in the energy sector due to their ability to ensure global optimality [22]. Pyomo, a Python library for optimization problem formulation, and GLPK, a software package for solving Linear Programming (LP) and MILP problems, are fundamental tools in this field. Real-world applications of MILP optimization include:

- Placement problems (PV system, wind system, charging station, etc.);
- Repair and maintenance problems (Wind farm, wind turbine, PV panels, etc.);
- Electricity generation and scheduling problems (Unit commitment, economic dispatch, etc.);
- Other (Gas storage, oil transmission, etc.)

The evolution of research on these optimization methods in the realm of electrical balancing has led to significant progress. Optimization efforts focus on linear mathematical models like MILP to ensure computational efficiency, balancing detailed modeling of load operations with implementation requirements in economically feasible home energy management systems. The mixed-integer aspect of these problems arises due to the integer or binary nature of some variables, such as whether a PV system is installed at a node (1) or not (0). This approach is crucial for accurately representing discrete decisions, such as

the installation of a PV system, which directly influences the efficiency and cost-effectiveness of home energy management systems. This research contributes to the development of Advanced Home Energy Management Systems (AHEMS) that optimize consumer energy resources. The application of complex models supports tariff design and contributes to achieving efficient and sustainable energy management.

2.2 Literature Gaps and Limitations

Demand Response (DR) in the residential sector is pivotal within the smart grid framework due to the significant energy consumption during peak times and the integration of local renewable energy generation with battery storage devices. Despite its importance, several limitations and challenges persist in the current state of demand response in homes equipped with distributed energy resources (DERs):

- **Optimization of Schedules:** The optimization of energy distribution schedules, which involves balancing local renewable sources, battery storage utilization, and household appliance consumption while considering both cost and comfort, remains a complex task [23].
- **Uncertainty Modeling:** Modeling parameter uncertainties, such as fluctuating renewable energy generation and variable consumption patterns, poses significant challenges. Users can mitigate energy consumption costs by reducing usage or shifting demand to off-peak periods [24].
- **Dynamic Modeling of Physics-Based Consumption:** Accurate dynamic modeling of energy consumption for various household appliances, both individually and at aggregated community levels, continues to be challenging.
- **User Comfort:** Minimizing inconveniences caused by delayed operation of programmable appliances and maintaining comfortable thermal levels for HVAC systems without exceeding user comfort limits is a significant issue.
- **Transition to Transactive Energy:** Transactive energy, a generalized form of DR that manages both supply and demand, requires real-time, autonomous, and decentralized decision-making, making the transition from traditional DR to transactive energy complex.

The challenges in implementing demand response in homes with distributed energy resources are numerous and multifaceted. Key challenges include:

- **Technological Challenges:** Integrating various technologies such as smart meters, energy management systems, and communication infrastructures is complex. Ensuring interoperability among these technologies is a significant hurdle.
- **Regulatory and Policy Challenges:** The lack of clear policies and regulations regarding the operation and compensation of demand response programs can hinder their widespread adoption.
- **Economic Challenges:** The economic viability of demand response programs is a primary concern. High initial investments required for the installation of necessary infrastructure can be a deterrent.
- **Consumer Participation:** Encouraging consumers to participate in demand response programs is challenging. This requires educating consumers about the benefits and providing incentives for participation.
- **Privacy and Security:** Protecting consumer privacy and ensuring the security of communication networks used for demand response are critical challenges.
- **Network Stability:** Managing network stability with high penetration of renewable energy sources and the dynamic nature of demand response is a complex task.

These challenges must be addressed to fully realize the potential of demand response in homes with distributed energy resources.

Optimization codes are essential tools for addressing DR issues. These codes manage and optimize energy usage, considering factors such as energy cost, the availability of DERs, and consumer needs. Key points include:

- **Optimization Techniques:** Various optimization techniques have been discussed in the literature for energy management problems, with hybrid techniques showing better performance due to their faster convergence speeds.
- **Appliance Scheduling:** Optimizing appliance scheduling strategies is crucial for residential users, requiring consumer flexibility and awareness [25].
- **Demand Management:** Demand management reduces energy acqui-

sition costs and associated penalties by continuously monitoring energy usage and managing appliance programs.

- **Peak Issues:** Optimizing energy demand for household appliances is challenging for both utilities and consumers, especially during peak hours when electricity consumption is highest [25].

These are just some ways optimization codes can address the challenges and limitations of DR. However, the effectiveness of these codes depends on various factors, including the quality of input data, the complexity of the energy system, and specific consumer requirements.

Optimization methods for managing DR present several limitations:

- **Computational Complexity:** Some optimization methods can be computationally intensive, particularly for large-scale problems [26].
- **Uncertainty and Variability:** The uncertainty associated with renewable energy resources and power system variability makes optimization challenging.
- **Demand Modeling:** Precise modeling of energy demand is difficult due to variability in consumer behavior.
- **Conflicts Between Objectives:** Multi-objective optimization problems face difficulties in obtaining exact optimized solutions for all objectives simultaneously [26].
- **Information Access:** Obtaining direct access to necessary information for optimal coordination in a large, distributed, and dynamic system is impractical and unnecessary.
- **Limitations of Intelligent Algorithms:** Intelligent algorithms used for DR are limited by their capacity to handle parametric load uncertainty associated with renewable energy sources (RES) and the power system [27].

These limitations represent significant challenges that must be addressed to enhance the effectiveness of optimization methods in managing DR.

Despite extensive literature on optimization models for DR, many models presented involve simplifications that deviate from reality. Consequently, there is a notable absence of effective models based on physical data. Most works focus solely on load optimization to reduce consumer bills while maintaining

comfort. Few consider the presence of renewable energy generation and battery storage, which are now ubiquitous but often in a centralized manner, either for a group of clients in an area or as part of microgrids [18]. For instance, the article [11] addresses the optimization problem of residential homes by considering them as microgrids equipped with smart appliances, distributed storage, and distributed generation.

This thesis investigates the benefits of household participation in demand response by adjusting loads. The household is equipped with an electrical storage (BESS), a photovoltaic system (PV), an electric vehicle (EV), an electric water heater (EWH) for hot water, and a thermal energy storage system (TESS) connected to an air-to-water heat pump (HP). A two-capacity heating model simulates the heating system's response to demand. The BESS smooths peaks in PV energy generation, while the TESS acts as a thermal flywheel supporting the heat pump. The EV battery can also serve as an additional intermittent storage system. A mixed-integer linear programming (MILP) formulation is employed to solve the problem through a mathematical programming approach. This formulation defines parameters, variables, and constraints that work together to optimize the objective function by minimizing the difference between the costs of imported power and the revenue from exported power to benefit the user.

However, many challenges remain. For example, the resolution speed of a MILP problem depends on the quality of the model formulation. If GLPK takes too long to solve a problem, exploring other solvers such as CPLEX, CBC from COIN-OR, SCIP, GUROBI, or IPOPT might be beneficial. In conclusion, while recent advancements are promising, there is still much to be done to fully harness the potential of MILP optimization methods in electrical balancing. Further research and developments are expected to bring additional improvements in this field [22], [28].

Chapter 3

Methodology

The methodology employed follows a systematic approach aimed at optimizing the response to the needs of a prosumer with distributed energy resources. The primary focus of this study is on the development of a Python code using the Pyomo optimization modeling language and the GLPK solver, specifically designed for MILP modeling the prosumer system and its connection to the Finnish distribution network.

In Fig. 3.1, the logical flow followed by the code, from reading input data and declaring decision variables to obtaining results, is depicted.

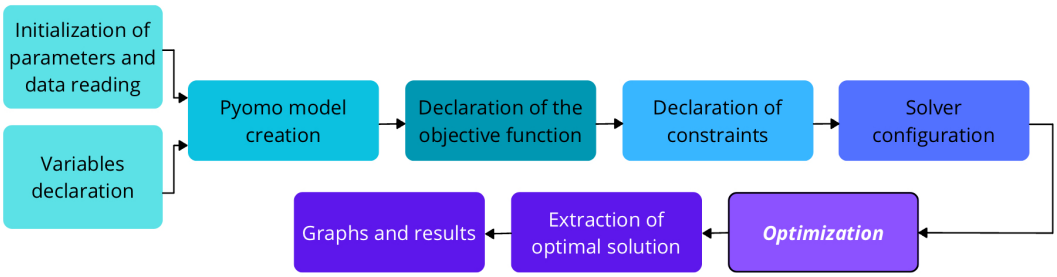

Figure 3.1: Main steps of the optimization code designed for the analysis.

The objective of this chapter is to model the system comprehensively. Firstly, a detailed geographical context of the prosumer is provided, analyzing energy market rules, with particular attention to the Day-Ahead price (DA_p) and energy constraints imposed by the Finnish government in the Uusimaa region, the most densely populated area in the country. Subsequently, relevant geographical data, including solar radiation and external temperature, are examined, and the system's schema on which the model is based is presented. Following that, each key element of the prosumer model is examined in detail,

analyzing every aspect and equation involved in its modeling. This chapter primarily aims to present the complexity of the considered prosumer in a clear and understandable manner, highlighting their energy consumption and demand while contextualizing the analysis and research within a broader framework. The ways in which the prosumer interacts with the distribution network and dynamically operates in the context are explored. In summary, the chapter aims to make the complexity of the considered user more accessible, providing a comprehensive overview of their interactions with the energy system and the surrounding context.

3.1 User Data and Localization

The user under examination is located in the Uusimaa Region of Finland (Fig.3.2), the country's most densely populated area, near the capital Helsinki (60.32° North, 24.47° East - Time and Zone from Greenwich 2)[1]. The customer owns a house situated at a distance from the urban center, allowing ample space to install all the necessary equipment for the analysis. Additionally, they benefit from a wide exposure to solar radiation, without hindrance from buildings or surrounding obstacles; the topography of the region is predominantly flat, characterized by small hills and extensive valleys, with numerous lakes and rivers, but lacking mountain ranges.

Figure 3.2: Uusimaa Region, Finland [29]. The highlighted area in orange represents the Helsinki district.

[1]Data source: IWEC Data 029740 WMO Station Number, elevation 56 m

To simplify the calculation of power produced by the user's solar panels, it was assumed that they are oriented towards the south with an optimal angle, utilizing input data for direct normal radiation.

Regarding the climate, the region experiences a cold temperate climate. Winter temperatures can drop significantly, leading to a pronounced increase in heating demand. In summer, temperatures are generally milder but still cool compared to other European regions. Concerning solar irradiance, during the southern Finnish summer, the sun can remain visible for many hours a day. However, in winter, sunlight hours can be limited, with the sun rising for only a few hours a day, impacting energy production during that period.

In the following sections, a detailed examination will be conducted on climatic data for analysis, variations in the DA_p, government energy constraints, and the critical load across different months of the year.

3.1.1 Climate Data

The pertinent climatic data, intended for subsequent use as input in the following chapters, has been collected and organized in *.csv* files. The data reading process was conducted using *Excel* software. The collection of the examined data occurred at an hourly resolution for each day of the year 2022 in the Helsinki area, utilizing the official data from the Finnish Meteorological Institute [30].

The Finnish Meteorological Institute employs climatic data comprising 8760 annual hours, provided free of charge. The official website contains a detailed list of historical climatic data retrieved and recorded from various weather stations throughout Finland. All data can be easily downloaded, allowing for clear and straightforward visual comprehension. Among the extensive dataset analyzed for the city of Helsinki, specific data points extracted include the outdoor temperature (T_h^{ext}) and irradiance (G_h). In Fig. 3.3 and Fig. 3.4, the annual graphs depicting the outdoor temperature in $^{\circ}C$ and irradiance in Wh/m^2 are presented, respectively.

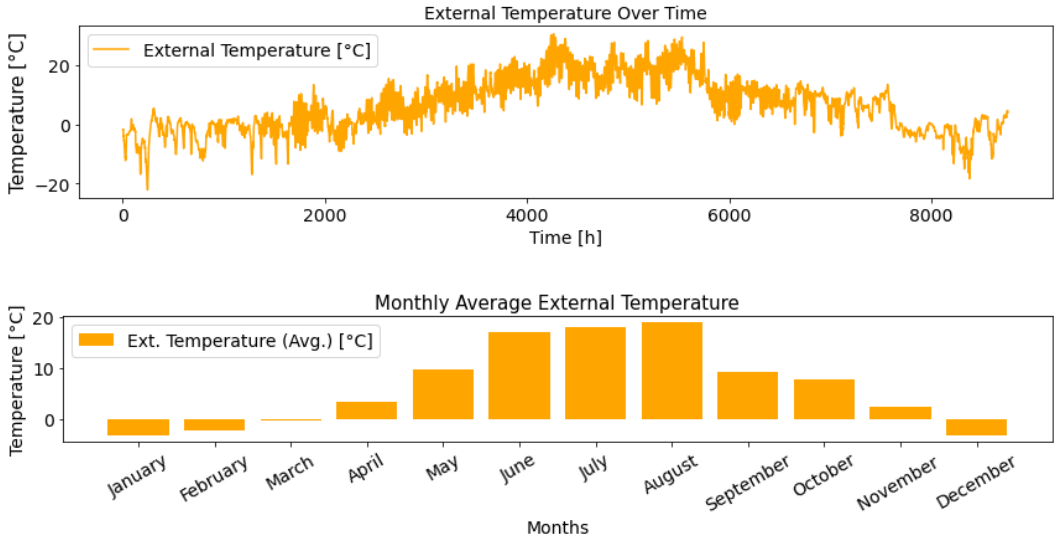

Figure 3.3: Temperature trend in $°C$ on an hourly basis, and monthly average of T_h^{ext}.

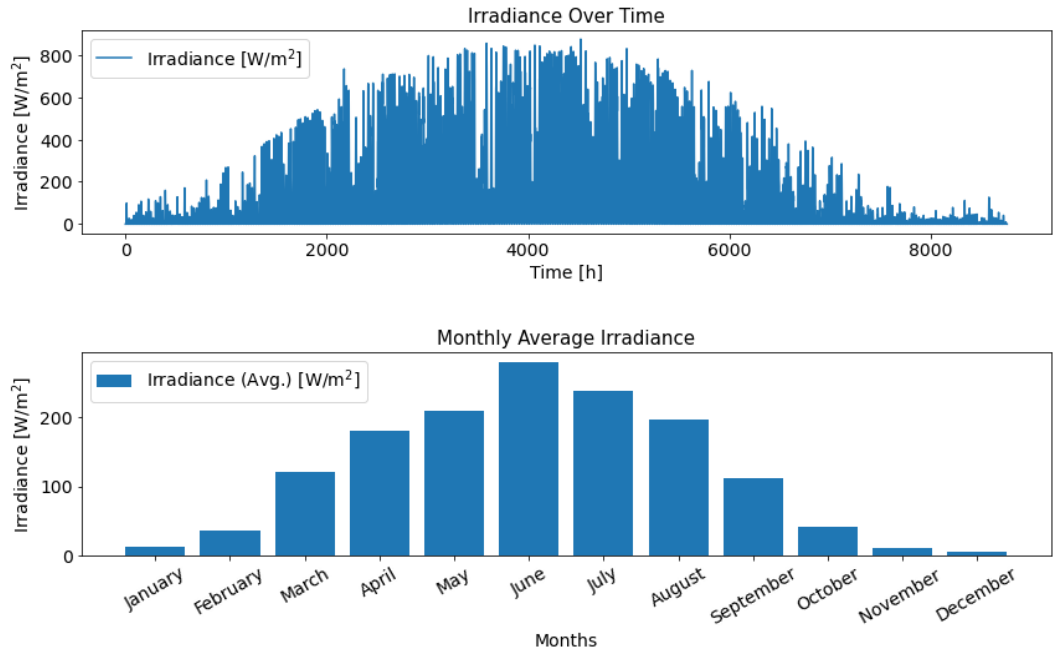

Figure 3.4: Irradiance trend in Wh/m^2 on an hourly basis, and monthly average of G_h.

It is crucial to emphasize that both figures contain duplicate graphs: for each one, the first illustrates the annual hourly resolution, while the second represents the monthly average. The inclusion of the monthly average has been intentional to provide an immediate overview of the trends on a monthly basis,

allowing for a clearer and visually comprehensible segmentation.

In Fig. 3.3, the marked variability of the external temperature (T_h^{ext}) throughout the year is evident, especially in the high-resolution hourly graph. The external temperature appears generally unpredictable, effectively adapting to the user's geographical context. It is immediately clear that the external temperature suits the user's location. During the winter months, particularly in January with an annual minimum of -22.1 $°C$ and in December, there is a considerable number of hours when the external temperature drops below zero. In contrast, during the summer period, the external temperature reaches moderately high values, peaking in June with an annual maximum of 30.6 $°C$.

The Fig. 3.4 illustrates the distribution of data related to irradiance (G_h) throughout the same year. As known, in regions located well north (latitude exceeding 60 degrees north relative to the equator), a complete scarcity of daily sunlight hours occurs, often falling below 5 hours, particularly during autumn and winter periods, with the opposite being true during spring and summer seasons. Both graphs, especially the one depicting the monthly average of irradiance (G_h), align perfectly with the external temperature trends. During autumn and winter, characterized by reduced solar illumination, a typical drastic drop in temperatures is observed, while the opposite occurs in the summer period. In detail, the month of June stands out as the brightest period of the year, undoubtedly favoring increased production from the installed photovoltaic system. Furthermore, it is easily inferable that the months with lower photovoltaic production will be January and December. During these periods, it is conceivable that the user may need to import a greater quantity of electrical energy from the distribution grid to meet energy demands.

In summary, the analyzed climatic data provide a comprehensive hourly overview throughout the year. These data, including information from years preceding 2022, serve as a valuable resource for deriving fundamental parameters crucial for optimization. Examples include the hourly power output of the photovoltaic system in watts, the maintenance of internal building comfort, the Coefficient of Performance (COP) of the air-to-water heat pump, among others.

It is important to highlight that the Finnish Meteorological Institute facilitates the collection of data from various meteorological stations in Finland. However, the scope can also be extended to areas outside Finnish territory (for

example, using softwre like *Climate Consultant 6.0* software could be employed to obtain representative climatic data for various regions of the world). Indeed, the developed Python code is versatile, capable of performing the necessary calculations and adapting to variations. Furthermore, the inclusion of historical climatic data allows for a deeper understanding of long-term trends and variations, providing a comprehensive historical context for the climatic conditions in the location under consideration anywhere in the world.

3.1.2 Day-Ahead Price Variations

In the context of the energy market, the "*Day-Ahead*" price (DA_p) is a crucial indicator that emerges from the daily implicit auction conducted by *Nord Pool*. This market allows operators to buy and sell electricity for delivery the next day. The price is determined based on the supply and demand for electric power.

Market operators submit their bids to buy and sell electricity for each hour of the following day. *Nord Pool* conducts an implicit auction, taking into account both the electricity price and the available transmission capacity between market areas. The auction establishes the electricity price for each hour of the following day, known as the DA_p.

The DA_p can vary significantly depending on various factors (Fig. 3.5), including the demand for electric power, the availability of generation capacity, weather conditions (which can impact renewable energy production), and the transmission capacity between market areas. *Nord Pool*, the leading energy market in Europe, offers day-ahead and intraday markets to its customers. This market allows operators to buy and sell electricity for delivery the next day or on the same day. *Nord Pool* operates in 15 countries (included Finland) and 21 bidding zones. Every day, more than 300 buyers and sellers place over 2000 orders. On an annual basis, approximately 500 TWh are traded. [31] *Nord Pool* provides a wide range of order types for buyers and sellers and publishes the available capacities on interconnectors and in the network at 10:00 CET. Buyers and sellers have until 12:00 CET to submit their final bids to *Nord Pool* for the auction for delivery hours of the next day. Submitted orders are matched with other orders in the pan-European market matching process. Hourly settlement prices are typically announced to the market at 12:45 CET or later. [31] After the publication of prices, individual results are

reported to each buyer and seller. The physical obligation to deliver/consume the purchased or sold energy follows as *Nord Pool* nominates transactions to the applicable imbalance settlement process in each country.

In the code, an optimization time window H has been implemented to maximize efficiency within the scheduled interval for declaring the new price list DA_p. The data used for this analysis is derived from the 2022 hourly energy prices, extracted from the *ENTSO-e* official website [32], as shown in Fig. 3.5.

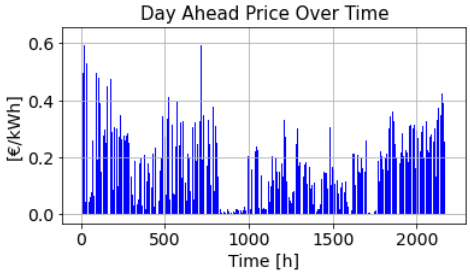

(a) *Season*: Autumn (September, October, November)

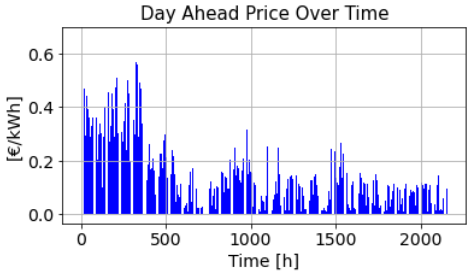

(b) *Season*: Winter (December, January, February)

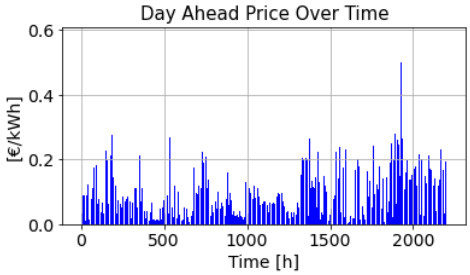

(c) *Season*: Spring (March, April, May)

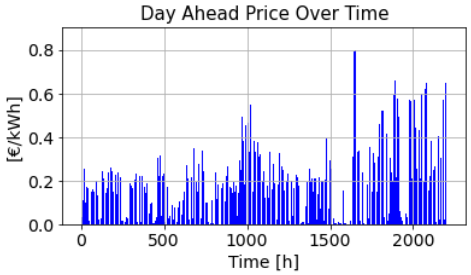

(d) *Season*: Summer (June, July, August)

Figure 3.5: Hourly resolution time plots representing the variation of DA_p in $€/kWh$. Data divided by seasons in the year 2022 [32].

The time window is defined by ($24\ hours \times number\ of\ days$) in the code is synchronized with the announcement of DA_p prices at 12:00 CET by *Nord Pool*. This aligns with the objective of the "*day-ahead*" market, which aims to determine energy prices for each hour of the following day.

It is crucial to note that although the model can optimize based on DA_p, these prices are influenced by multiple real-time factors already included in the 2022 *ENTSO-e* annual data. In 2022, electricity prices surged due to geopolitical tensions, while in 2021, they experienced an upswing towards the year-end owing to the energy crisis. In 2020, prices continued to align with the

preceding years, maintaining lower levels. Presently, 2022 has been selected as it holds the potential to yield improved model results, given the higher price differentials observed on an hourly basis. These factors include fluctuations in energy demand, the availability of generation capacity, weather conditions, and transmission capacity between different market areas.

Furthermore, using historical data for hourly energy prices implies that the model cannot predict future market prices. The model results should be interpreted as an indication of how energy could have been optimized in 2022, rather than as a forecast for the future. However, it is possible to conduct a future study on price prediction and integrate it into the existing code.

The primary focus of the current work is not price prediction but rather providing code applicable to various contexts, capable of optimizing energy organization based on prices to maximize user benefit. Overall, the developed code provides a solid foundation for future studies, including those related to economics and accurate forecasting models.

3.1.3 Prosumer Critical Loads

In the residential context, the management of critical electrical loads is of paramount importance to ensure energy efficiency and the safety of the dwelling. Critical loads within a residence may encompass essential devices (such as refrigerators, security systems, etc.) that must remain powered even in the event of a power outage. Other loads, such as non-essential lighting or appliances, can be temporarily deactivated to prevent overloads. A meticulous system programming generally allows for the recording of energy consumption values, providing statistical data on consumption based on users and time slots. These pieces of information can be instrumental in further optimizing energy usage within the dwelling.

For a comprehensive analysis of the case study, data on the user's critical loads (a family of 3-4 individuals) were collected throughout the entire year of interest. In Fig. 3.6, the graph depicting the critical loads on an hourly resolution for the entire year 2022 is presented, with a zoom on the first week of January for a more detailed view.

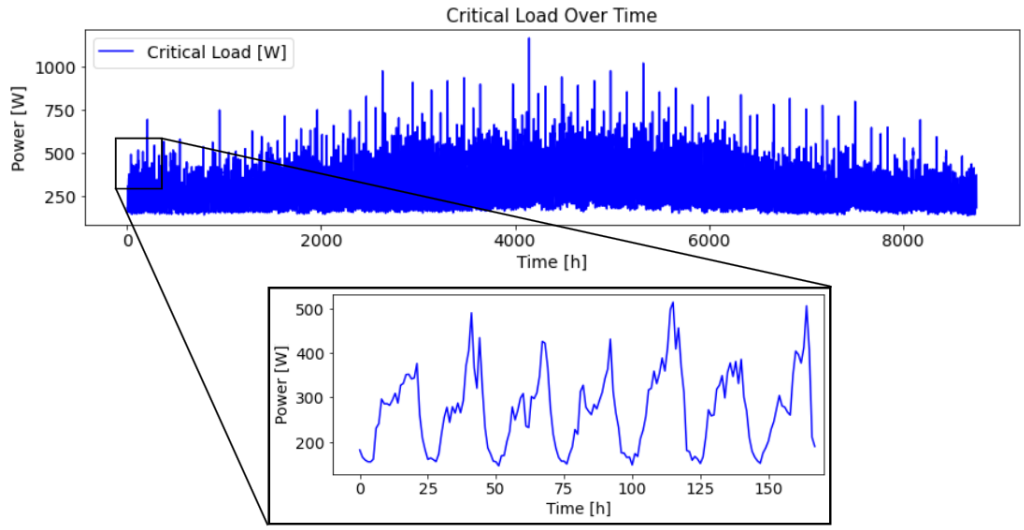

Figure 3.6: Customer critical load over time in W; data from the first week of January in the box.

The management of critical loads in the residential domain is a fundamental aspect in ensuring both energy efficiency and the safety of the residence. Additionally, the incorporation of home automation systems could significantly facilitate this management, allowing for automated control of energy consumption and cost reduction.

3.1.4 Import/Export Energy Constraints

Promotion of the use of renewable energy is part of the energy and climate policy that aims for sustainable energy production and consumption to curb climate change. In Finland, the Energy Authority is responsible for the implementation of the EU renewable energy policy and the national renewable energy policy.

The Energy Authority governs the feed-in tariff scheme for renewable energy subsidies, arranges auctions for renewable energy subsidies and transport infrastructure projects, as well as collects wind power charges. Furthermore, the Energy Authority oversees compliance with the sustainability of biofuels and fuel quality, the guarantee-of-origin system for renewable electricity and educational establishments for mechanics involved in the installation of renewable energy systems. The Energy Authority also provides energy advice for consumers, municipalities and enterprises, as well as carries out impact assessments on renewable energy policy actions and prepares related reports and statistics [33].

For this reason, considering that the feed-in tariffs are determined by the

Energy Authority in Finland and may be adjusted to promote the adoption of renewables, it would be challenging to obtain precise reference numbers for the feed-in tariff. Consequently, the following logic has been hypothesized at the user-grid connection point (Fig. 3.7). It is emphasized that, due to the variability of the energy context, it is still possible to modify the methodology by which the costs and tariffs for the purchase/sale of electricity from the grid by the prosumer are considered and identified in Finland.

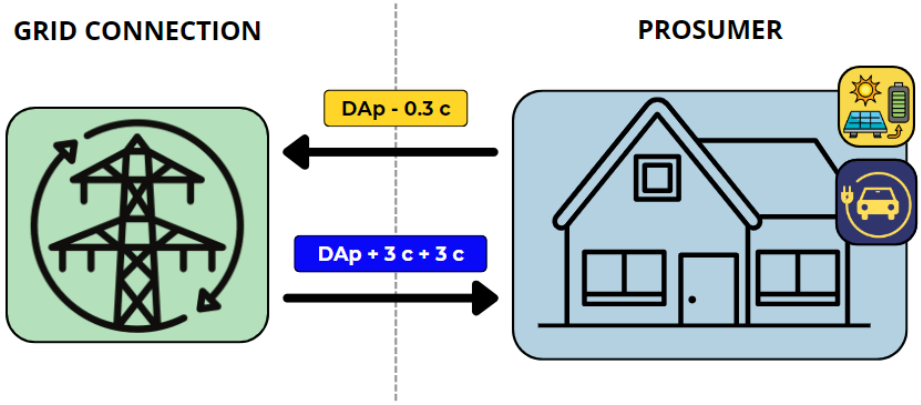

Figure 3.7: Hourly tariff assumed for the import and export of electricity in €/kWh.

In the context of the Finnish energy landscape, it is important to note that the acquisition of electrical energy from the grid is not exclusively limited to the DA_p; it also includes additional charges associated with distribution and energy taxation, administered by the local distribution entity. In this study, additional costs related to energy importation compared to the Day-Ahead price have been hypothesized at 3 *cents* per kWh for both distribution and energy taxation. These factors should be considered in the assessment of the overall costs related to energy importation.

Concerning the sale of energy to the grid, the transaction also occurs at the DA_p but is subject to a specific deduction of 0.3 *cents* per kWh. This reduction constitutes a penalty affecting the economic return for the prosumer. It is essential to emphasize that these dynamics may vary depending on energy policies and prevailing tariffs. Therefore, constant monitoring of regulatory and tariff elements is recommended to ensure that the analysis and results closely align with the reality of the situation.

In Finland, the prevalent standard for electrical connections among distribution system operators (DSOs) is typically $3 \times 25\ A$. This selection is likely informed by technical and safety considerations, alongside the usual power demands of residential and small commercial structures. Such connections are well-suited for properties like detached houses, semi-detached houses, leisure dwellings, or community maintenance buildings. Determining the size of the main fuse, typically set at $25\ A$ per phase, should involve consultation with an electrical designer or contractor. However, the specific rationales may vary among different DSOs and depend on factors such as network capacity, regulations, and customer requirements. These entities are part of a broader network of DSOs in Finland, as outlined on the *Energiavirasto* website [33]. In the context of a low-voltage three-phase network connection (which in Finland operates at $400\ V$ and $50\ Hz$), it can be asserted that the user can draw or inject a maximum power, denoted as $P_{\text{threshold}}$ in kW. This power is calculated based on the ampere limit set by the DSOs.

3.1.5 Objective Function and Logic

The objective function in this Pyomo optimization model represents the total cost associated with the power exchange between the building and the grid over the specified optimization horizon. The objective function is defined as the sum of the cost of importing power from the grid and the revenue from exporting power to the grid at each hour, considering the day-ahead electricity prices (DA_p).

The expression for the objective function is represented by the Eq. 3.1:

$$Minimize \quad \sum_{h \in H} [P_{imp,h} \cdot (DA_{p,h} + c^{imp}) - P_{exp,h} \cdot (DA_{p,h} - c^{exp})] \tag{3.1}$$

Where:

- $c^{imp} = 3\ cents/kWh + 3\ cents/kWh$
- $c^{exp} = 0.3\ cents/kWh$

The objective function comprises two key terms: one addresses the cost of imported power, represented by $P_{imp,h}$, which reflects the electrical power at hour h drawn from the grid at an associated hourly cost. The expression $(DA_{p,h} + c^{imp})$ captures this cost, with added variations for taxation.

Conversely, the second term concerns the profit from exported power, denoted by $P_{exp,h}$, signifying power at hour h sent to the grid. The expression $(DA_{p,h} - c^{exp})$ represents the total benefit, with a small additional negative variation.

The logic underlying the analysis is based on minimizing an objective function of the household. By defining the model and implementing the variables that regulate it, it is possible to optimize energy management for the single. The simulation period is denoted as H. The proposed model starts at hour $h = 0$. Input parameters for the subsequent hours are read. These parameters are then used in the optimization model discussed in the following sections. The input data is loaded into *Pyomo* for optimization. The optimization process generates decision trajectories for the period, minimizing the objective function dependent on the read DA_p. Subsequently, the process is repeated, with new input parameters read for each iteration. This approach allows for

the optimization of decisions based on real data provided for each selected hourly interval throughout the entire length of H. The model developed for each user is represented in the block diagram in Fig. 3.8.

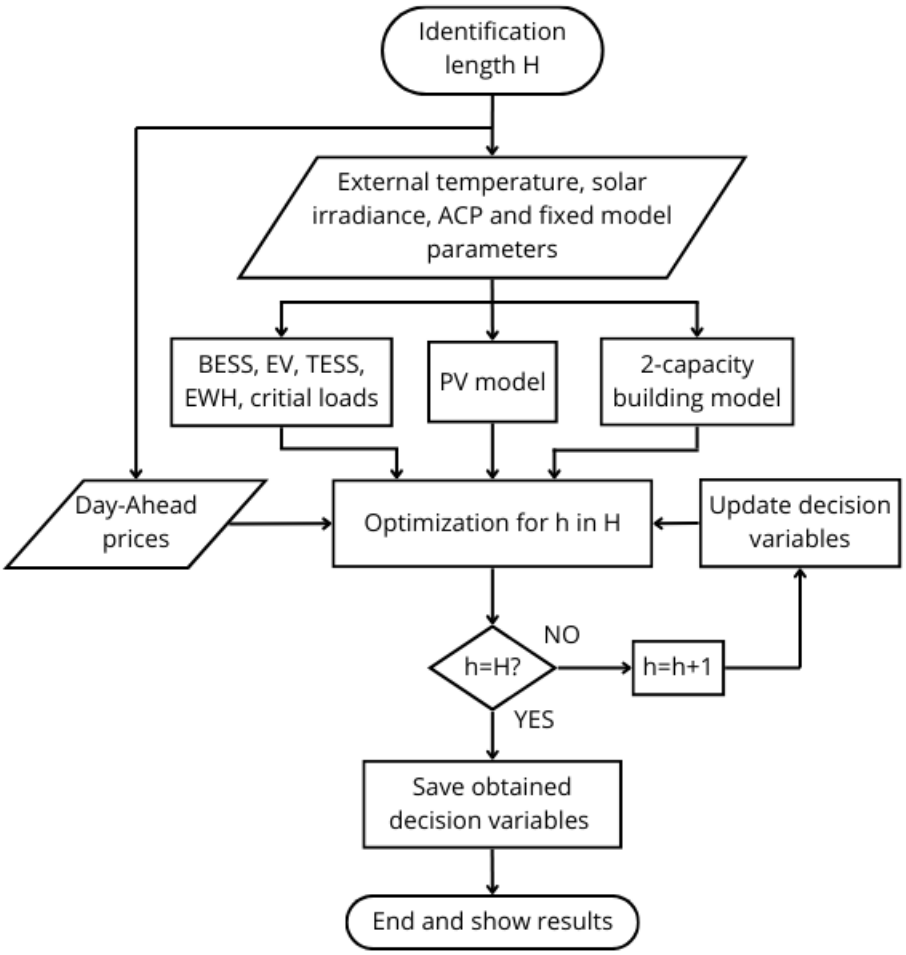

Figure 3.8: Block diagram for the proposed framework.

The objective is to minimize the total cost, which includes the cost of imported power and the penalty/reward for exporting power. It was subject to some technical constraints and limits which ensure convenience of the user. The above-mentioned constraints will be explained in the next section by thoroughly analyzing the components of the model representing the prosumer-grid connection system.

3.2 Prosumer-Grid Framework

The Prosumer-Grid integration system, implemented in the examined Finnish house equipped with a PV system as a RES for generation, reveals an innovative perspective towards a transition to a more sustainable and intelligent energy network [34]. This interconnected ecosystem is based on a solid foundation consisting of the Point of Common Coupling (PCC) and the MV/LV transformer. The PCC is the point in the microgrid's electrical circuit connected to the main electrical grid. This system allows the villa to receive energy from the main electrical grid, serving as a junction node between decentralized production and centralized distribution of energy [35]. On the other hand, the MV/LV transformer is a static electrical machine operating in alternating current and based on the phenomenon of electromagnetic induction. This device is responsible for converting voltage from one level to another, ensuring that energy is transported and distributed efficiently in the local electrical network. As is now known, with the presence of the photovoltaic system, the connection system is further enriched. The solar panels are connected to an inverter, essential for transforming the DC electrical energy generated by the panels into AC usable in the domestic field and suitable for injection into the grid. The inverter, therefore, constitutes the bridge between the self-produced solar energy and the connection to the PCC and the MV/LV transformer. This advanced configuration offers several advantages. Firstly, the house can benefit from clean and locally produced renewable energy, reducing dependence on conventional sources and contributing to environmental sustainability. Secondly, the use of an energy storage system such as the BESS allows for storing excess energy produced for future use, improving energy consumption efficiency. The integration of technologies such as the TESS and the EWH adds a further layer of flexibility and sustainability. Finally, the inclusion of an EV in the system expands the possibilities of using solar energy. The EV can be recharged (and discharged as needed) using self-produced energy, contributing to sustainable mobility and reducing the use of fossil fuels. In this section, the comprehensive scheme of the entire household and the equations that model it will be described.

3.2.1 Prosumer Scheme: Model Description

Below in Fig. 3.9, the complexity of the prosumer's structure connected to the grid is depicted. It is specified that the electric power flows are highlighted in black, while water flows are highlighted in red (for the sake of simplicity in the diagram, the inverter has not been depicted and the return and the outgoing have been represented as a single flow; furthermore, the HP is represented internally as a single unit.).

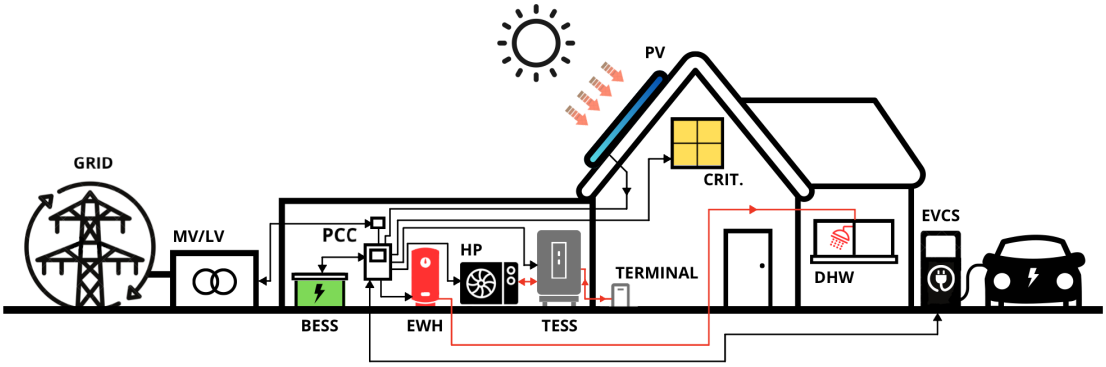

Figure 3.9: Simplified scheme of the prosumer under examination connected to the distribution grid.

The scheme depicts a typical house located, as mentioned, near Helsinki. It is inhabited by a family, assumed to consist of 4 people. The house includes a technical room where BESS, TESS, EWH and an air-to-water HP that powers the building's HVAC system are located. Air-to-water HP provides heat to the heating water circulation system for heating, and absorbs heat from it for cooling. On the roof, as mentioned, there is a PV system as a source of on-site generation. Critical loads and domestic hot water (DHW) demand are simply highlighted. It is assumed that the user has an Electric Vehicle Charging Station (EVCS) outside the house. On the left, the transformer is present with the subsequent connection to the national electrical grid. The entire system communicates through the PCC and the meter that calculates how much energy is imported and exported every hour. It is emphasized that the diagram is simplified, and not all individual connections constituting the electrical and heating/cooling systems of the building are represented.

3.2.2 PV Modeling

A simple model for calculating the PV output was used in Ref. [36]. The model is based on irradiance and temperature data, as well as PV characteristics, which can be found in manufacturer's datasheet. The model is presented in Eqs. 3.2 and 3.3.

$$P_h^{PV} = \frac{P_{max}^{PV} \cdot G_h}{G_{ref}} \cdot \frac{ln(I_{SC})}{ln(\frac{I_{SC}}{G_h} \cdot G_{ref})} \cdot \frac{T_{ref}^{PV}}{T_h^{PV}} \tag{3.2}$$

$$T_h^{PV} = T_h^{ext} + \frac{NOCT - 20}{80} \cdot S \tag{3.3}$$

The Eq. 3.2 calculates the output power of the photovoltaic module by correcting for solar irradiance, short-circuit current, and temperature. The second term in Eq. 3.3 represents the contribution to heating due to the normal operating cell temperature and insulation level. The factor of 80 in the denominator appears to be a normalization factor to scale the difference between NOCT and 20 to a range that influences the heating contribution.

In order to investigate various evidences with different PV system sizes, the hourly production in per unit (PU) has been computed (Fig. 3.10).

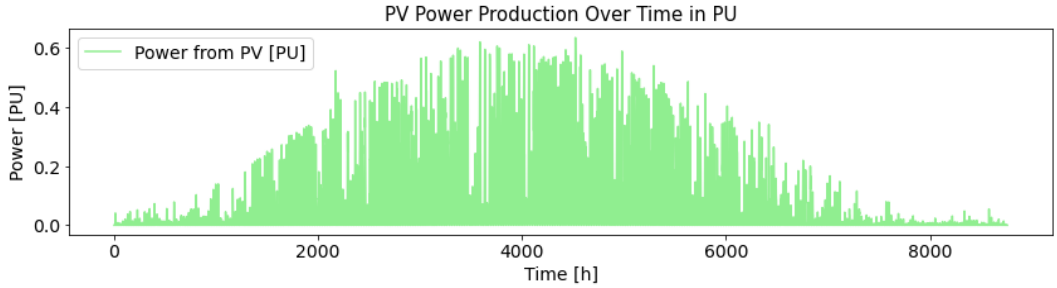

Figure 3.10: PV hourly production PU waveform.

Consequently, the values will consistently range between zero and one, facilitating the maintenance of the proportionality of the waveform under examination for the analyzed year. However, it will be multiplied by a factor P_{peak}^{PV} to establish the maximum size of the system using the peak value obtainable from market-supplied technical specifications provided by manufacturers. By dynamically adjusting the peak-watt value of P_{peak}^{PV} in the code, it becomes feasible to conduct diverse experiments in distinct scenarios by manipulating the installed plant size.

Below, in Tab. 3.1, organized input data regarding the user's PV in the Base Case can be found. It is important to note that for subsequent cases, only the P_{peak}^{PV} value will be modified – the sole governing factor determining the system size once the generation waveform in per-unit has been identified, as explained earlier.

Table 3.1: PV data (Base Case).

Parameter	Unit	Value
G_{ref}	Wh/m^2	1000
P_{peak}^{PV}	kW	5
I_{SC}	A	10
T_{ref}^{PV}	$°C$	25
$NOCT$	$°C$	45
S	mW/cm^2	300

3.2.3 BESS Modeling

Electrochemical generators, or secondary batteries, harness electrical energy from stored potential within electrochemical bonds. These rechargeable accumulators boast efficiencies surpassing 90% [37]. Lithium-ion batteries dominate modern energy storage, requiring caution against risks in electrical or thermal overload, mandating meticulous cell voltage balancing and battery management systems. A battery-equipped system regulates mismatches between electricity load and PV generation by storing surplus PV power and discharging to meet remaining demand. This achieves the goal of maximizing renewable energy use and effectively reducing PV rejection rates [38], [39], [40].

In order to simulate the precise charging and discharging behavior of the BESS system, the model employed in Ref. [41] was adhered to. The charging and discharging power of the BESS is bounded in Eqs. 3.4 and 3.5, and to prevent simultaneous charging and discharging, binary decision variables are constrained as in Eq. 3.6. It is assumed that the nominal charging and discharging power of the battery are equivalent to each other.

$$P_{ch,h}^{BESS} \leq b_{ch,h}^{BESS} \cdot P_{nom}^{BESS} \qquad \forall h \in H \tag{3.4}$$

$$P_{dch,h}^{BESS} \leq b_{dch,h}^{BESS} \cdot P_{nom}^{BESS} \qquad \forall h \in H \tag{3.5}$$

$$b_{dch,h}^{BESS} + b_{ch,h}^{BESS} \leq 1 \qquad \forall h \in H \tag{3.6}$$

The State of Charge (SOC) of the BESS in any time slot h may be determined by constraint 3.7 while Eq. 3.8 bounds the state of charge for the purpose of increasing the life cycle.

$$SOC_h^{BESS} = SOC_{h-1}^{BESS} + \epsilon_c^{BESS} \cdot P_{ch,h}^{BESS} - \frac{P_{dch,h}^{BESS}}{\epsilon_d^{BESS}} \qquad \forall h \in H \tag{3.7}$$

$$SOC_{min}^{BESS} \leq SOC_h^{BESS} \leq SOC_{max}^{BESS} \qquad \forall h \in H \tag{3.8}$$

The Eq. 3.7 represents a SOC model for a BESS, where:

1. ϵ_c^{BESS} is the charging efficiency, representing the percentage of electrical energy effectively stored in the battery during the charging phase.
2. ϵ_d^{BESS} is the discharging efficiency, representing the percentage of electrical energy that can be effectively extracted from the battery during the discharging phase.

These efficiencies take into account energy losses that occur during the charging and discharging processes. For example, a portion of the electrical energy supplied to the battery during charging is dissipated as heat due to the internal resistance of the battery; moreover, it is important to also consider losses from the converters used for the charging and discharging processes. Similarly, during discharge, not all stored energy can be extracted due to internal losses.

The Eq. 3.8 imposes a constraint on the SOC, specifying that the SOC at each hour h must be within SOC_{min}^{BESS} and SOC_{max}^{BESS}. This constraint ensures that the battery is neither overcharged nor excessively discharged, both conditions that could potentially damage the battery and reduce its lifespan [42], [43]. These limits have been set to mitigate: battery stress; battery degradation (both full charge to 100% and complete discharge to 0% can lead to faster battery deterioration); charge cycles (the number of charge cycles, i.e., a full charge and discharge of the battery, affects battery lifespan). For optimal battery lifespan and performance, aim to keep the battery charge between 20% and 80% of its nominal capacity.

Given the objective of minimizing imports, the solver tends to discharge the battery towards the end of this period. To prevent complete discharge at the end of the last day, a condition is employed where the state of charge (SOC) at the end equals that at the beginning. Specifically, the SOC of the BESS is set to half of its maximum capacity at the end of the interval H. Without this condition, the optimization model treats the energy charged initially as "free" and utilizes it until the end. These additional constraints are outlined in equation (Eq. 3.9).

$$SOC^{BESS}_{h=(first\ hour)} = SOC^{BESS}_{h=(H-1)} = 0.5 \cdot C^{BESS}_{nom} \tag{3.9}$$

In the following table (Tab. 3.2), all the necessary data for modeling the BESS in the Base Case are provided [2].It's worth noting that the implemented code enables real-time adjustment of multiple parameters to conduct supplementary simulations as needed. This includes defining the battery size and charge/discharge power according to the installed device. The model, as previously described, operates to minimize the objective function by adjusting the BESS system's charging and discharging in response to price fluctuations.

Table 3.2: BESS data (Base Case).

Parameter	**Unit**	**Value**
C^{BESS}_{nom}	kWh	13.5
P^{BESS}_{nom}	kW	5
SOC^{BESS}_{min}, SOC^{BESS}_{max}	kWh	$(0.2 \cdot C^{BESS}_{nom})$, $(0.8 \cdot C^{BESS}_{nom})$
ϵ^{BESS}_{c}, ϵ^{BESS}_{d}	$-$	0.95, 0.90

In the realm of BESS sizing, similar to PV systems, adopting proper sizing practices is crucial for significant energy savings. Oversizing the storage system poses the risk of high investment costs that may not be economically advantageous in the long run, considering the battery's lifespan. However, delving into the sizing and overall life cycle costs of storage systems alongside PV installations is complex and isn't the primary focus of this study.

[2] BESS data source: Tesla Powerwall 2 datasheet

3.2.4 EVCS Modeling

To model the charging profile of the EV, three parameters are essential: the rated charging power, the plug-in time, and the state of charge of the battery [44]. The power demand of the EV is also influenced by the Demand Response (DR) control signal received from an external source, such as a home controller or a utility considered by the code. Regarding the EV's rated charging power, EV driving patterns are used to determine the energy storage status, i.e., the battery SOC. The assumed daily distance traveled by the EV in a distribution circuit is fixed and determined by a decrease of approximately 50% of the maximum capacity. It is presumed that the vehicle covers the same distance during the non-connection period, arriving at the connection point with the same SOC percentage each time (any brief recharges during the journey are neglected).

In the experimental phase, annual hourly data of the available charging power (ACP) were gathered for a generic user. The ACP is derived from the time of the car being parked and connected to a charger. These data were subsequently compiled in an additional *.csv* file, which was read by the input code (as illustrated in Fig. 3.11).

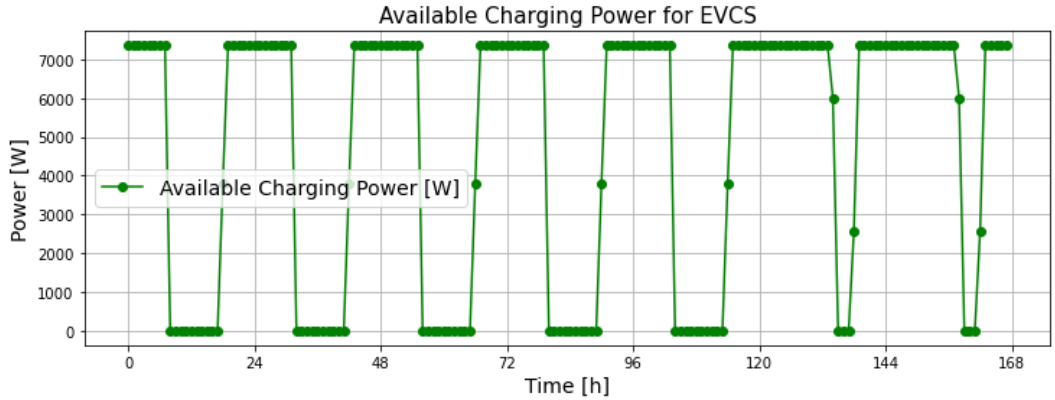

Figure 3.11: Example: Available Charging Power for the EV, data from the first week of January.

Before detailing the equations modeling the EVCS logic, let's review a code snippet that manipulates data concerning the EV's connection to the charging station, followed by a brief explanation of its functionality.

Two lists of values are identified through a loop iterating over a set of temporal indices (H):

- $T_{arrival}$ represents a list containing the initial temporal index, initialized with 0;
- $T_{departure}$ is an empty list that will be used to store the temporal indices when the available charging power transitions from a positive value to zero, based on the dataframe containing the values of Electric Vehicle Power (EVP).

The code's loop checks if the current temporal index is greater than 0 and if there is positive ACP at the current temporal index. If the condition is true, and the ACP at the previous temporal index was zero, it adds the previous index to $T_{arrival}$. This indicates the beginning of the connection.

The code then proceeds to identify the departure times ($T_{departure}$):

- It checks if the current temporal index is greater than 0 and if the charging power at the current temporal index is zero;
- If the condition is true, and the charging power at the previous temporal index was positive, it adds the previous index to $T_{departure}$. This indicates the end of charging.

Finally, a binary representation of the charging state (w_{EV}) occurs: a list w_{EV} is created containing binary values (1 or 0) based on time the charging power at each temporal index is greater than zero or not.

In summary, the code processes data on charging power, identifies the start and end times of charging events, and creates a binary representation of the charging state (w_{EV}).

The equations, similarly to the BESS case, that model the behavior for the charging and discharging power of the EV are as follows (Eqs. 3.10, 3.11, 3.12); it is assumed that the nominal charging and discharging power of the battery are equivalent to each other:

$$P^{EV}_{ch,h} \leq b^{EV}_{ch,h} \cdot P^{EV}_{nom} \qquad \forall h \in H \tag{3.10}$$

$$P^{EV}_{dch,h} \leq b^{EV}_{dch,h} \cdot P^{EV}_{nom} \qquad \forall h \in H \tag{3.11}$$

$$b_{dch,h}^{EV} + b_{ch,h}^{EV} \leq 1 \qquad \forall h \in H \tag{3.12}$$

In addition, it was necessary to consider a constraint ensuring that both the charging and discharging powers of the EV remain consistently lower than the ACP each hour(P_h^{ACP}). Consequently, the vehicle cannot charge or discharge, in favor of the user, a power quantity exceeding that available each hour. This is identified in Eqs. 3.13, 3.14:

$$P_{ch,h}^{EV} \leq P_h^{ACP} \qquad \forall h \in H \tag{3.13}$$

$$P_{dch,h}^{EV} \leq P_h^{ACP} \qquad \forall h \in H \tag{3.14}$$

Once the vector w_{EV} is identified, it will be possible to determine the time intervals during which the electric vehicle is connected or disconnected. The aforementioned vector contains only binary values (0 and 1). The two different scenarios expressed in the system 3.15 are explored (it is considered that for the first iteration, the SOC of the EV is set equal to the value SOC_{in}^{EV}):

$$\begin{cases} SOC_h^{EV} = SOC_{h-1}^{EV} + \epsilon_c^{EV} \cdot P_{ch,h}^{EV} - \frac{P_{dch,h}^{EV}}{\epsilon_d^{EV}} & if: \quad w_{EV}[h] = 1 \\ P_{ch,h}^{EV} + P_{dch,h}^{EV} = 0 & if: \quad w_{EV}[h] = 0 \end{cases} \tag{3.15}$$

The first equation in 3.15 represents a SOC model for a EV battery, where (similarly to the BESS model, energy losses occurring during the charging and discharging processes are taken into account):

1. ϵ_c^{EV} is the charging efficiency, representing the percentage of electrical energy effectively stored in the EV battery during the charging phase.
2. ϵ_d^{EV} is the discharging efficiency, representing the percentage of electrical energy that can be effectively extracted from the EV battery during the possible discharging phase.

Furthermore, in the second equation in 3.15, when the vector w_{EV} has a zero entry, the sum of the charging and discharging powers from the perspective of the charging station is necessarily zero since the vehicle is not connected.

To identify that the vehicle is consistently discharged by the same percentage of SOC, it has been established that for each $T_{arrival}$, it holds that (Eq. 3.16):

$$SOC_h^{EV} = SOC_{in}^{EV} \qquad \forall h = T_{arrival} \; and \; \forall \; h \in H \tag{3.16}$$

Furthermore, it is desired that the EV battery is fully charged in the last hour before departure, ensuring that the user has the vehicle fully charged when needed. For each $T_{departure}$, it holds that (Eq. 3.17):

$$SOC_h^{EV} = SOC_{max}^{EV} \qquad \forall h = T_{departure} \; and \; \forall \; h \in H \tag{3.17}$$

For the same reasons explained earlier in section (3.2.3), being that it is, in any case, an electric storage system, it imposes a constraint on the SOC, specifying that the SOC of EV at each hour h must be within SOC_{min}^{EV} and SOC_{max}^{EV} (Eq. 3.18).

$$SOC_{min}^{EV} \leq SOC_h^{EV} \leq SOC_{max}^{EV} \qquad \forall h \in H \tag{3.18}$$

Below, in Tab. 3.3, the data for an electric vehicle are presented [3], featuring a nominal capacity of 50 kWh and a maximum AC charging power of 11 kW [45]. The value 7.36 kW represents the upper limit set by the charging station (maximum value in the ACP set). It is possible to make changes by modifying the EV data based on the specific model owned by the user (for other typical values, it is possible to refer to [45]).

Table 3.3: EV data (Base Case).

Parameter	**Unit**	**Value**
C_{nom}^{EV}	kWh	50
P_{nom}^{EV}	kW	11
SOC_{in}^{EV}	kWh	$0.6 \cdot C_{nom}^{EV}$
SOC_{min}^{EV}, SOC_{max}^{EV}	kWh	$(0.2 \cdot C_{nom}^{EV})$, $(0.8 \cdot C_{nom}^{EV})$
ϵ_c^{EV}, ϵ_d^{EV}	$-$	0.95, 0.90

[3] EV data source: Tesla Model 3 datasheet

3.2.5 EWH Modeling

In this section, an examination of the EWH model will be conducted. The DHW profile is depicted in Fig. 3.12. According to statistics provided in [46], the total daily DHW consumption considered here is well suitable for a dwelling occupied by 3–4 persons in Finland.

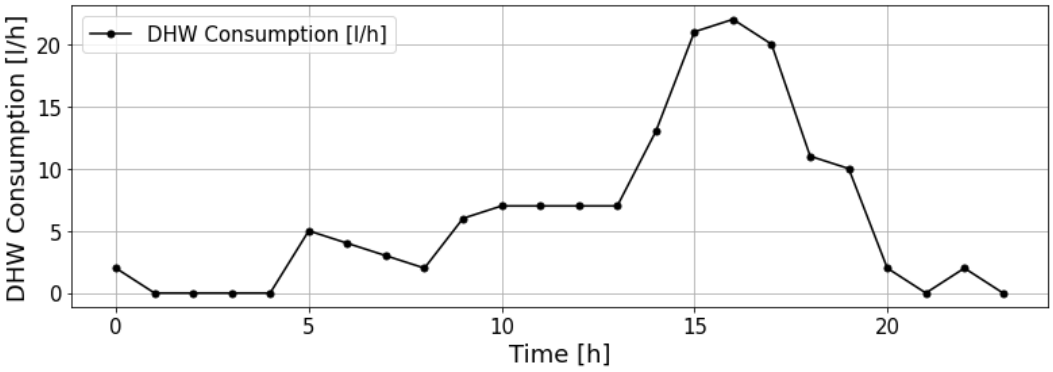

Figure 3.12: Daily DHW consumption profile of a household in liters/h.

The physical model proposed in Refs. [41], and [47] is followed in this work. The temperature of DHW at hour h inside a tank may be calculated as in Eq. 3.19. A distinction from the model proposed in the papers lies in the consideration of thermal losses through the tank enclosure in this study. The DHW usage action triggers the operation of EWH to maintain the DHW temperature inside the tank. However, the users may allow a small deviation from the set point to participate in the DR program offered by the aggregator. In this regard, the EWH may be scheduled at any time slot regardless of the usage profile concerning the comfort levels of each user. The DHW temperature must remain in specified comfort limits as in Eq. 3.20. For simplicity, it is assumed that EWH can operate at any continuous level bounded by the maximum rating in Eq. 3.21.

$$T_h^{DHW} = \frac{T_{h-1}^{DHW} \cdot (1 - \frac{\phi_T^{EWH}}{100}) \cdot (V^{EWH} - V_{use,h}^{DHW} \cdot \Delta h)}{V^{EWH}} + \\ + \frac{T_{in}^{EWH} \cdot V_{use,h}^{DHW}}{V^{EWH}} \cdot \Delta h + \frac{P_h^{EWH}}{(c_w/3600) \cdot V^{EWH}} \cdot \frac{\Delta h}{60\ min/h} \qquad \forall\ h \in H \tag{3.19}$$

$$T_{min}^{DHW} \leq T_{h}^{DHW} \leq T_{max}^{DHW} \qquad \forall h \in H \tag{3.20}$$

$$0 \leq P_{h}^{EWH} \leq P_{max}^{EWH} \qquad \forall h \in H \tag{3.21}$$

Below, in Tab. 3.4, all data related to the electric water heater model is presented (Base Case). It is noteworthy that the system type is that of an electric boiler equipped with an internal resistance to heat the water when necessary, in order to comply with Finnish regulations on buildings [48] regarding the temperature of domestic hot water. It should be emphasized that the tank is connected to the aquifer, ensuring a constant replenishment to maintain a water level above a certain limit. In general, the temperature of the water from the aquifer can vary, depending on external conditions and geographic location. For simplicity, a temperature of 10 $°C$ has been assumed. Furthermore, the temperature inside the tank must be controlled and sufficiently high to limit the risk of legionella and scaling, as referenced in [49], thereby enabling the safe use of domestic hot water by the users. It was decided to set a preferred range between 58 and 60 $°C$.

Table 3.4: EWH and DHW data (Base Case).

Parameter	**Unit**	**Value**
c_w	$J/kg/°C$	4186
T_{min}^{DHW}, T_{max}^{DHW}	$°C$	58, 60
T_{in}^{DHW}	$°C$	10
V^{EWH}	l	200
P_{max}^{EWH}	kW	2
ϕ_{EHW}^{EWH}	$-$	0.5%

3.2.6 TESS Modeling

Regarding the TESS model, the choice has been made to incorporate a tank that operates simultaneously with the building's HVAC system. Various types of systems are available, and it has been chosen to utilize a mode similar to those shown in Refs. [50], [51]. The only difference is that the tank can be heated via direct electricity to address peak loads, especially during the coldest periods of the year. Positioned in series with the HP, as illustrated in Fig. 3.9, this tank aligns with the model presented in a simplified form in [52]. More specifically, it has been decided to show the connection between the tank and the heat pump used, as depicted in Fig. 3.13.

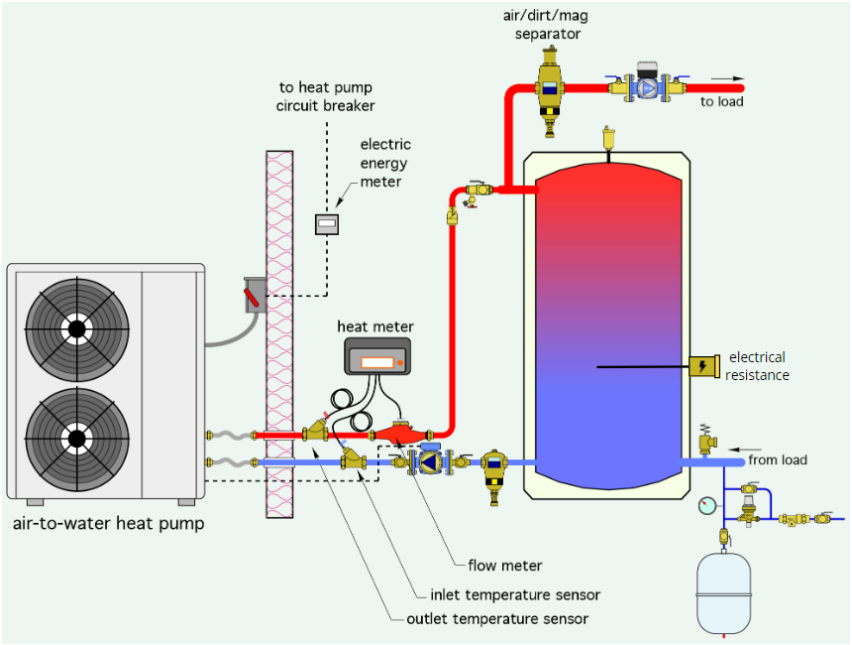

Figure 3.13: Design detail for air-to-water HP with electrical resistance [53].

The tank serves as a thermal reservoir, akin to a flywheel. It can be heated during the charging phase, typically when energy prices are favorable. Later, as needed, the tank releases hot water to the terminals, utilizing the stored thermal energy. The advantage of this heating system lies in its cost efficiency, attributed to the COP of the heat pump, which makes heating the water in the tank economical. In extremely cold weather, when the COP drops, an electric heater assists in maintaining the water temperature. The heat pump uses a thermodynamic cycle to capture thermal energy from the external air, even at lower temperatures, and transfer it to the water in the internal heating system.

Ultimately, the heat transfer fluid from the heat pump provides additional thermal energy to the TESS, improving the overall efficiency of the system. The heated water can be used to warm the environment, for example, through a heating system, and then it is sent to the terminals. Even when heating is not active (summer period), the heat pump is used to cool indoor spaces. In this case, the tank could serve as a thermal reservoir for the heat removed from the spaces during the cooling process.

In the Nordic energy market system, an aggregator is mandated to communicate the power proposal for the upcoming day to the corresponding DSO ahead of the actual energy delivery phase. The tank contains warm water with a temperature ranging from $30°C$ to $90°C$. Exploring efficient interaction in the context of a smart grid between a residential customer and an electric aggregator, the latter serves as an intermediary for electricity procurement, facilitating mechanisms for triggering demand response. Equipped with a system of heating with flexible charging capacity, the customer, with the aid of the established communication infrastructure and a smart meter, receives communicated prices for the next 24 hours from the aggregator. This orchestrated system empowers users to identify optimal times to minimize imported power from the grid, strategically drawing power during periods of lower market prices. Consequently, the system meets energy needs while offering support for heating during peak pricing, fostering significant energy savings. Responsibility for flexible load planning at the customer level is entrusted to a home energy management system, contributing to a cohesive and responsive energy consumption strategy.

At the beginning it's possible to identify the constraints for tank charging and discharging power, considering that the water temperature in the tank remains within the specified limits T_{min}^{TESS} and T_{max}^{TESS}, ensuring it stays within an acceptable temperature range. The charging power and discharging power in each time interval h cannot exceed the maximum rated power of the TESS system when the binary variables are equal to 1 (Eqs. 3.22, 3.23). The sum of the coefficients indicating the decision to charge the tank and the decision to discharge the tank in each time interval cannot exceed 1, implying that only one of the two operations can occur at a time (3.24).

$$P_{ch,h}^{TESS} \cdot b_{ch,h}^{TESS} \leq P_{max}^{TESS} \qquad \forall h \in H \tag{3.22}$$

$$P_{dch,h}^{TESS} \cdot b_{dch,h}^{TESS} \leq P_{max}^{TESS} \qquad \forall h \in H \tag{3.23}$$

$$b_{ch,h}^{TESS} + b_{dch,h}^{TESS} \leq 1 \qquad \forall h \in H \tag{3.24}$$

Regarding the constraint for tank energy balance in the time intervals, the tank's SOC is determined based on the previous interval's value, charging power, discharging power, and heat losses through the tank (Eq. 3.25). For the first interval, the initial tank's SOC is set proportionally to the half of tank's capacity in liters and this represents the initial preparation of the system.

$$SOC_h^{TESS} = SOC_{h-1}^{TESS} \cdot (1 - \phi_T^{TESS}) + (P_{ch,h}^{TESS} - P_{dch,h}^{TESS}) \cdot \Delta h \qquad \forall h \in H \tag{3.25}$$

The state of charge in Wh is upper-bounded by the maximum capacity (Eq. 3.26).

$$SOC_h^{TESS} \leq V^{TESS} \cdot c_w \cdot (T_{max}^{TESS} - T_{min}^{TESS}) \cdot \frac{1}{3600} \qquad \forall h \in H \tag{3.26}$$

The state of charge of the tank at the last hour, is set to be equal to the initially calculated state of charge to ensure appropriate continuity in the model (Eq. 3.27).

$$\begin{aligned} SOC_{h=(first\ hour)}^{TESS} &= SOC_{h=(H-1)}^{TESS} = \\ &= \frac{V^{TESS}}{2} \cdot c_w \cdot (T_{max}^{TESS} - T_{min}^{TESS}) \cdot \frac{1}{3600} \end{aligned} \tag{3.27}$$

It is emphasized that a 1-1 conversion has been adopted for the thermal and electrical power of charge and discharge from the TESS due to the appropriate level of detail for the work context. It is underscored that the efficiencies of the heating systems and storage losses depend on the house structure, heat distribution, and the storage unit's location.

TESS heat losses contribute partially within the building envelope, reducing overall losses. However, it is acknowledged that there are also small losses in the heat distribution system. It is concluded that the mentioned simplifications

partially offset each other, influencing the overall efficiency.

In the following table (Tab. 3.5), all relevant values for modeling the TESS system (Base Case) are summarized and grouped. It is emphasized that the tank in question is used exclusively for the plant water (PW) and not for the DHW.

Table 3.5: TESS data (Base Case).

Parameter	**Unit**	**Value**
c_w	$J/kg/°C$	4186
T_{min}^{TESS}, T_{max}^{TESS}	$°C$	30, 95
V^{TESS}	l	500
P_{max}^{TESS}	kW	4
ϕ_{EHW}^{EWH}	$-$	0.5%

In summary, the model dynamically regulates the charging and discharging of a thermal tank within the context of an HVAC system, balancing the water temperature in the tank and adhering to the maximum charging and discharging capacities of the HVAC system.

3.2.7 Building Thermal Model

A wide range of thermodynamic models has been proposed in the literature to estimate heating or cooling loads. Complex models are burdensome for practical applications, while overly simple models do not yield accurate results. Therefore, it is necessary to strike a balance between accuracy and simplicity. In this work, two-capacity building model is employed to estimate the heating or cooling requirements by analyzing the variation in indoor temperature relative to the external temperature [54], [41], [55].

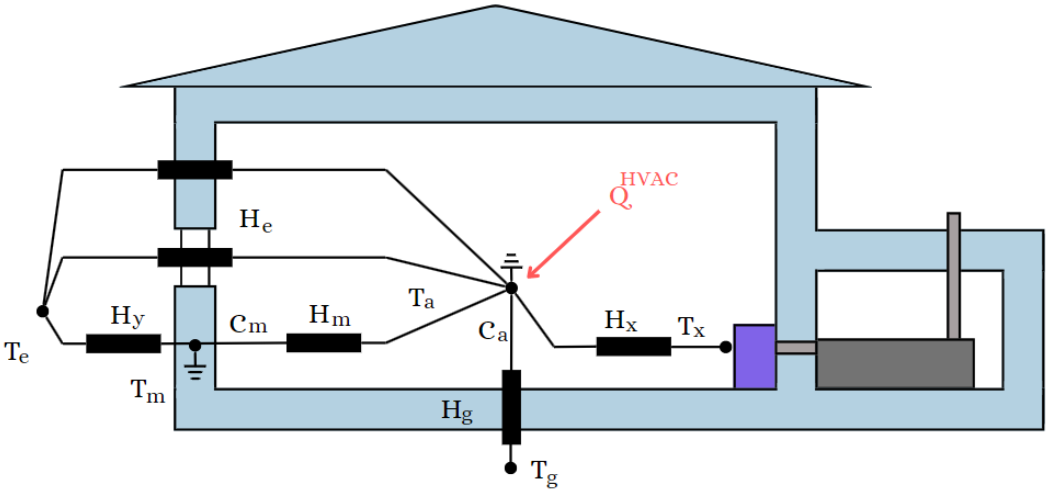

Figure 3.14: Two-capacity building model prototype.

As depicted in Fig. 3.14, this model utilizes two thermal capacities. One capacity is assigned to the building mass, C_m, while the other is distributed to the indoor air, C_a. This model involves two unknown temperatures, $T_{a,h}$ and $T_{m,h}$. It is assumed that the HVAC unit, responsible for conditioning flows, is set to operate at a constant temperature, T_x. The generated air is of convective type and is allocated to the indoor air node. For heat flows, T_g needs to be considered. The windows installed in the building have a small thermal mass compared to the building structure. Nodes T_e, T_a, T_m, T_g, in Fig. 3.14, and the HVAC unit are interconnected through thermal conductance or, in the presence of heat flow, they are connected through thermal capacity. The building mass node is positioned at an undefined depth within the building and thus embodies the mean temperature of the building mass. The energy balance of this model is represented by a simplified discrete form as follows in Eqs. 3.28, 3.30.

$$T_{a,h} = \frac{T_{a,h-1} + \frac{\Delta h}{C_a} \cdot \left(H_m T_{m,h-1} + H_e T_h^{ext} + H_g T_g + H_x T_x + Q_h^{TOT}\right)}{1 + \frac{\Delta h}{C_a}(H_m + H_e + H_g + H_x)} \qquad \forall h \in H \tag{3.28}$$

Where:

$$Q_h^{TOT} = Q_h^{HVAC} - P_{ch,h}^{TESS} + P_{dch,h}^{TESS} \tag{3.29}$$

$$T_{m,h} = \frac{T_{m,h-1} + \frac{\Delta h}{C_m}(H_m T_{a,h} + H_y T_h^{ext})}{1 + \frac{\Delta h}{C_m}(H_m + H_y)} \qquad \forall h \in H \tag{3.30}$$

In Finland, the indoor temperature of residences is consistently maintained at a comfortable level throughout the year. During the winter months, when the external temperature drops below freezing, the interior of a Finnish home is consistently kept at approximately $21°C$ [48]. This practice contributes to the creation of a comfortable and welcoming indoor environment, notwithstanding the severe winter temperatures prevalent in the country. Constraint 3.31 bounds the indoor temperature in a predefined dead band tunable by the occupants. HVAC unit can consume any power level between 0 and maximum level as expressed in Eq. 3.32.

$$T_{a,min} \leq T_{a,h} \leq T_{a,max} \qquad \forall h \in H \tag{3.31}$$

$$0 \leq |Q_h^{HVAC}| \leq Q_{max}^{HVAC} \qquad \forall h \in H \tag{3.32}$$

For a more detailed analysis of the air conditioning system, consideration has been given to the variation of the COP of the heat pump. It is hypothesized that there is an air source HP with external air intake, exhibiting a variable COP. This factor significantly influences the conversion of thermal power to electrical power. In the case of an air source HP, where the temperature of the low-temperature heat source undergoes more pronounced variations, an averaging expression is employed. Drawing on a recent study [56], which compared nine brands of commercial air source HPs, an equation for averaging (Eq. 3.33) with a high coefficient of determination ($R^2 = 0.983$) can be derived for external air temperature ($°C$).

$$COP_h^{HP} = 3.45 \cdot exp(0.03 \cdot T_h^{ext}) \tag{3.33}$$

Heat pumps represent an innovative technology in the field of heating and environmental conditioning, exploiting the principle of heat transfer from a source at a lower temperature to a source at a higher temperature. The assessment of the efficiency of such systems is often expressed through the COP, which quantifies the ratio between the delivered thermal power and the absorbed electrical power. The fundamental formula governing the conversion of thermal power to electrical power in a heat pump is given by the generic Eq. 3.34:

$$P_{el} = \frac{Q_{th}}{COP} \tag{3.34}$$

The application of this formula provides a measure of the energy efficiency of the system, highlighting the performance in the transformation of thermal energy into electrical energy. In the following graph, shown in Fig. 3.15, the trend of the COP of the heat pump is depicted in relation to the external temperature. A higher value indicates greater efficiency, emphasizing the heat pump's ability to generate a significant amount of thermal power compared to the amount of electrical power absorbed. It is important to note that this ideal calculation does not account for any energy losses or inefficiencies in the system, which may result from various sources, such as heat dissipation or electrical resistances. Therefore, actual performance may vary based on operational conditions and the specific design of the HP.

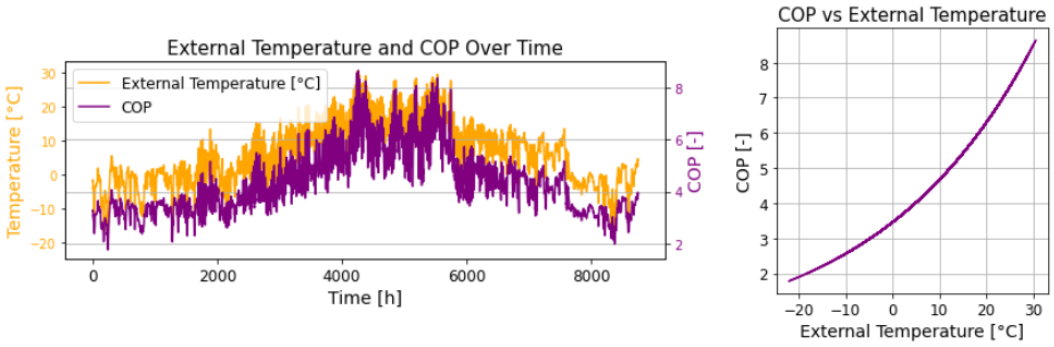

Figure 3.15: Charts representing respectively the trend of COP_h^{HP} and T_h^{ext} throughout time, and the relationship between COP_h^{HP} and T_h^{ext}.

It is worthwhile to note that Q_h^{HVAC} can take both positive and negative values depending on the external temperature. Positive values of Q_h^{HVAC} in Eq. 3.28 indicate that the HVAC unit is operated in heating mode, while negative values represent the cooling operation when the external temperature is higher than the HVAC set point temperature [55].

The model initially takes the form of a challenging MINLP model, where existing methods or commercial solvers struggle to guarantee a global solution, despite the potential for a high-quality outcome. To address this, the MINLP model is transformed into a more manageable MILP model, suitable for seamless integration into a AHEMS. The conversion of a product involving binary and continuous variables into linear expressions is straightforward. However, to linearize the nonlinear term associated with the absolute function, two positive auxiliary variables are introduced. Binary variables, ensuring the precision of the linearization technique, are incorporated as the absolute value is not part of the objective function [41], [55]. The procedural details are outlined in Eqs. 3.35, 3.36, 3.37, 3.38, 3.39.

$$Q_h^{HVAC} = Q_h^a - Q_h^b \qquad \forall h \in H \tag{3.35}$$

$$|Q_h^{HVAC}| = Q_h^a + Q_h^b \qquad \forall h \in H \tag{3.36}$$

$$Q_h^a \leq b_h^a \cdot Q_{max}^{HVAC} \qquad \forall h \in H \tag{3.37}$$

$$Q_h^b \leq b_h^b \cdot Q_{max}^{HVAC} \qquad \forall h \in H \tag{3.38}$$

$$b_h^a + b_h^b \leq 1 \qquad \forall h \in H \tag{3.39}$$

The considered house was a two-floor building with a total floor area of 200 m^2 and the parameter values of the two-capacity model for this house are listed in Tab. 3.6. Please note that the given parameters regarding the building itself (without consider the plant size) are applicable to Finnish detached houses only.

Table 3.6: Building thermal model data (Base Case).

Parameter	Unit	Value
H_e, H_y, H_m, H_x, H_g	$W/°C/m^2$	0.29, 0.33, 5.16, 0.48, 0.05
C_a, C_m	$Wh/°C/m^2$	3.616, 31.14
T_g, T_x	$°C$	10, 18
$T_{a,min}$, $T_{a,max}$	$°C$	21, 22
Q_{max}^{HVAC}	kW	6

In conclusion, the proposed model provides an approach for the thermal management of the building in Finland in question, utilizing air-source heat pump technology, hot water storage tanks, and conditioning terminals [57]. This system enables the optimization of the building's energy efficiency while simultaneously reducing environmental impact.

3.2.8 Power Balance

To conclude the modeling equations for the system, it is imperative to elucidate the electrical power balance equation at the PCC (Eq. 3.40). It is noteworthy that the charging and discharging powers of the tank for plant water have already been encompassed within the HVAC system power. In other words, the power required by the system to maintain the desired indoor temperature for comfort purposes is already calculated to include the power needed by the heat pump in series with the tank.

$$\begin{aligned} P_h^{PV} + P_{dch,h}^{BESS} + P_{dch,h}^{EV} + P_{imp,h} = \\ = P_{ch,h}^{BESS} + P_{ch,h}^{EV} + P_h^{EWH} + P_h^{HVAC} + P_h^{crit} + P_{exp,h} \qquad \forall h \in H \end{aligned} \tag{3.40}$$

This equation represents the balance for the individual hour h under consideration and accounts for all elements that play a specific role in the system. It must be satisfied throughout the entire interval H.

The models were solved on a laptop equipped with an Intel(R) Core(TM) i7-8750H processor, featuring a base frequency of 2.20 GHz and a maximum frequency of 2.21 GHz, and 16.0 GB of RAM. The MILP optimization computation was carried out using the *Python* programming language, utilizing the *Pyomo* library. The solver used, in this case GLPK, ensures that this equality is verified for each hour. If this were not the case for even a single hour, the

optimal solution would not be found, leading to an infeasible condition.

The power calculated hour by hour represents the average instantaneous consumption or generation of energy in each hour of the day. The code sets up a mathematical optimization model to optimize energy management considering all the factors mentioned above over a specified time horizon covering one or more days.

3.2.9 Performance Index

To discuss the performance of the entire system, the Load Matching Index (LMI) is used. This index is a metric used to evaluate how well an energy system is able to meet energy demand with the available production. It measures the effectiveness with which renewable energy production (such as solar, as analyzed in this case) aligns with energy demand, helping determine how much reliance on conventional or backup energy sources is necessary. A higher LMI indicates better correspondence between production and energy consumption. The LMI is calculated using Eq. 3.41.

$$LMI = \frac{1}{H} \cdot \sum_{h \in H} min\left(1; \frac{g_h + bb_h}{l_h}\right) \tag{3.41}$$

The term H denotes the considered time interval, which is significantly influenced by the duration and frequency of the time intervals used for the calculation. This underscores the importance of precise temporal definition within the analysis context. Moreover, the components of the numerator, g_h and bb_h, play a crucial role in determining the index value. The former, g_h, represents the energy generation from renewable sources (RES) in hour h, highlighting the contribution of sustainable energy resources in the system. The latter, bb_h, indicates the balancing provided by electrical storage systems, reflecting the effectiveness of storage technologies in optimizing energy utilization. Meanwhile, the term in the denominator reflects the total load during hour h, resulting from the sum of all power demands of the system at that time. This measure represents the overall level of energy demand, emphasizing the importance of aligning energy supply with the system's requirements within a specific time interval.

Chapter 4

Results

4.1 Base Case Power Flows

In this chapter, graphical representations and outcomes related to the Base Case, in accordance with the facility sizes outlined in the preceding section, will be presented. These visuals are structured seasonally, aligning with the format depicted in Figure 3.5. The exhibited solutions underscore the proficiency of the implemented code in minimizing the objective function 3.1. The primary goal is to narrow the cost difference between imported and exported power, by implementing energy management strategies to optimize utilization, enhance efficiency, and align production and consumption, thus minimizing reliance on higher-cost energy imports or lower-cost energy exports. The overarching goal is to maximize the economic value of energy while concurrently reducing comprehensive costs associated with procurement and disposition. Graphs will illustrate exported and imported energy quantities between the electrical grid and the user, as well as the SOC for BESS, EV batteries, and TESS, along with their associated charging and discharging power values. Furthermore, graphical representations will be generated to depict the electrical power profiles of EWH and the HVAC system. The extraction of graphical data and results is accomplished through the combined use of the *Pandas* and *NumPy* libraries in the Python environment. *Pandas*, specialized in the processing and analysis of tabular data, synergistically integrates with *NumPy*, which provides advanced data structures and mathematical functions for numerical and scientific operations. The values of decision variables are obtained using the GLPK solver, adopting a MILP approach. GLPK is an open-source library

specialized in solving linear and mixed-integer linear programming (LP, MILP) problems, making it relevant for the present case. Pyomo, an optimization framework in Python, provides an interface for the definition and solution of mathematical optimization models, including linear and integer ones. The Pyomo's interface allows users to code tasks in algebraic form, simplifying the process of model formulation and solution.

Before proceeding with the detailed analysis of the results, it has been chosen to closely examine the results for the temporal sequence of the first 3 days of May. In this context, BESS, TESS, and EV can actively engage with the distribution network through the PCC. It is noteworthy that the ability to exchange power with the grid via a PCC is contingent upon the design and specific configuration of each system. Consequently, all outcomes presented herein result from simulations applied to the aforementioned scenario.

Battery Energy Storage System The chart depicting the BESS system's charging and discharging power, along with the corresponding SOC (Fig. 4.1), shows a consistent trend influenced by energy prices. The green curve represents charging power, while the red curve represents discharging power. It's worth noting that the SOC curve of the battery is closely linked to both charging and discharging powers through equation 3.7. The optimized system effectively maintains the battery's charge level between maximum and minimum thresholds, as explained earlier, allowing charging during excess production and favorable energy prices. The impact of charging and discharging efficiencies is visible in the slope of the SOC hourly segments. Higher efficiency would facilitate faster charging and discharging, benefiting the end-user.

Electric Vehicle A similar rationale is applied to the electric vehicle battery. The only difference from the BES system is that the EV is not always available and simultaneously acts as a load for the user and a potential source of flexibility. As depicted in Fig. 4.2, the vehicle is connected and disconnected from the charging station during predefined hours highlighted by the blue and magenta pins, respectively. Once connected, the vehicle has an SOC equal to the maximum possible value reduced by the portion consumed during the traveled distance. The connection to the station does not automatically initiate charging; the vehicle may be charged or discharged, as evident and possibly, to balance loads and minimize the imposed objective function. However, it becomes a

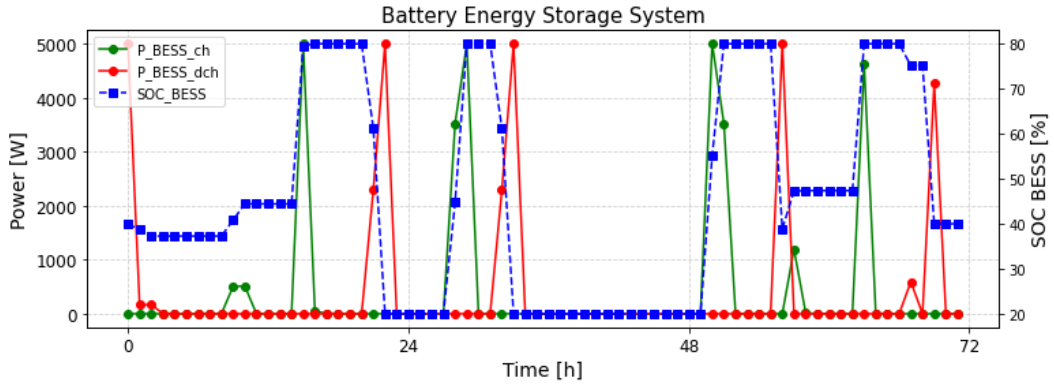

Figure 4.1: Results of the BESS for the three days of May (hourly time resolution).

periodically fixed load as it is required to reach the maximum allowable capacity before departing, ensuring that the user always has a fully charged vehicle whenever it is needed. Additionally, it is noted that as a constraint, the charging and discharging powers cannot exceed the ACP, and the SOC is calculated as zero during the period when the vehicle is not connected to the station.

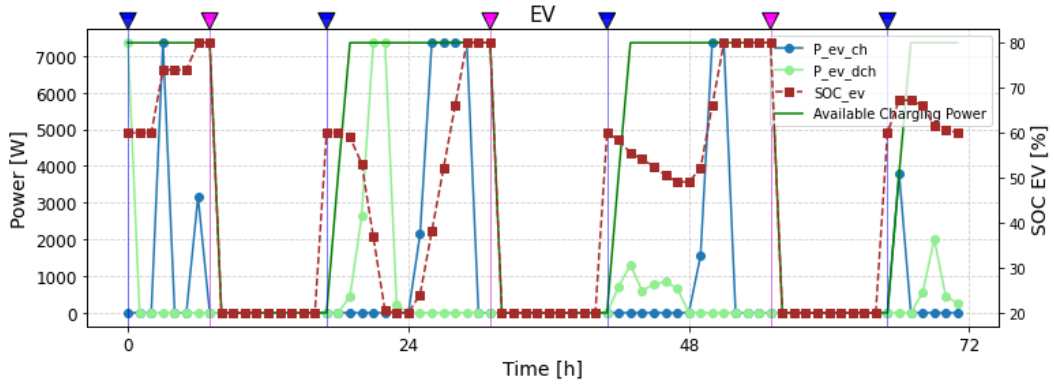

Figure 4.2: Results of the EV for the three days of May (hourly time resolution).

Thermal Energy Storage System Regarding the use of the tank for PW, it is observed in Fig. 4.3, that the charging and discharging powers and SOC operate similarly to the two previous systems. The main difference, already evident in the plots of the selected days but also extended in a broader analysis, is that the tank utilization decreases with the increase in external temperature: Colder periods require greater support for the heating system and, consequently, a more dynamic utilization of the tank itself. Furthermore, the

SOC will never remain stable due to system losses through the tank enclosure.

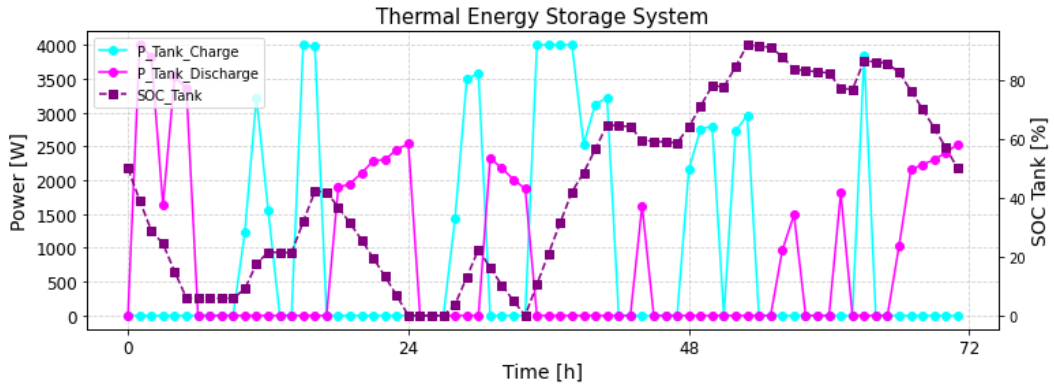

Figure 4.3: Results of the TESS for the three days of May (hourly time resolution).

HVAC and Electric Water Heater In Fig. 4.4, there is a noticeable substantial variation in the power required by the HVAC system. The dark green curve highlights the inclusive power of both charging and discharging of the TESS support to the heat pump. An increase in power demand is observed when the external temperature drops, and a decrease is noted when it rises, all aimed at maintaining the desired indoor temperature. Regarding the power of the EWH for hot water, it follows a similar pattern over the 24 hours, as explained in the modeling chapter of this system. It is clarified that the plotted power fraction related to the heat pump is the electrical power already converted through the COP of the heat pump itself.

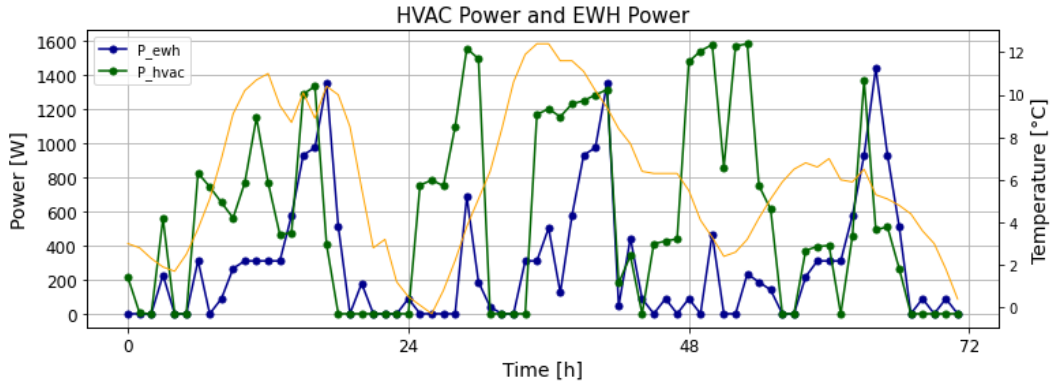

Figure 4.4: Results of the HVAC and EWH for the three days of May (hourly time resolution).

To gain a clearer understanding based on seasons instead, it has been chosen to analyze how the power demand of the system varies according to external conditions and the analysis period. It was preferred to separately analyze the months divided into seasons. This is justified by the fact that the results of a single day are not yet fully comparable due to the variability of external conditions and energy prices. This reflects on the variation in terms of the power generated locally by the PV and a significant fluctuation in the loads and power demanded by the system as a whole.

4.1.1 Autumn

For the autumn period, Fig. 4.5 is examined, comprising a stacked bar chart illustrating the demand mix and a pie chart displaying the percentage breakdown of generation for the autumn season.

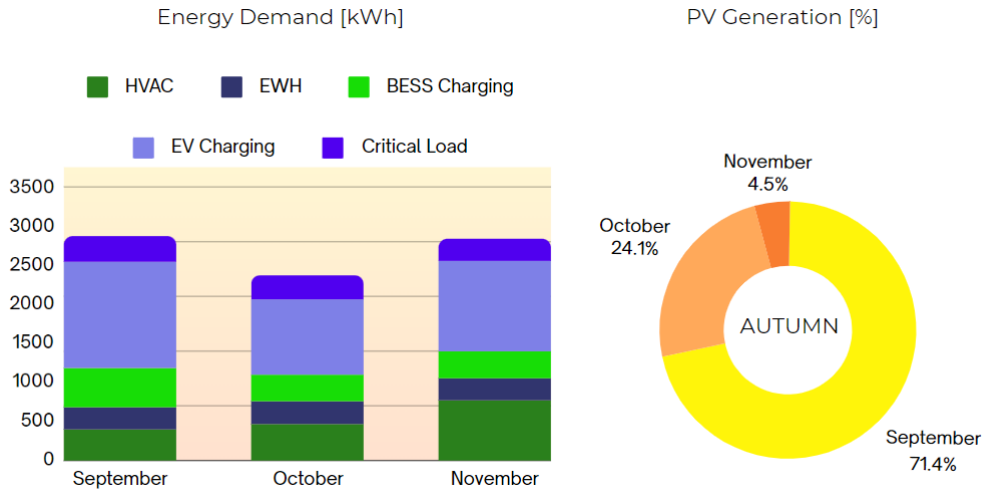

Figure 4.5: Results for energy demand and PV generation for the autumn period.

In the left graph, it's notable that the power demand of the HVAC system displays the most pronounced variability, with a significant increase observed from September to November. This surge is primarily attributed to a corresponding drop in external temperatures during this period. Concurrently, there's a noticeable decline in the energy generated by the photovoltaic system, largely due to reduced solar irradiance. To illustrate, the total power output declines significantly from 209.20 kWh in September to 13.14 kWh in November.

4.1.2 Winter

During the winter season, a graph akin to the one before is generated. As depicted in Fig. 4.6, there's a notable average seasonal surge in total demand, amounting compared to autumn.

This increase is largely attributed to the heightened usage of heating systems. Given the harsh and frigid winter conditions in Finland, external temperatures plummet significantly during this period.

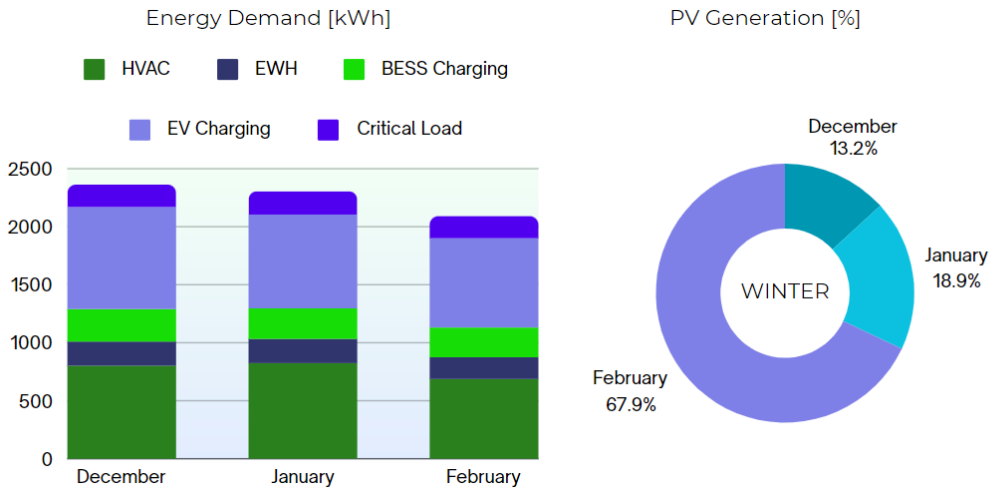

Figure 4.6: Results for energy demand and PV generation for the winter period.

When it comes to photovoltaic generation, no significant differences are observed among the three winter months. This is largely due to Finland's limited sunlight availability during this period, coupled with meteorological conditions that inhibit sunlight penetration through dense cloud cover. As evidenced, there's a marked reduction compared to the autumn period: throughout winter, the total generation amounts to 81.90 kWh over the three months, whereas in autumn, a significantly higher value of 293.02 kWh is recorded.

It's evident that during this timeframe, the SOC percentage of storage systems such as BESS, which rely directly on photovoltaic power, reaches its lowest point for the entire year. This underscores the significant challenges imposed by winter conditions on both renewable energy generation and storage within the region, highlighting the need for robust solutions to mitigate these seasonal fluctuations.

4.1.3 Spring

For the spring period, reference is made to the graphs presented in Fig. 4.7. These graphs provide valuable insights into the trends and patterns observed during this transitional season.

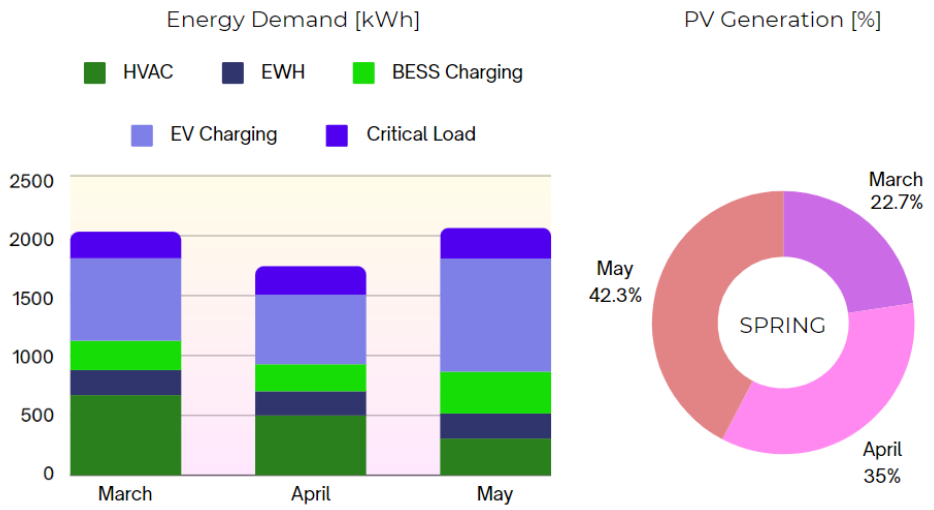

Figure 4.7: Results for energy demand and PV generation for the spring period.

After an initial rise in energy demand from HVAC systems starting in March, there's a gradual decline leading up to the beginning of summer. Despite lower energy demand in May, the total demand for this month exceeds that of the two previous months due to fewer weekends, impacting electric vehicle charging demand and raising the overall demand to 944.16 kWh. This emphasizes the importance of efficient energy management strategies to ensure a reliable power supply during peak periods.

For photovoltaic generation, there's a gradual percentage increase from March to May, correlating with the expected rise in daylight hours during this period. Specifically, the total generation is as follows: 245.78 kWh in March, 380.12 kWh in April, and 458.83 kWh in May. This upward trend in photovoltaic generation corresponds with the declining power demand in May, suggesting a surplus of renewable energy that could be stored or efficiently utilized to optimize energy consumption and lessen dependence on non-renewable sources during peak periods.

4.1.4 Summer

For the upcoming summer period, analogous graphs to those employed previously will be utilized. Distinctions are less discernible during transitional seasons but are markedly pronounced during diametrically opposite periods, notably winter and, indeed, summer. Reference is made to Figure 4.8.

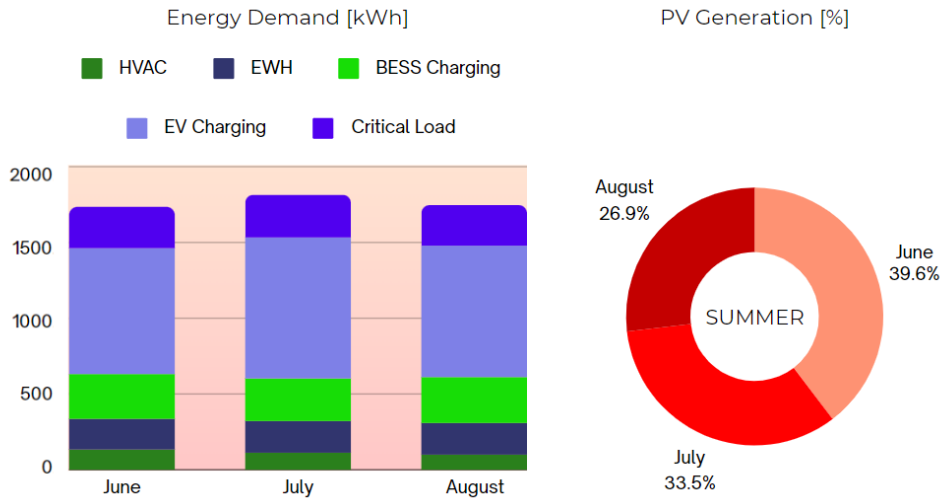

Figure 4.8: Results for energy demand and PV generation for the summer period.

It is immediately apparent that there is a significantly low percentage of energy demanded by HVAC relative to the total energy consumption. Additionally, the overall demand is observed to be lower compared to previous months. Specifically, there is around 84% reduction in the total amount of energy required by HVAC from the winter period to the summer period. This substantial decrease underscores the seasonal variation in power usage and highlights the efficiency of HVAC systems during warmer months.

In terms of generation, there's been a significant surge from winter, where the total amount was 81.90 kWh, to 1542.21 kWh during summer. June and July stand out as the most productive months, contributing to around 73.1% of the total quarterly production. This increase highlights the seasonal variability and the importance of maximizing solar energy utilization during peak months, aligning with the input data shown in Fig. 3.4 and emphasizing the significance of strategic planning in optimizing renewable energy production.

4.1.5 Whole Analyzed Year

To provide a comprehensive overview of the two analyzed quantities, it has been decided to incorporate the annual comprehensive graph (Fig. 4.9). This graph vividly illustrates the smooth, variable trend of the load demanded by HVAC. Moreover, upon examining the generation graph, one can discern that the highest percentage of generated energy relative to the annual total occurs during the months of June and July, with nearly identical percentage slices. Moreover, it is interesting how BESS is more active during summer months due to the excess of PV generation, which requires charging.

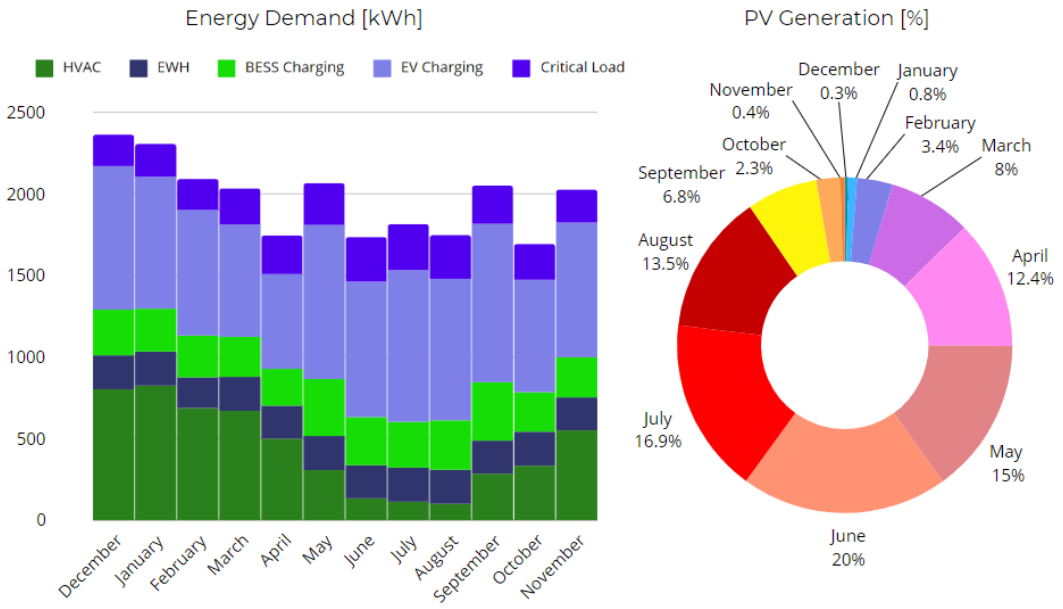

Figure 4.9: Results for energy demand and PV generation for the analyzed year.

Conducting a preliminary comparative analysis was imperative to understand the distribution of power required by the user across the months, which have been further categorized into seasons. This preliminary exploration serves as an essential foundation for subsequent, more in-depth analysis in the following section. In the upcoming analysis, the imported and exported energy amounts will be examined in detail, alongside the net costs incurred by the user. Furthermore, the analysis will showcase how optimization strategies can effectively alter the demand, aiming to align it as closely as possible with generation patterns. This will provide valuable insights into optimizing energy usage and cost-efficiency.

4.2 Deep Analysis of Optimized Results

In this section, the achieved results are analyzed, and considerations are made regarding the main differences observed among the different periods of the year (price data for 2022).

4.2.1 Net Cost fot the User

The data presented in Table 4.1 provides a comprehensive overview of monthly variations in both imported and exported energy, accompanied by their corresponding financial implications for the user. Additionally, the table includes the monthly financial impact on the user, where a negative figure signifies an actual financial gain in the context of electrical energy. The management system is intricately designed to efficiently navigate energy dynamics, specifically geared towards maximizing cost savings for the user. It is important to emphasize that the costs referred to here are those stated in the objective function, specifically electricity bills. The analysis does not include the cost of equipment and installation. More details in *Appendix B* (Tabs. B-2, B-3, B-4).

Table 4.1: Summary of energy and cost metrics per month (Base Case).

	Total Imported Energy $[kWh]$	Total Exported Energy $[kWh]$	Total Cost of Imported Energy [€]	Total Revenue from Exported Energy [€]	Net Cost for the User [€]
September	1721.27	758.16	289.26	282.05	7.21
October	1406.36	313.20	166.18	85.30	80.88
November	1641.54	287.00	321.45	80.50	240.94
December	1912.12	284.48	460.85	116.00	344.85
January	1875.00	235.97	235.88	42.36	193.52
February	1663.25	265.98	171.18	37.85	133.33
March	1565.22	308.99	173.76	70.62	103.15
April	1207.04	273.46	123.60	53.74	69.85
May	1539.52	771.53	182.04	175.63	6.42
June	1155.37	736.99	123.10	172.74	−49.64
July	1310.34	781.51	180.37	212.91	−32.53
August	1340.04	741.45	223.24	332.50	−109.26
Tot.	18 337.07	5758.72	2650.91	1662.20	988.72

From the table analysis, it is evident that colder months with lower sunlight exposure, such as winter months, incur a higher net cost compared to warmer months. This phenomenon can be attributed to the higher and more prolonged irradiance values and external climate conditions, which lead warmer months to entail lower air conditioning loads and higher local photovoltaic production. While these observations are intuitive, they are not the sole reasons for the monthly variation in net cost.

Indeed, the monthly DA price trend varies, as depicted in Fig. 3.5. To provide a more immediate yet less detailed overview, the monthly average values of DA_p for 2022 are represented in Fig. 4.10. Simultaneously, the curves of the total cost of imported energy and the total revenue of exported energy are also depicted monthly, which exhibit a close correlation with DA_p (**0.838** and **0.792** respectively are the correlation coefficients). Additionally, to offer a comprehensive view, the user's net cost is represented monthly as well. It is noticeable that this cost will be higher in colder months, decreasing and becoming negative in warmer months, indicating a higher quantity of energy being sold to the grid (there is a high negative correlation coefficient of **-0.801** between the user's net cost and the exported energy in kWh). This signifies a strong negative correlation between the two variables. In other words, there is a significant opposite trend between the amount of exported energy and the net cost. Such a strong negative correlation suggests that higher exported energy is associated with a substantial reduction in the overall net cost.

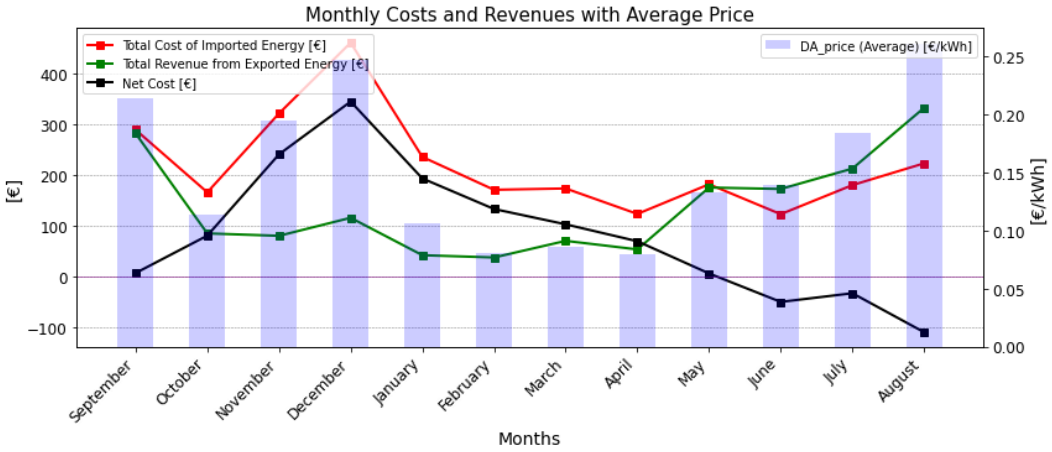

Figure 4.10: Variation of the monthly user net cost for the year 2022 (Base Case).

The monthly results of exported and imported energy are depicted in the chart in Fig. 4.11. It is evident that the exported energy (negative) never exceeds the imported energy (positive). However, the optimized system is capable of managing energy in such a way that, when possible, the user may not incur any expenses at the end of the month, or even generate a profit through exportation during periods of favorable prices (such as June, July, and August).

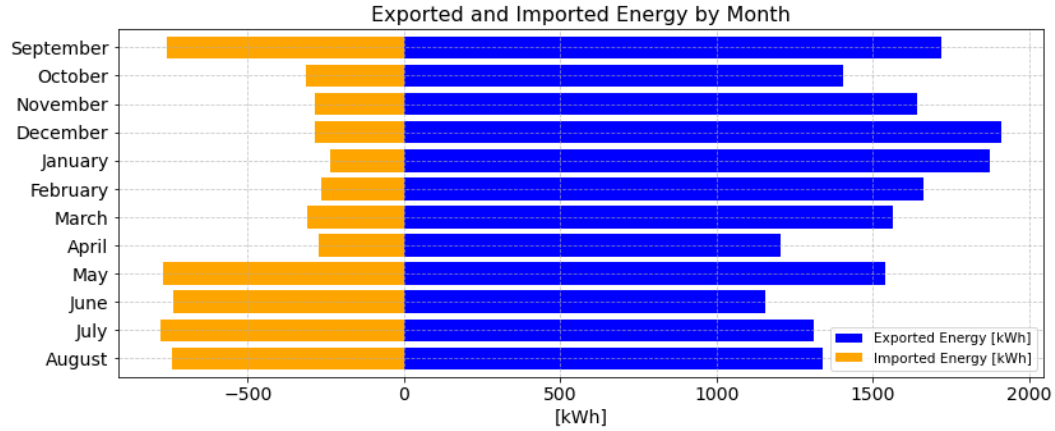

Figure 4.11: Total imported and exported energy variation for the year 2022 (Base Case).

For a comprehensive overview of the energy exchange dynamics and total demand throughout different seasons with daily average resolution for the Base Case, please refer to *Appendix A*. (Figs. A-1, A-2, A-3, A-4).

4.2.2 Load Matching Index

Another conducted analysis involves the Load Matching Index. The LMI assesses the alignment or equilibrium between PV generation and local demand. Specifically, it quantifies the proportion of the total load met by on-site generation. The LMI was computed for simulated loads and PV generation using Eq. 3.41, with the results depicted in Fig. 4.12. In this particular case, the LMI was notably low due to reduced PV generation during winter and autumn. The diurnal cycle of PV posed a constraint, preventing the complete satisfaction of the load exclusively through PV, even in the summer and spring seasons. Furthermore, it is emphasized that all generation was effectively managed to minimize user costs and promote savings.

It should be reminded that the LMI value depends on the number of intervals considered. It has been chosen to calculate the LMI for the seasons to provide a summary view of how it is influenced by external conditions. Indeed, from the calculation of correlation coefficients, it is found that the correlation between the average monthly generation and the monthly LMI value is **0.908**.

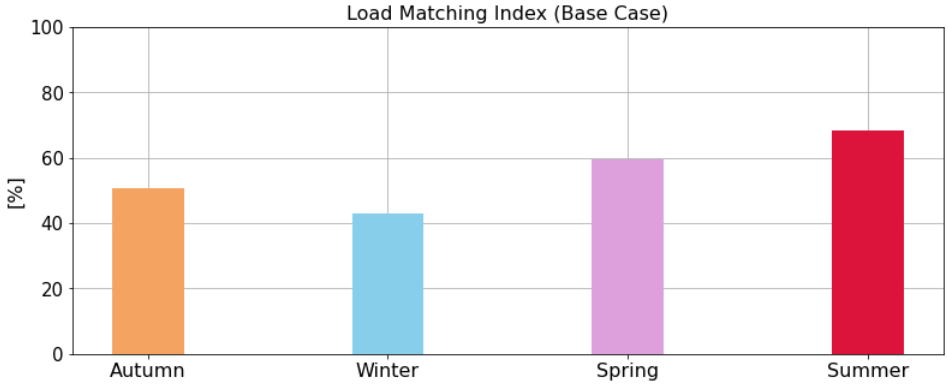

Figure 4.12: LMI comparison for different seasons in Base Case.

In general, LMI index values tend to decrease when energy management efficiency is low. Subsequently, a case will be examined where the absence of systems enhancing system flexibility leads to a drastic drop in LMI values. Consequently, the values obtained from the baseline case analysis not only appear acceptable, as they surpass the scenario without flexibility systems, but also align with the trend of photovoltaic production. For instance, a percentage increase of 59.57% is observed from the winter period (characterized by lower LMI) to the summer period (characterized by higher LMI), or a decrease of -26.16% from the transition from summer to autumn. It is noteworthy that an increase in LMI value indicates a greater system capacity to effectively manage the increase in photovoltaic production. Furthermore, as renewable energy production becomes more predominant, the utilization of storage systems and DR becomes more dynamic and exerts a positive impact on the index itself. These systems can help adapt energy load more efficiently to renewable energy availability and demand variations. Another factor influencing the index is the total load, which, being in the denominator in equation 3.41, tends to increase the LMI value during periods of lower load and decrease it during periods of higher load.

4.2.3 Optimized Load Balance

In order to explain how decisions are made within the system, it was decided to analyze a three-day timeframe for the sake of clarity and visual understanding. Three days in the month of May were selected (the same pattern is visible in any analyzed time interval, with appropriate deviations due to external conditions). The first graph essential for understanding how optimization works is a zoom on the trend of DA_p for these three analyzed days (Fig. 4.13).

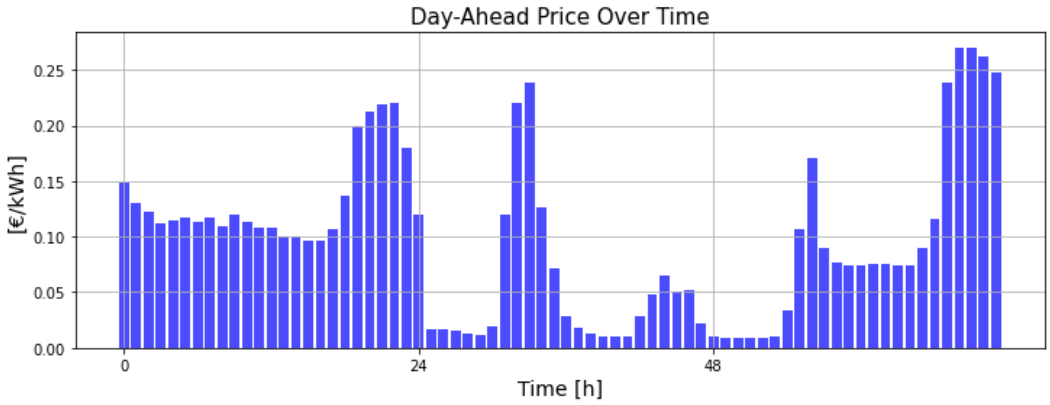

Figure 4.13: DA_p variation for a three-day timeframe of May.

These three days were selected because they exhibit clear fluctuations in energy prices. The price oscillates between high and low values rapidly, even within hourly intervals. However, this extreme variability is not as pronounced on the first day, for instance. The consequence of this selection is that it allows for an analysis of how the system responds to significant fluctuations in energy prices. This enables the evaluation of optimization strategies' effectiveness in managing such fluctuations and stabilizing the system, particularly compared to periods with lower price variations. Additionally, it provides a more comprehensive overview of the overall system performance in volatile energy market conditions.

For comprehensive analysis, it is essential to plot the graph to demonstrate the true benefits of the conducted analysis. It was chosen to represent two graphs in Fig. 4.14 depicting the load balance of the household. The first graph without optimization and the second graph optimized as explained earlier.

Figure 4.14: Respectively, the load balance of the household without optimization and with optimization is depicted in the three-day timeframe.

As detailed in the legend, the total demand is represented by the magenta curve. With the optimized version, it is observed that the load curve is adjusted to overlap with the generation from RES whenever possible. Load peaks primarily arise from the need to charge the electric vehicle, which are quite evident since, for the remaining hours, being May a relatively warm month compared to others, it is not characterized by a high heating load.

Examining the illustration depicted in Figure 4.13, it is evident that in the

optimized approach (while always adhering to imposed constraints), energy import occurs during time slots characterized by low selling prices. This stands in contrast to the non-optimized approach, where such optimization does not occur. The significant reduction in costs for the user becomes apparent when considering the trend of the curve representing exported power.

In the non-optimized scenario, power is exported only when necessary based on the availability of generation exceeding the load, and when the electric vehicle, once connected, relinquishes power to meet the load. Subsequently, the vehicle proceeds to charge with the maximum available power to be fully charged (at 100% fot the EV battery SOC) an hour before departure. This behavior is not dynamic but rather mechanical, as the system merely aims to fulfill imposed constraints without considering energy optimization for the user's benefit.

Conversely, in the optimized scenario, the electric vehicle only discharges when it serves to reduce the overall net cost for the user (as indicated by the absence of the second peak of exported power). Both scenarios witness proper functioning of energy storage systems, albeit in the optimized system, they assume a central and dynamic behavior. When discharging, if the price is favorable, they export a percentage to the grid to achieve greater and more sensible revenue. Furthermore, observing the LMI value for this time interval, it is evident how the optimized energy usage promotes a much more pronounced adherence between generation and load compared to the non-optimized scenario. In the former scenario, the load is not adjusted to follow the generation, although the user could benefit from on-site generation facilitating potential exports. However, this advantage is not exploited, rendering the system significantly less energy-efficient. By adopting the DR technique, a drastic increase in the LMI is observed. For example, such an increase is already noticeable over the three days analyzed, with a value of 55.26%. The final evaluation emerges from the analysis of the user's net cost at the end of the three days (which can be extended to any time interval). Over the three non-optimized days, the net cost for the user stands at 12.90€, while in the optimized case, the value is 2.03€. Therefore, the user adopting an optimized energy management system as described transitions from an expenditure to a gain. Hence, the user has a percentage gain of approximately around -84.34%, indicating a reduction in net cost compared to the non-optimized scenario. The percentage is negative because the transition is from a loss to a gain.

4.3 Discussion on Research Limitations

Despite the model's satisfactory performance, several limitations must be considered. Below, we examine the relevant constraints in detail:

- **Model Complexity:** The implemented code is based on a rather intricate model that incorporates numerous variables and constraints. This complexity necessitates significant computational resources for optimization. Computation times increase substantially with larger time intervals H, posing challenges for practical applications requiring real-time or near-real-time solutions.
- **Simplified Assumptions:** The model relies on simplified assumptions regarding data and parameters. For instance, it assumes the electric load for the EWH repeats periodically over 24 hours, while actual demand may fluctuate based on user behavior. Fixed departure and arrival times, routes, and SOC percentages for electric vehicles are considered, which might not reflect real-world variability where users have dynamic schedules and energy consumption patterns. Additionally, critical loads and heating/cooling demands are influenced by numerous unpredictable factors, including user comfort preferences. The model focuses solely on energy consumption to maintain internal temperatures within specified bounds, ignoring other consumption sources like electrical equipment, lighting, and occupancy. Furthermore, potential variations in yields or losses not accounted for in the model introduce additional uncertainty into the analysis.
- **Data Representation:** The model reads data from a *.csv* file, making the quality and completeness of this data crucial to the results. Errors or omissions in the data can significantly impact the model's performance. Additionally, the model does not predict future data, only considering a fixed time interval, which limits its applicability in scenarios requiring long-term planning and adaptation to dynamic conditions.

The limitations extend beyond technical and code-related aspects, encompassing choices related to the system itself:

- **Geolocation:** This study is confined to the Finnish context, utilizing user geolocation data specific to Finland. Ground temperature and weather conditions, which can vary considerably across different geographical

locations, significantly influence the efficiency and management of energy systems. Building insulation characteristics also directly impact heating and cooling needs, affecting overall energy consumption. Therefore, analyses conducted in other geographical regions must account for these factors to provide accurate assessments of energy dynamics and optimization opportunities.

- **User Isolation:** The model does not account for participation and cooperation within a renewable energy community. Consequently, the analyzed user cannot share and optimize energy collaboratively, missing out on the benefits of shared renewable energy resource management. In a community energy context, users can coordinate to balance energy production and consumption, enhancing the efficiency of resource utilization. Operating in isolation prevents users from fully exploiting optimization potential, thus forfeiting economic and environmental benefits associated with collaborative energy management. User isolation represents a significant limitation in maximizing the efficiency and sustainability of renewable energy resources.
- **Variety of Renewable Sources:** The current model relies solely on photovoltaic generation, limiting the consideration of other renewable sources such as wind energy. Dependence on a single RES source reduces the flexibility and resilience of the energy system, as diverse sources can offer complementary advantages regarding energy availability and production. Incorporating other technologies, such as wind energy, could facilitate more efficient management of energy resources and enhance overall system stability, particularly given variations in Finnish sunlight availability and weather conditions. Expanding the model to include multiple renewable sources would likely improve the resilience and sustainability of the energy system.

Chapter 5

Sensitivity Analysis

In the chapter concerning sensitivity analysis, four cases with variations made to the base model will now be examined. The main deviations will be analyzed, and a discussion will be conducted on the best and most cost-effective model for the user. This type of analysis is necessary as it aims to provide an order of magnitude regarding the benefits resulting from more or less efficient configurations of the prosumer model. It is intended to demonstrate how the advantage of an optimization system is not only vertical but also horizontal, favoring both greater economic return and a more heterogeneous utilization of the installed technological resources.

5.1 Load Flexibility and Plant Sizes

The research aimed at achieving a genuine advantage in understanding the optimal configuration for household continues with the modification of the parameters involved. A wide range of scenarios is being explored to assess the benefits and drawbacks of different configurations. Initially, a baseline case without the implementation of flexibility systems and without considering DR is examined. Subsequently, other cases involving variations in the size of the installed PV system and the nominal capacity of the BESS are considered, as well as the possibility of not utilizing the TESS to support the HP.

For an overview of all the analyzed cases, Table 5.1 highlights the main differences among them. Elements such as the size of the heat pump or the volume of the EWH, which are not included in the table, remain unchanged across all cases.

Table 5.1: Summary table of the analyzed cases.

	Base Case	Case 1	Case 2	Case 3	Case 4
DR	Yes	No	Yes	Yes	Yes
PV size [kWp]	5	5	5	2	10
BESS size [kWh]	13.5	/	13.5	6.4	16
BESS P_{nom} [kW]	5	/	5	3.3	10.24
EV size [kWh]	50	50	50	50	50
EV P_{nom} [kW]	11	11	11	11	11
TESS	Yes	No	No	Yes	Yes

To gain insight into the annual generation curve trends with varying plant sizes on a monthly resolution compared to the average of monthly irradiance values, please refer to *Appendix A* (Fig. A-5).

5.1.1 Case 1

The first scenario presented concerns a user who lacks devices for thermal and electrical flexibility, thus being a producer-consumer without storage capacity. The user only has a photovoltaic system as a production source, but does not have access to the TESS thermal storage system to support the HP, nor the BESS system. The electric vehicle solely acts as a load, and therefore the charging station is set only to charge the vehicle's battery. Additionally, the case where the DR is not active is also considered, hence the demand will not be adjusted as much as possible to the generation. The power of the photovoltaic system is 5 kW peak, while the maximum power for the HVAC system remains unchanged compared to the Base Case, which is 6 kW.

It is important to note that in this configuration, the absence of DR causes exportation only when generation is lower than load. The system does not take into account market prices or user needs. The user's demand will therefore remain unchanged due to the absence of flexibility systems. The decision was made to keep the electric vehicle as a load to ensure a more accurate comparison. However, it should be noted that if the owned vehicle were not electric but traditional, the net annual cost would certainly be lower as a result of the system, but it would not include the monthly expenses incurred by the user for fuel, which combined with the bill costs would definitely exceed those of other cases, due to the higher prices of fuels compared to electricity. An appreciable

rise in the annual net cost for 2022 is anticipated relative to the Base Case, alongside a notable decrease in the LMI across all seasons (for instance, a reduction of the winter LMI compared to the Base Case amounts to 83.60%).

For completeness, the annual graph with hourly resolution of the demand for Case 1 is shown in Figure 5.1.

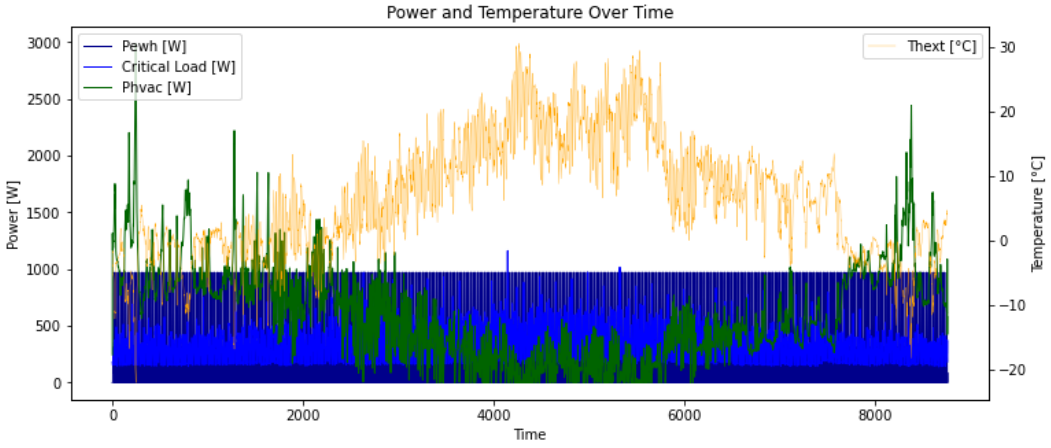

Figure 5.1: Hourly load of the household for analyzed year (Case 1).

5.1.2 Case 2

The second scenario involves utilizing the same user configuration as in the baseline case but without TESS support for the air-to-water HP. A system with a TESS supported by an air-to-water HP and a system with only a HP can differ in several aspects. Firstly, the TESS-enabled system has the ability to store thermal energy in a thermal storage tank, allowing for energy accumulation when it is abundantly available (such as during off-peak hours or when there is excess renewable energy) and release it when needed. A system with only a HP lacks this thermal energy storage capacity. Additionally, thanks to its storage capability, the TESS-supported system can be more flexible in adapting to variations in energy demand or the availability of energy from renewable sources. It can be programmed to utilize stored energy when energy prices are higher or when there is a need to reduce the load on the grid. Its usage can improve the overall system efficiency (affecting LMI values) as it enables optimal utilization of available energy (on average, the TESS system is effectively utilized to store or release thermal energy for a value ranging monthly between 70% and 80%).

The system can be designed to operate optimally, for example, by reducing the need to run the HP during peak hours when energy costs are higher.

Regarding economic differences, a TESS system tends to have higher initial costs compared to a system with only a HP (typically initial costs including purchase and installation hover around 1000€, looking at current market prices), due to the addition of the thermal storage tank and associated control systems. However, in the long run, it can offer significant savings on operational costs due to better energy management. For example, from the simulation, it is obtained that annually, the total savings for the year are 101.97€; this value represents the total net savings for the user throughout the year using the TESS system instead of not using it. Assuming that the installation and purchase have an initial expense of 1000€ and that the savings trend is constant annually, the payback period will be approximately 10 years, a time still shorter than the average lifecycle of a tank which is typically around a minimum of 20 years. For Case 2, the reduction in LMI compared to the Base Case is present in all seasons but less pronounced than the deviation that Case 1 exhibits from the Base Case (for example, there is a reduction of just over 1% compared to the Base Case in summer). In summary, adding a TESS to a HP system can lead to greater operational flexibility, improve overall energy efficiency, and offer long-term economic benefits, although it entails higher initial costs.

5.1.3 Case 3

The third scenario involves using a system identical to the baseline case but with smaller photovoltaic and battery energy storage system capacities. Specifically, a PV system with an installed capacity of 2 kWp and a BESS with a nominal capacity of 6.4 kWh with a charge and discharge nominal power of 3.3 kW. were used[1]. By reducing the capacities compared to the baseline case, one can expect lower photovoltaic generation and energy storage capacity, potentially leading to an unsatisfactory load fulfillment with power primarily sourced from the grid rather than on-site generated power, and certainly reducing energy export (approximately 30% relative to the Base Case). The overall system efficiency decreases due to the reduced capacity, impacting the user's net cost with greater grid dependence and influencing the total energy cost. Indeed, for Case 3, there is a notable decrease in investment costs compared to the Base

[1]BESS data source: Tesla Powerwall 1 datasheet

Case. The analyses suggest that, given the assumptions made, the net annual cost for 2022 will rise by approximately 98.66% compared to the Base Case.

5.1.4 Case 4

The fourth scenario aims to highlight the system's behavior with larger PV and BESS capacities. It represents the opposite case of Scenario 3. Indeed, with an increase in both PV system and BESS capacities, one can expect greater photovoltaic generation and energy storage capacity. This could result in decreased energy import from the grid and potentially increased energy export. The overall system efficiency might improve due to the expanded capacity, potentially reducing the user's net cost by decreasing grid dependence and positively impacting the total energy cost. Specifically, the PV system size would be 10 kWp, and the BESS nominal capacity would be 16 kWh [2], with a charge and discharge nominal power of 10.24 kW. In contrast to Case 3, the investment costs for a larger-scale facility (Case 4) have increased by 38.46% compared to the Base Case. However, there is a significant reduction in the net annual costs for 2022. This is primarily due to the increased capacity of both the photovoltaic system and the BESS. Additionally, the exported energy in the same year has increased by 42.43% compared to the Base Case, while the imported energy remains nearly unchanged.

For all scenarios, the same set of input data for critical loads, price conditions, temperature, and irradiance, as well as the same geographical location, were assumed. This was done to ensure a focused analysis on system organization and management to determine which configuration best meets the user's needs. Therefore, it is effectively an analysis in favor of the user, as it will be their choice how to design the system and allocate expenses accordingly.

[2]BESS data source: RJ-Tech LiFePO4 Manufacturer, model: RJ-LFP51314-F

5.2 Analysis of Parameters Deviations

The analysis of deviations will now be conducted. Differences across various domains will be examined through the deviations recorded from the results obtained for the various cases analyzed.

5.2.1 Self-consumption of PV Energy

The LMI extends beyond simply measuring how well the system balances energy demand and supply; it aims to reflect a broader concept of systemic efficiency. This index not only assesses the system's ability to meet energy demands but also evaluates how efficiently this process operates, both operationally and economically. In practice, a higher load matching index not only indicates better alignment between energy demand and supply but also suggests more efficient management of the system as a whole. This implies that the system not only delivers energy when required but does so optimally, minimizing waste and costs while maximizing overall operational and economic efficiency. In summary, systemic efficiency is integrated into the analysis of the load matching index, which evaluates not only the alignment between energy demand and supply but also the system's capability to manage this balance efficiently on both operational and economic fronts. In Fig. 5.2, the LMI values for the four seasons analyzed across the four cases discussed previously are depicted in comparison to the Base Case.

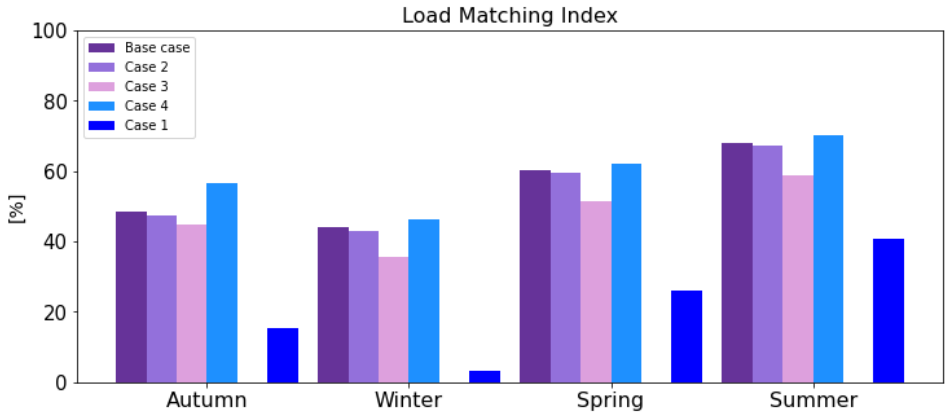

Figure 5.2: Comparison of LMI in seasonal resolution among the various cases analyzed and the Base Case.

From the same graph, it's readily apparent how the absence of storage

systems significantly impacts the LMI. Focusing on the difference between the Base Case and Case 1, indeed, there's a substantial reduction observed in every season, affecting the overall system efficiency.

In Table 5.2, the percentage increments or decrements of the LMI relative to the Base Case are reported for the cases studied. This table has been created to provide a better understanding of how the LMI values are influenced by the system configuration.

Table 5.2: Increase or decrease of the LMI compared to the Base Case, in percentage.

Change in LMI from the Base Case				
Season	Case 1	Case 2	Case 3	Case 4
Autumn	-68.74%	-2.90%	-7.89%	+16.59%
Winter	-92.73%	-2.99%	-19.38%	+4.59%
Spring	-56.75%	-1.28%	-14.73%	+3.18%
Summer	-40.31%	-1.36%	-13.88%	+3.04%

The reduction in LMI in Case 2 without TESS underscores a dependency on thermal energy management within the energy system. The lack of flexibility is evident: TESS balances the supply and demand of thermal energy, preventing discrepancies that would otherwise diminish the LMI. Without TESS, additional resources would be needed to regulate temperature or provide thermal energy as required, thereby increasing system costs and complexity, with negative impacts on LMI. Furthermore, TESS balances energy demand by utilizing excess thermal energy when needed. Without this capability, adapting production to load fluctuations would be more complex, adversely affecting LMI. In general, the absence of TESS would limit the energy system's ability to adapt to demand fluctuations, resulting in greater discrepancies between thermal energy supply and demand, thus impacting LMI.

The sizing of energy storage systems, referring to Cases 3 and 4, can influence the Load Matching Index (LMI) in various ways:

- **Adequate sizing**: Properly sized energy storage systems can reduce the gap between energy supply and demand. They store excess energy during times of surplus and provide it during peak demand, potentially improving the LMI.

- **Insufficient sizing**: Undersized energy storage systems may fail to store enough energy to cover demand peaks or balance intermittent renewable energy production. This could lead to a decrease in LMI as the system struggles to meet demand optimally.
- **Excessive sizing**: Oversized energy storage systems may incur extra costs and resource wastage. However, efficient management can help align energy demand and supply, potentially improving the LMI despite the excess capacity.

For the analyzed cases, the effect of the sizing of energy storage systems on LMI depends on their ability to balance intermittent energy production from renewable sources with energy demand. Plant sizes in Case 3, in fact, show a reduction in the capacity to adapt the load to generation, while in Case 4, a plant sized larger than the Base Case leads to a more accurate management of energy and improves overall energy efficiency and the system's LMI. However, increasing the size of both the PV system and the BESS excessively becomes very costly for the user, who must bear higher investment costs, and does not bring obvious benefits either in terms of savings or LMI.

5.2.2 Cost Analysis

Transitioning to cost analysis, a comparison is sought among Cases 1, 2, 3, and 4 with the Base Case. To adequately analyze costs for the purpose of achieving as realistic an assessment as possible, despite employing simplifying assumptions (see, for instance, Fig. 3.7 and Eq. 3.1), initial investment cost ranges for different configurations have been sought.

It has been chosen to report in Tab. 5.3 the net costs to the user in the year 2022 for comparable Cases 1, 2, 3, 4. For a better understanding of how useful it is to have a system like the one analyzed, a consumer case with the same loads as the Base Case but without any generation and TESS has also been calculated.

Table 5.3: Comparison of the net costs across different configurations for the year 2022.

	Net cost for the user [€]					
Months	Consumer	Base Case	Case 1	Case 2	Case 3	Case 4
September	301,89	7,21	236,67	28,95	122,68	-69,51
October	206,06	80,88	198,32	95,84	136,47	59,36
November	338,62	240,94	342,42	247,32	290,13	223,05
December	467,48	344,85	275,95	356,73	392,96	307,58
January	272,21	193,52	470,61	201,36	229,16	166,78
February	197,31	133,33	195,18	138,62	172,43	105,47
March	211,56	103,15	134,07	110,29	163,94	53,84
April	177,59	69,85	130,69	74,16	143,27	9,09
May	214,93	6,42	134,07	12,53	109,11	-93,98
June	189,55	-49,64	74,86	-45,60	70,64	-175,03
July	232,82	-32,53	114,60	-28,73	91,25	-163,11
August	307,92	-109,26	176,08	-100,78	42,24	-265,94
Tot.	3117,94	988,72	2483,52	1090,69	1964,28	157,60

Through a personal market analysis and consultation with industry experts (*Tesla*, *GreenPower*, *Otovo*), tables of costs for each type of installation have been compiled, selecting an indicative average final investment cost for each range. In all cases, the presence or absence of the TESS system has been taken into account with a hypothesized overall relative cost, as mentioned earlier, of 1000€, Tab. 5.4. Furthermore, for better comprehension, the Base Case has been compared to the consumer case, without any RES or storage system but with identical loads.

Table 5.4: Initial investment costs (indicative values).

User Configuration	PV Plant size [kWp]	Range [€]	BESS size [kWh]	Range [€]	Total Initial Investment (i.v.) [€]
Consumer *	[-]	/	[-]	/	0
Base Case	5	6000-7500	13,5	17550-20250	26650
Case 1 *	5	6000-7500	[-]	/	6750
Case 2 *	5	6000-7500	13,5	17550-20250	25650
Case 3	2	2400-3000	6,4	8320-9600	12600
Case 4	10	12000-15000	16	20800-24000	36900

In addition to estimating the investment cost for PV, BESS, and TESS installations[3], it is important to consider that these costs do not include those related to HP, EWH, EV installations, and the construction of the building itself, as it is assumed that such costs are uniform across all configurations.

After conducting simulations, the monthly net costs for all configurations throughout the year 2022 have been calculated. Consequently, an annual net cost has been obtained for each configuration. Assuming that this net cost repeats annually without variations (such as reductions in solar panel efficiency, battery storage capacity, or changes in weather conditions), it is possible to generate the four comparison graphs illustrated in Figure 5.3.

For the analysis of cumulative costs, a discount rate of **3%** has been adopted until 2022, based on [58]. The reference point is 2021 (the year of investment), indicated by a dashed black vertical line. With actual data available for 2022, discounting has been performed from this year starting from 2023 until the last expected year of the facilities' useful life. The discount rate is a crucial parameter used in financial analysis to calculate the present value of future cash flows. It represents the rate at which future cash flows are discounted to their present value. This rate takes into account the time value of money, reflecting the opportunity cost of investing funds elsewhere or the cost of financing. By updating the discount rate beyond 2022, the analysis takes into account possible changes in economic conditions, inflation rates, and other factors that may influence the cost of capital and the time value of money. This approach ensures that the analysis remains, albeit simplified, relevant and reflects the financial implications of the investment for the entire duration of its useful life.

[3]The marked cases in the table indicate the absence of TESS and its initial cost

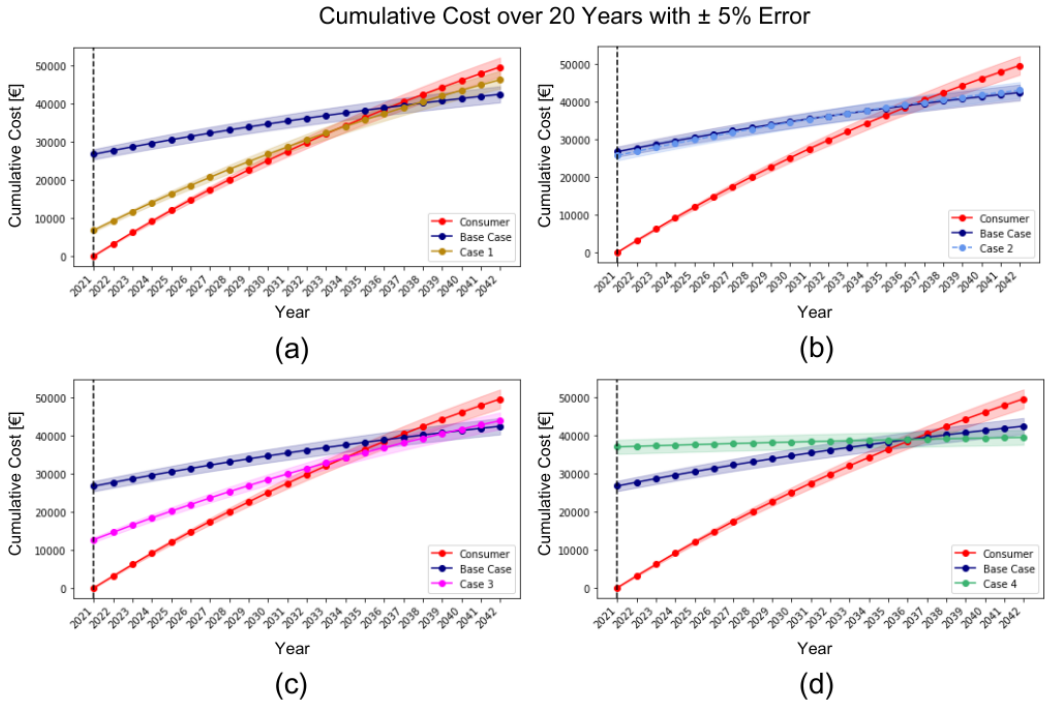

Figure 5.3: Cumulative costs over a 20-year plant lifecycle, comparison across different configurations.

The above graphs represent the annual cumulative net costs incurred by the user in different configurations. The colored band around each curve represents the error of ± 5% because the exact trend of prices in future years is not known. Each graph analyzes the trend of cumulative costs over the typical lifespan of the installation, which is assumed to be 20 years from installation. Therefore, an installation is hypothetically assumed to commence operations from first day of January, 2022. In all scenarios, each configuration guarantees final cumulative costs lower than those of the consumer configuration case. This implies that despite necessitating higher initial financial outlays, it remains economically advantageous to invest in order to realize savings on the bill.

In *(a)*, spanning the sixteenth to the twentieth year, the cumulative costs incurred by the consumer configuration exceed those of the Base Case; moreover, after the eleventh year, the cumulative costs of Case 1 start to exceed those of the Consumer configuration due to the presence of generations systems.

In *(b)*, from the midpoint of the tenth year through the twentieth, as previously mentioned, the savings relative to Case 2 confirm that the implementation of TESS still provides an advantage, albeit proportionally minimal in economic terms.

In *(c)* and *(d)*, it's possible to observe the two instances of system size modification (referred to as Case 3 and Case 4). In the former, a lower initial cost is evident; however, after the seventeenth year, there is an increase in cumulative costs compared to the Base Case. Conversely, for the Case 4 configuration, a very slight slope of the tangent to the curve is observed, attributed to the system's ability to export energy more efficiently during advantageous periods, thanks to larger system sizes relative to the Base Case.

At the conclusion of the 20-year period, a lower cumulative cost relative to the Case 4 is evident. Nevertheless, this is accompanied by a significantly larger initial investment. Therefore, the decision regarding the extent and manner of investment is left to the user, considering their economic resources. It is essential to note that the assumptions of no system wear or performance degradation, as well as maintenance expenses, have been excluded. However, for a more informed decision-making process, these factors should be duly considered. More details in *Appendix B* (Tab. B-1).

5.2.3 Power Trade Framework

In the following section, analysis will be conducted on how the system employs the distribution network as a source for drawing energy when necessary or convenient for users, as well as a medium for exporting excess energy. The discrepancies in imported and exported energy on a monthly basis are depicted in Figs. 5.4 and 5.5, respectively.

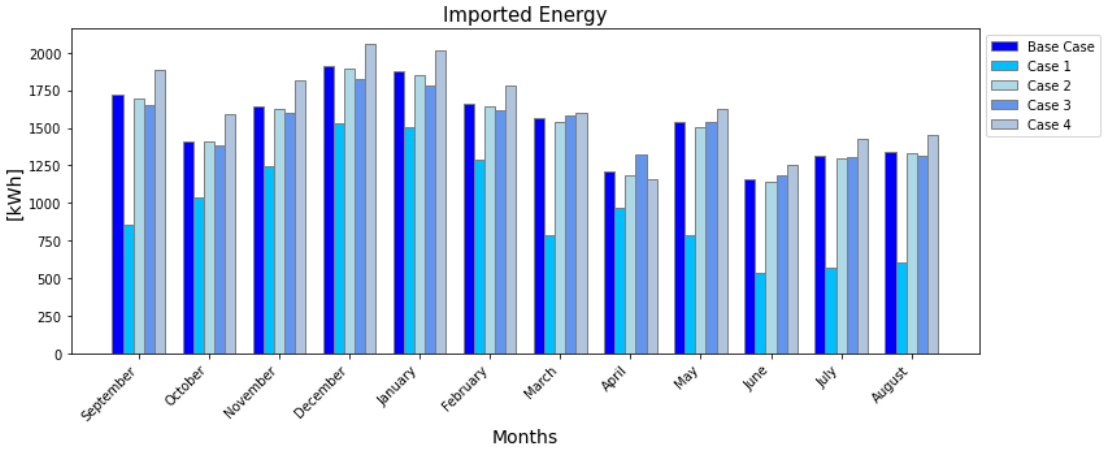

Figure 5.4: Imported energy bar chart per each case in year 2022.

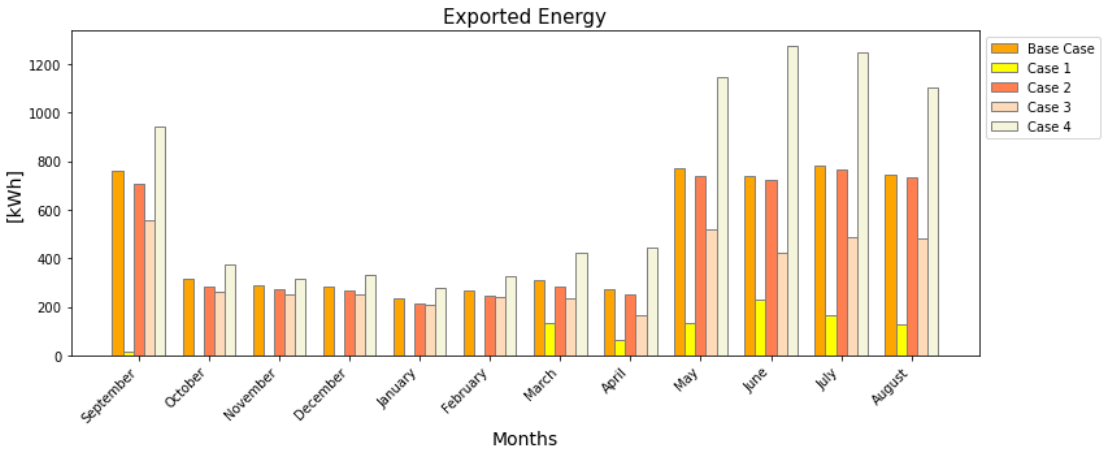

Figure 5.5: Exported energy bar chart per each case in year 2022.

The results show the configurations that stress the network the most. In the year 2022, indeed, by grouping all the monthly data and organizing them in Fig. 5.6, it can be observed that the main difference among the various cases lies in the export capacity.

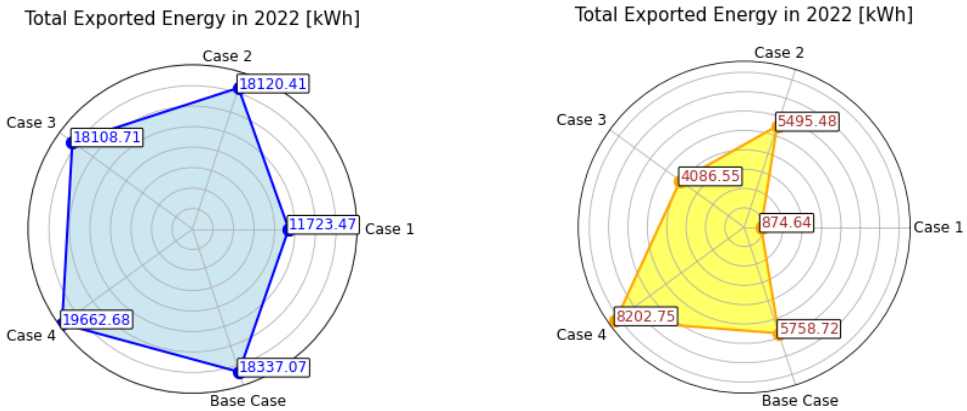

(a) **(b)**

Figure 5.6: Total imported (a) and exported (b) energy in year 2022.

Total Import : Case 4 (PV 10 kWp and Storage 16 kWh) and the Base Case, which is very similar to Case 2, have the highest total importation. This is likely due to the significant variability in prices. Having storage systems with higher capacities makes them rely more on the grid to fulfill their objective, resulting in larger energy exchanges and putting more strain on the grid. However, this increased reliance on the grid also efficiently benefits the user.

Although these cases have higher importation compared to others, the monthly quantity is not significantly higher than the other cases (except for Case 1 due to the absence of storage systems).

Total Export : In Case 4, there is a significantly higher energy export compared to other cases. This is attributed to both the increased generation capacity and storage capacity, enabling the system to accumulate excess energy during periods of overproduction or low prices, to be released when needed. There is a notable disparity across almost all months of the year in Fig. 5.5, relative to other cases; this trend is also reflected in Fig. 5.6 *(b)*. Additionally, it is observed that Case 1 is capable of exporting a truly minimal amount of energy, particularly evident during winter months; this system behavior is entirely contingent upon the non-programmability of renewable sources.

Case 4 appears to exert higher stress on the grid in terms of total importation, yet it significantly contributes to the grid by exporting excess energy. Conversely, Case 1 seems to impose the least stress on the grid regarding importation, albeit making a lesser contribution to energy exportation. It could potentially represent a more balanced configuration concerning grid load.

Further exploration is warranted into how these configurations may affect grid efficiency and stability. Configurations with higher energy importation may strain grid components such as transformers and transmission lines during peak periods. Should multiple users exhibit similar behavior concurrently, this could necessitate additional investments to reinforce such components to manage demand effectively.

Cases incorporating storage systems (Base Case, Case 2, Case 3, and Case 4) demonstrate greater capacity to balance load and contribute to the grid through excess energy exportation. This leads to enhanced grid stability, as mentioned earlier, and improved demand management.

Although Case 4 appears to stress the local grid more in terms of imports, its significant contribution to energy exports results in higher revenues for the system owner. Consequently, optimizing to minimize the gap between import costs and export revenues reflects a prudent strategy to maximize the overall economic value of the system and ensure efficient utilization of generated energy.

This means that the algorithm plans imports when prices are low and exports when they are high, thus following market indications. Market prices

are determined by the bids of generators and consumers, as well as potential congestion on the transmission network. Therefore, by buying when prices are low and selling when they are high, one contributes to optimizing the transmission network and the production system. However, it is important to note that this strategy may not be suitable for the local distribution network, which may be overloaded at certain times. Currently, prices do not reflect local distribution issues.

In conclusion, while the algorithm's market-driven approach appears to enhance revenue generation and grid efficiency at the macro level, localized challenges within the distribution network warrant separate consideration and management to ensure overall system stability and reliability.

5.3 Connection Capacity

Until now, all results have been attained while maintaining a constant $P_{threshold}$ of $3 \times 25\ A$ (considering a $cos\phi \approx 0.95$ the value is around 16 kW), serving as both import and export limits. Currently, the focus is on examining how a reduction in the electrical grid's capacity affects the hourly power import and export quantities, consequently impacting the overall net cost to users across diverse configurations. A fluctuation in $P_{threshold}$ precipitates a discernible effect even within truncated time spans, such as 24 hours. For instance, Fig. 5.7 illustrates the import and export power dynamics, respectively, during the initial week of May, exhibiting variations in threshold power values. At first glance, it is evident that modifying the threshold power values results in variations across all analyzed cases, except for Case 1. The latter does not involve any DR or energy storage mechanisms, thus remaining unaffected by variations as long as the threshold value in a specific hour is lower than the corresponding load value. This translates into the infeasibility to meet the constraints (no optimal solution found) in the code.

Five measurements were carried out, including the case with 16.5 kW, each with progressively lower values of $P_{threshold}$. Some cases do not have a total of five points, resulting in a shorter curve, indicating that no solution can be calculated for that value of $P_{threshold}$. Only Case 4 has five points because, despite having a limit of 4 kW, it manages, with a larger system, to handle the limited power exchange capability with the grid.

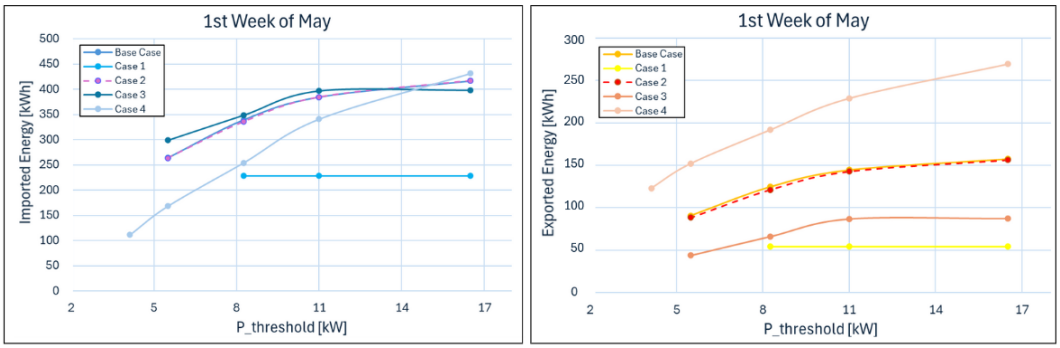

Figure 5.7: Respectively: imported energy (a) / exported energy (b) varying with the threshold value for the first week of May.

Except for Case 1, which, as mentioned earlier, remains unchanged by threshold adjustments, all other cases exhibit a significant decrease in imported energy throughout the week, particularly noticeable in graph *(b)* for exported power. Consequently, by varying the threshold power limit and observing the exported or imported energy data, the graph depicted in Figure 5.8 illustrates the fluctuation in the user's net cost.

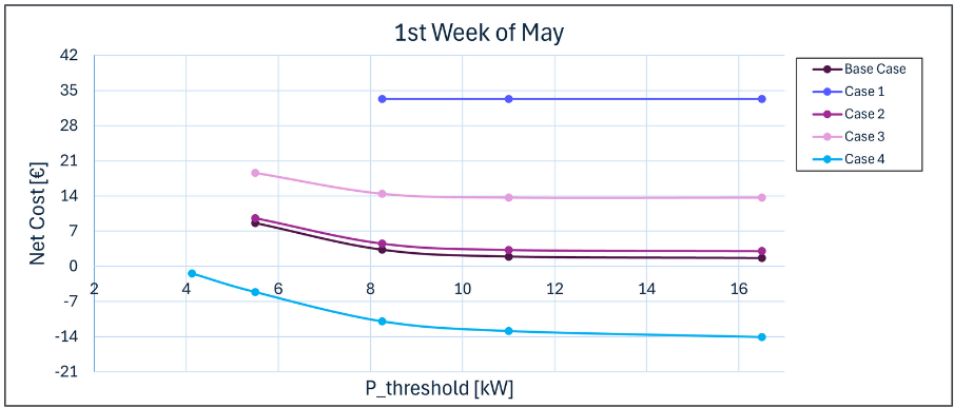

Figure 5.8: Net cost for the user varying with the threshold value for the first week of May.

Observing the above graphs, several considerations can be made. Reducing the maximum power limit that the prosumer system can draw from or inject into the electrical grid can influence various aspects:

- **Operational system capacity**: A reduced limit decreases the maximum amount of power the system can exchange with the electrical grid. This limits the ability to draw energy from the grid when needed or to sell excess generated energy.

- **Flexibility in energy usage**: A reduced limit restricts flexibility in energy usage; one is no longer fully able to utilize electricity from the grid when prices are low or when there is a shortage of energy from other renewable sources.
- **Financial effects**: Limiting the amount of power to be drawn or injected has financial impacts. It reduces the opportunity to save money by purchasing energy from the grid when prices are low, but also reduces the opportunity to generate revenue from selling excess energy.
- **Network stability**: However, by reducing the maximum power limit, the local electrical grid may become more stable, as lower limits decrease the likelihood of overloads or other load management issues. However, it may also limit the grid's ability to absorb energy spikes or respond to sudden fluctuations in energy demand.

In general, reducing the maximum power limit entails a trade-off between operational flexibility and network stability. Naturally, the lower the threshold value, the greater the stability of the grid, reducing the risk of potential issues associated with it. However, this comes at the expense of the user's system, which has fewer means to freely manage the energy needed to meet loads, resulting in increased energy bill prices. The results obtained for this analyzed time interval have implications for every chosen time interval, highlighting the importance of optimally balancing these factors based on the specific system needs and conditions of the local electrical grid. It's important to consider the issue of network congestion. Due to DR, some power flows will be shifted in time, potentially leading to multiple households shifting their load to the same hour. This can cause a power spike, creating congestion issues. While this analysis focuses on one household, it's crucial to anticipate the broader effects across multiple households. In addressing this, it's suggested that network connection capacities could be temporarily reduced below 16.5 kW in order to alleviate congestion. The analysis conducted demonstrates that certain strategies are more tolerant to reduced capacity than others. For instance, lowering the threshold power may not significantly affect imported and exported power, depending on the extent of the threshold reduction. This highlights the need for careful consideration and balancing of strategies to mitigate both immediate and potential future grid challenges.

Chapter 6

Conclusions

The focal point of this research has led to a deeper understanding of managing energy through Demand Response to promote households equipped with distributed energy resources. Utilizing previously discussed rigorous methodologies and the GLPK solver for MILP optimization, a comprehensive analysis of input data for a residence located in the Uusimaa region, Helsinki district, Finland, was conducted. The research primarily focused on analyzing a Base Case in the year 2022: the user is equipped with a photovoltaic system for local generation, an energy storage system, a thermal storage system with integrated electric resistance connected to a variable COP air-to-water heat pump, which, along with terminals, constitutes the HVAC system, an electric vehicle as an alternative to a traditional one, and an electric water heater for domestic hot water. This complex system takes into account loads generated to meet user needs, such as supplying domestic hot water at predetermined times, maintaining indoor temperature within a defined temperature range, considering a building's two-capacity thermal model, full electric vehicle charging, critical loads such as lighting, appliances, and more. The system is grid-connected through the Point of Connection to Distribution (PCC), adhering to legal limits set at 3×25 A for both energy withdrawal and injection into the grid. Hourly average power flows are managed and calculated to ensure power balance at the PCC and minimize the objective function. The latter aims to minimize the hourly difference between the cost of imported energy and the cost of exported energy, considering Day-Ahead energy prices and their respective buying and selling modes discussed in the main body of this work.

Initially, optimization results were examined in terms of hourly average

power. Through a detailed analysis of the first three days of May 2022, the State of Charge (SOC) trend and the charge and discharge power of the following components (Figs. 4.1, 4.2, 4.3): BESS, EV, and TESS were examined. Subsequently, the study also included the HVAC system demand graph, integrating support from the tank for plant water and the EWH (Fig. 4.4). These results confirm the robustness of the proposed methodology: all prosumer system elements synergistically operate to minimize the objective function, respecting the limits defined during the composition of the Python code. Data collected for the Base Case were aggregated seasonally and annually. A trend in energy demand for heating/cooling emerged consistent with annual temperature variations, with a peak of 824 kWh recorded in January. Additionally, it was observed that the most significant component of monthly energy demand is represented by electric vehicle charging, averaging 40% of the total. It is also noteworthy that the BESS is more active during summer months due to increased photovoltaic generation during that period. Subsequently, Table 4.1 was presented to analyze the user's monthly net costs. These costs stem from the difference between the cost of imported energy and the gain from exported energy, both strongly correlated with the monthly average energy price. At the end of 2022, the user incurred a net cost of approximately 988€. It is interesting to note that despite the amount of exported energy being less than imported energy each month, the user's net costs can be negative (indicating a gain) thanks to optimization. Furthermore, maintaining seasonal breakdown, a decision was made to evaluate the load matching index to provide an assessment of self-consumption effectiveness. The obtained values were in line with expectations: intermediate for spring and autumn, with a minimum of 42.86% during winter and a maximum of 68.43% during summer. To further emphasize the importance of energy optimization, a comparison was made between optimized and non-optimized systems for the first three days of May. Compared to the non-optimized case, an increase in the load matching index from 36% to 59% was recorded, accompanied by reduced net costs, shifting from positive (indicating an expense) to becoming a gain.

The main conclusions of the study highlight how the developed code has the capability to optimize load management to adapt and align as closely as possible with the local generation curve (Fig. 4.14), thus maximizing self-consumption and generating a higher percentage value of the load matching index compared to a non-optimized scenario. The method employed also allows for effective

management of significant fluctuations in Day-Ahead price values, enhancing system flexibility.

Further investigations were conducted to evaluate the impact of different configurations compared to the base case on self-consumption, costs, and quantities of energy exported and imported. Four distinct configurations were selected based on installation size, use of demand response mechanisms, and presence of a thermal storage system. It was found that the presence or absence of the thermal storage system (Case 2) has minimal impact on these variables. Conversely, installation sizes of the photovoltaic and energy storage system (Cases 3 and 4) are more significant: a smaller size compared to the base case leads to reduced self-consumption and grid export, despite lower initial costs. On the contrary, a larger installation size has a greater capacity for grid export, positively influencing user net costs, increasing self-consumption percentage but requiring a higher initial investment. A substantial difference was noted when the demand response mechanism is not active (Case 1). In this scenario, the monthly net amount is significantly lower compared to the base case, with considerably higher monthly costs and exports occurring only when photovoltaic production exceeds load. Subsequently, an analysis was focused on a week in May, assessing import/export variations and consequently net costs as the connection power limit decreases. It was concluded that by reducing the power limit imposed at the grid connection point, there is a decrease in energy exchanged with the grid and an increase in net costs for the user. Moreover, the more flexible the user, the greater the potential to reduce the power limit. In the analysis of different configurations, more specifically, a particularly low Load Matching Index (LMI) was observed in Case 1, with a winter minimum of only 3.21% and a summer maximum of 70.24% in Case 4. All examined configurations, except for Case 4, showed a reduction in LMI compared to the Base Case, highlighting that demand response mechanism and plant capacity increase favor self-consumption, but achieving an LMI index of 100% is not feasible. Regarding costs, the Case 4 has the lowest net cost at the end of 2022, although with an initial investment of around 37000€. Evaluating discounted cumulative costs for the average system lifespan, all configurations were more cost-effective compared to the decision of not installing any system, with cumulative costs at the end of the twentieth year amounting to 49505€. This highlights how the presence of a flexibility system positively influences both the user and the distribution network. Closely tied to cost analysis is the

examination of quantities of energy exchanged with the electrical grid. Case 4 stands out for the highest total of imported (19662.68 kWh) and exported (8202.75 kWh) energy compared to other cases considered in the analyzed year. Although Case 4 appears to put more pressure on the local grid in terms of imports, its significant contribution to energy exports translates into higher revenues for the system owner, highlighting that, despite energy system optimization aiming to maximize revenues following market indications, local challenges in the distribution grid require separate management to ensure overall system stability. The impact of reducing the value of $P_{threshold}$ led to an increase in net costs for all cases involving demand response. Analyzing the first week of May, an increase in net costs for all cases was observed, with particular emphasis on Case 2. Consequently, an investigation was conducted on how the capacity of the common connection point (PCC) could influence potential demand response and locally generated PV energy utilization. By reducing the size of the PCC connection, operational issues for DSOs (Electricity Distribution System Operators) could be avoided, primarily voltage rise and network capacity. However, reducing the size of the connection could create a bottleneck and lead to curtailment of energy produced by both large-scale and local systems. In summary, the results analysis confirmed the effectiveness of the proposed methodology in optimizing prosumer energy systems, highlighting significant improvements in demand management and cost reduction. Seasonal and annual data revealed patterns consistent with climatic variations, emphasizing the predominant role of electric vehicle charging in the overall energy balance. Optimization showed a positive influence on self-consumption and profitability even in the presence of substantial initial investments, as seen in Case 4. However, cost and network requirements analysis underscored the complexity of local energy management and the need to balance user interests with system stability needs. Finally, parameter variations, such as $P_{threshold}$, emphasized the importance of carefully considering the implications of such changes on operational management and network safety.

The code developed to support the analyses presents a complex model to optimize an integrated energy system, which includes renewable sources, energy storage, electric vehicles, and thermal management of buildings. This approach to energy optimization is highly promising for the future, aiming to maximize the efficiency and sustainability of available energy resources. Looking ahead, further developments in this field can be expected. With advancing

technology and increasing availability of real-time data, optimization models will become increasingly sophisticated and accurate. For example, integrating machine learning algorithms could allow the system to dynamically adapt to operating conditions and learn from historical data to improve performance over time. Moreover, with growing interest in transitioning towards a low-carbon economy, demand for energy optimization solutions is expected to increase. Governments, businesses, and communities are increasingly adopting ambitious clean energy and emission reduction goals, and models like the one presented can play a crucial role in supporting such efforts. Finally, ongoing technological innovation is expected to lead to more convenient, scalable, and accessible solutions for energy optimization. This could include developments in the field of storage batteries, integration of electric vehicles with the electric grid, and automation of smart buildings. The future of energy optimization solutions is very promising, and they are expected to play an increasingly important role in achieving global energy sustainability goals.

In summary, the research examines the optimal management of energy resources in a Finnish household, focusing on the role of the prosumer. It is acknowledged that what is optimal for individual users may not always be advantageous for the local distribution grid. Additionally, the importance of a flexible system that promotes self-consumption is emphasized, as this leads to greater overall system efficiency and savings on the energy bill. These conclusions are of significant importance in the context of optimized energy management, suggesting possible directions for further studies and practical applications. This situates the current master's thesis work in an extremely relevant and timely context.

Bibliography

[1] Vahid Arabzadeh et al. “Deep decarbonization of urban energy systems through renewable energy and sector-coupling flexibility strategies”. In: *Journal of Environmental Management* 260 (2020), p. 110090. ISSN: 0301-4797. DOI: https://doi.org/10.1016/j.jenvman.2020.110090. URL: https://www.sciencedirect.com/science/article/pii/S0301479720300281.

[2] M. Gomez-Gonzalez et al. “Novel optimization algorithm for the power and energy management and component sizing applied to hybrid storage-based photovoltaic household-prosumers for the provision of complementarity services”. In: *Journal of Power Sources* 482 (2021), p. 228918. ISSN: 0378-7753. DOI: https://doi.org/10.1016/j.jpowsour.2020.228918. URL: https://www.sciencedirect.com/science/article/pii/S0378775320312192.

[3] Peter Anuoluwapo Gbadega and Akshay Kumar Saha. “Impact of Incorporating Disturbance Prediction on the Performance of Energy Management Systems in Micro-Grid”. In: *IEEE Access* 8 (2020), pp. 162855–162879. DOI: 10.1109/ACCESS.2020.3021598.

[4] Peter Anuoluwapo Gbadega and Yanxia Sun. “Primal–dual interior-point algorithm for electricity cost minimization in a prosumer-based smart grid environment: A convex optimization approach”. In: *Energy Reports* 8 (2022). 2022 The 5th International Conference on Renewable Energy and Environment Engineering, pp. 681–695. ISSN: 2352-4847. DOI: https://doi.org/10.1016/j.egyr.2022.10.144.

[5] Rehman Zafar et al. “Prosumer based energy management and sharing in smart grid”. In: *Renewable and Sustainable Energy Reviews* 82 (2018), pp. 1675–1684. ISSN: 1364-0321. DOI: https://doi.org/10.1016/j.rser.2017.07.018.

[6] Peter Anuoluwapo Gbadega and Olufunke Abolaji Balogun. “Modeling and Control of Grid-Connected Solar-Wind Hybrid Micro-Grid System with Multiple-Input Ćuk DC-DC Converter for Household amp; High Power Applications”. In: *International Journal of Engineering Research in Africa* 58 (Feb. 2022), pp. 191–224. DOI: 10.4028/www.scientific.net/JERA.58.191.

[7] Peter Anuoluwapo Gbadega and Akshay Kumar Saha. “Dynamic Tuning of the Controller Parameters in a Two-Area Multi-Source Power System for Optimal Load Frequency Control Performance”. In: *International Journal of Engineering Research in Africa* 51 (Dec. 2020), pp. 111–129. DOI: 10.4028/www.scientific.net/JERA.51.111.

[8] Giovanni Brusco et al. “Energy Management System for an Energy District With Demand Response Availability”. In: *IEEE Transactions on Smart Grid* 5.5 (2014), pp. 2385–2393. DOI: 10.1109/TSG.2014.2318894.

[9] *Statistics Finland - Energy consumption in households*. URL: https://www.stat.fi/til/asen/kas_en.html.

[10] Carlos Henggeler Antunes, Maria João Alves, and Inês Soares. “A comprehensive and modular set of appliance operation MILP models for demand response optimization”. In: *Applied Energy* 320 (2022), p. 119142. ISSN: 0306-2619. DOI: https://doi.org/10.1016/j.apenergy.2022.119142.

[11] *ACER submitted the framework guideline on demand response to the European Commission – first step towards binding EU rules*. URL: https://acer.europa.eu/news-and-events/news/acer-submitted-framework-guideline-demand-response-european-commission-first-step-towards-binding-eu-rules.

[12] Amir-Hamed Mohsenian-Rad et al. “Autonomous Demand-Side Management Based on Game-Theoretic Energy Consumption Scheduling for the Future Smart Grid”. In: *IEEE Transactions on Smart Grid* 1.3 (2010), pp. 320–331. DOI: 10.1109/TSG.2010.2089069.

[13] Amir-Hamed Mohsenian-Rad and Alberto Leon-Garcia. “Optimal Residential Load Control With Price Prediction in Real-Time Electricity Pricing Environments”. In: *IEEE Transactions on Smart Grid* 1.2 (2010), pp. 120–133. DOI: 10.1109/TSG.2010.2055903.

[14] Hee Tae Roh and Jang Won Lee. “Residential demand response scheduling with multiclass appliances in the smart grid”. English. In: *IEEE Transactions on Smart Grid* 7.1 (Jan. 2016). Publisher Copyright: © 2015 IEEE., pp. 94–104. ISSN: 1949-3053. DOI: 10.1109/TSG.2015.2445491.

[15] K.M. Tsui and Shing Chan. “Demand Response Optimization for Smart Home Scheduling Under Real-Time Pricing”. In: *Smart Grid, IEEE Transactions on* 3 (Dec. 2012), pp. 1812–1821. DOI: 10.1109/TSG.2012.2218835.

[16] Phani Chavali, Peng Yang, and Arye Nehorai. “A distributed algorithm of appliance scheduling for home energy management system”. English. In: *IEEE Transactions on Smart Grid* 5.1 (Jan. 2014), pp. 282–290. ISSN: 1949-3053. DOI: 10.1109/TSG.2013.2291003.

[17] Amir Niromandfam, Ahmad Sadeghi Yazdankhah, and Rasool Kazemzadeh. “Modeling demand response based on utility function considering wind profit maximization in the day-ahead market”. In: *Journal of Cleaner Production* 251 (2020), p. 119317. ISSN: 0959-6526. DOI: https://doi.org/10.1016/j.jclepro.2019.119317.

[18] Muhammad Hussain and Yan Gao. “A review of demand response in an efficient smart grid environment”. In: *The Electricity Journal* 31.5 (2018), pp. 55–63. ISSN: 1040-6190. DOI: https://doi.org/10.1016/j.tej.2018.06.003.

[19] Sereen Althaher, Pierluigi Mancarella, and Joseph Mutale. “Automated Demand Response From Home Energy Management System Under Dynamic Pricing and Power and Comfort Constraints”. In: *IEEE Transactions on Smart Grid* 6.4 (2015), pp. 1874–1883. DOI: 10.1109/TSG.2014.2388357.

[20] Mahmoud Elkazaz et al. “A hierarchical two-stage energy management for a home microgrid using model predictive and real-time controllers”. In: *Applied Energy* 269 (2020), p. 115118. ISSN: 0306-2619. DOI: https://doi.org/10.1016/j.apenergy.2020.115118.

[21] Sibo Nan, Ming Zhou, and Gengyin Li. “Optimal residential community demand response scheduling in smart grid”. In: *Applied Energy* 210 (2018), pp. 1280–1289. ISSN: 0306-2619. DOI: https://doi.org/10.1016/j.apenergy.2017.06.066.

[22] *A novel MILP decomposition algorithm ensuring global optimality for the predictive design of complex multi-energy systems*. URL: https://hdl.handle.net/10589/151285.

[23] Rajasekhar Batchu and Naran M. Pindoriya. "Residential Demand Response Algorithms: State-of-the-Art, Key Issues and Challenges". In: *Wireless and Satellite Systems*. Ed. by Prashant Pillai et al. Springer International Publishing, 2015. DOI: 10.1007/978-3-319-25479-1_2.

[24] Tehreem Nasir et al. "Recent Challenges and Methodologies in Smart Grid Demand Side Management: State-of-the-Art Literature Review". In: *Mathematical Problems in Engineering* 2021 (2021), p. 16. DOI: 10.1155/2021/5821301.

[25] Amit Shewale et al. "An Overview of Demand Response in Smart Grid and Optimization Techniques for Efficient Residential Appliance Scheduling Problem". In: *Energies* 13.16 (2020). ISSN: 1996-1073. DOI: 10.3390/en13164266.

[26] Pravat Kumar Ray et al. "Multi-Objective Optimization for Demand Response Management". In: (2019), pp. 121–126. DOI: 10.1109/ICIT48102.2019.00028.

[27] Ioannis Antonopoulos et al. "Artificial intelligence and machine learning approaches to energy demand-side response: A systematic review". In: *Renewable and Sustainable Energy Reviews* 130 (Sept. 2020), p. 109899. DOI: 10.1016/j.rser.2020.109899.

[28] *Python implementation of optimization models with Pyomo and Docplex: a case study*. URL: http://webthesis.biblio.polito.it/id/eprint/17334.

[29] *Uusimaa Region - Finland*. URL: https://commons.wikimedia.org/wiki/File:Uusimaa_SOTE.svg.

[30] *Finnish Meteorological Institute*. URL: https://en.ilmatieteenlaitos.fi/.

[31] *Day-ahead market | Nord Pool*. URL: https://www.nordpoolgroup.com/en/the-power-market/Day-ahead-market/.

[32] *Transparency Platform | ENTSO-e*. URL: https://transparency.entsoe.eu/.

[33] *Energy Authority - Renewable energies Finland*. URL: https://energiavirasto.fi/en/renewable-energy.

[34] O. H. Abdalla and A. A.A. Mostafa. "Technical Requirements for Connecting Solar Power Plants to Electricity Networks". In: (Nov. 2019). DOI: 10.5772/intechopen.88439.

[35] Brian K. Perera, Phil Ciufo, and Sarath Perera. "Point of common coupling (PCC) voltage control of a grid-connected solar photovoltaic (PV) system". In: (2013), pp. 7475–7480. DOI: 10.1109/IECON.2013.6700377.

[36] A. D. Jones and C. P. Underwood. "A modelling method for building-integrated photovoltaic power supply". In: *Building Services Engineering Research and Technology* 23.3 (2002), pp. 167–177. DOI: 10.1191/0143624402bt040oa.

[37] Benjia Li et al. "Review on photovoltaic with battery energy storage system for power supply to buildings: Challenges and opportunities". In: *Journal of Energy Storage* 61 (2023), p. 106763. ISSN: 2352-152X. DOI: https://doi.org/10.1016/j.est.2023.106763.

[38] Vanika Sharma, Mohammed H. Haque, and Syed Mahfuzul Aziz. "Energy cost minimization for net zero energy homes through optimal sizing of battery storage system". In: *Renewable Energy* 141 (2019), pp. 278–286. ISSN: 0960-1481. DOI: https://doi.org/10.1016/j.renene.2019.03.144.

[39] D.A. Perez-DeLaMora et al. "Roadmap on community-based microgrids deployment: An extensive review". In: *Energy Reports* 7 (2021), pp. 2883–2898. ISSN: 2352-4847. DOI: https://doi.org/10.1016/j.egyr.2021.05.013.

[40] Tiago Sousa et al. "Peer-to-peer and community-based markets: A comprehensive review". In: *Renewable and Sustainable Energy Reviews* 104 (2019), pp. 367–378. ISSN: 1364-0321. DOI: https://doi.org/10.1016/j.rser.2019.01.036.

[41] Arslan Ahmad Bashir et al. "A novel energy scheduling framework for reliable and economic operation of islanded and grid-connected microgrids". In: *Electric Power Systems Research* 171 (2019), pp. 85–96. ISSN: 0378-7796. DOI: https://doi.org/10.1016/j.epsr.2019.02.010.

[42] Bo Wang, Cuo Zhang, and Zhao Yang Dong. "Interval Optimization Based Coordination of Demand Response and Battery Energy Storage System Considering SOC Management in a Microgrid". In: *IEEE Transactions on Sustainable Energy* 11.4 (2020), pp. 2922–2931. DOI: 10.1109/TSTE.2020.2982205.

[43] Kumar Shivam, Jong-Chyuan Tzou, and Shang-Chen Wu. "A multi-objective predictive energy management strategy for residential grid-connected PV-battery hybrid systems based on machine learning technique". In: *Energy Conversion and Management* 237 (2021), p. 114103. ISSN: 0196-8904. DOI: https://doi.org/10.1016/j.enconman.2021.114103.

[44] Shengnan Shao, Manisa Pipattanasomporn, and Saifur Rahman. "Development of physical-based demand response-enabled residential load models". In: *IEEE Transactions on Power Systems* 28.2 (2013), pp. 607–614. DOI: 10.1109/TPWRS.2012.2208232.

[45] Robin Filip et al. "Analyzing the Impact of EV and BESS Deployment on PV Hosting Capacity of Distribution Networks". In: *Energies* 15.21 (2022). DOI: 10.3390/en15217921.

[46] Kaiser Ahmed, Petri Pylsy, and Jarek Kurnitski. "Hourly consumption profiles of domestic hot water for different occupant groups in dwellings". In: *Solar Energy* 137 (2016), pp. 516–530. ISSN: 0038-092X. DOI: https://doi.org/10.1016/j.solener.2016.08.033.

[47] Shengnan Shao, Manisa Pipattanasomporn, and Saifur Rahman. "Development of physical-based demand response-enabled residential load models". In: *IEEE Transactions on Power Systems* 28.2 (2013), pp. 607–614. DOI: 10.1109/TPWRS.2012.2208232.

[48] *The National Building Code of Finland*. URL: https://ym.fi/en/the-national-building-code-of-finland.

[49] Kaiser Ahmed, Petri Pylsy, and Jarek Kurnitski. "Monthly domestic hot water profiles for energy calculation in Finnish apartment buildings". In: *Energy and Buildings* 97 (2015), pp. 77–85. ISSN: 0378-7788. DOI: https://doi.org/10.1016/j.enbuild.2015.03.051.

[50] Stefano Aneli et al. “Improvement of energy self-sufficiency in residential buildings by using solar-assisted heat pumps and thermal and electrical storage”. In: *Sustainable Energy Technologies and Assessments* 60 (2023), p. 103446. ISSN: 2213-1388. DOI: https://doi.org/10.1016/j.seta.2023.103446.

[51] *200-liter Thermal Accumulator Tank for hot/cold Technical Water*. URL: https://www.energyduegi.com/it/home/bollitori-ed-accumuli/accumuli-per-acqua-refrigerata/volano-termico-da-200-litri-per-acqua-tecnica-caldo-freddo.1.5.377.gp.158716.uw.

[52] Mubbashir Ali et al. “A market-oriented hierarchical framework for residential demand response”. In: *International Journal of Electrical Power Energy Systems* 69 (2015), pp. 257–263. ISSN: 0142-0615. DOI: https://doi.org/10.1016/j.ijepes.2015.01.020.

[53] *Air-to-water heat pump systems, Caleffi*. URL: https://www.caleffi.com/sites/default/files/media/external-file/Idronics_27_NA_Air-to-water%20heat%20pump%20systems.pdf.

[54] Mubbashir Ali, Amir Safdarian, and Matti Lehtonen. “Demand response potential of residential HVAC loads considering users preferences”. In: (2014), pp. 1–6. DOI: 10.1109/ISGTEurope.2014.7028883.

[55] Arslan Ahmad Bashir et al. “Matching of Local Load with On-Site PV Production in a Grid-Connected Residential Building”. In: *Energies* 11.9 (2018). ISSN: 1996-1073. DOI: 10.3390/en11092409.

[56] Ron Zevenhoven and Özer Arnas. “The effect of air humidity on the exergy efficiency of domestic heat pumps”. In: *Energy Conversion and Management* 221 (2020), p. 113054. ISSN: 0196-8904. DOI: https://doi.org/10.1016/j.enconman.2020.113054.

[57] Merkebu Zenebe Degefa. “Energy efficiency analysis of residential electric end-uses: Based on statistical survey and hourly metered data”. In: (2010). URL: https://aaltodoc.aalto.fi/items/d34e0d67-b64e-40f2-b111-2af67a6c1361.

[58] *IEA50-The Cost of Capital in Clean Energy Transitions, business models and indicative WACCs of utility-scale solar PV projects,* URL: https://www.iea.org/articles/the-cost-of-capital-in-clean-energy-transitions.

Appendix A

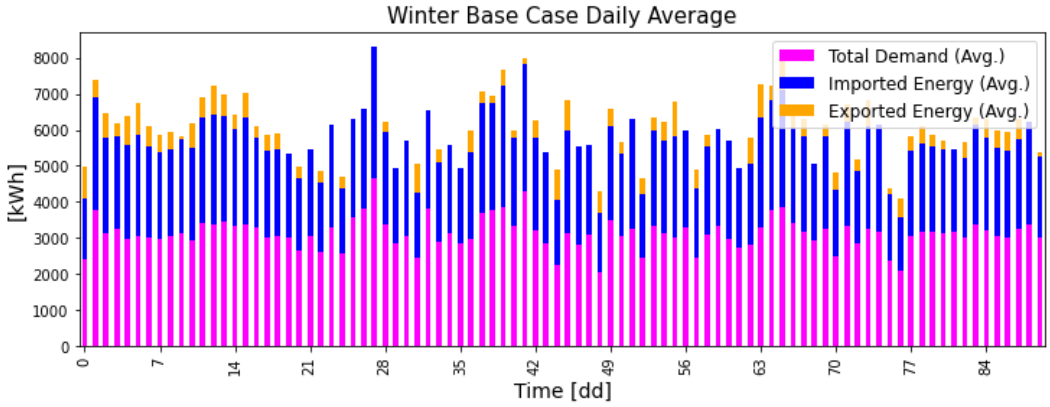

Figure A-1: Exchange of power and total demand for the Base Case winter.

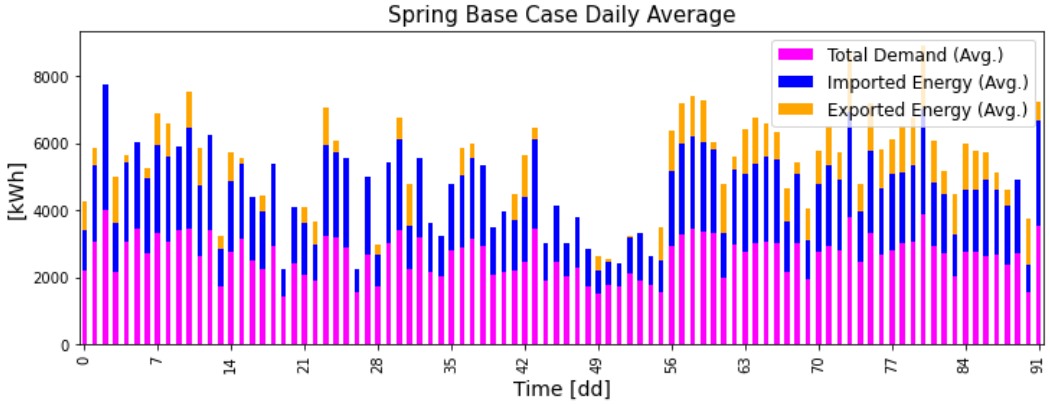

Figure A-2: Exchange of power and total demand for the Base Case spring.

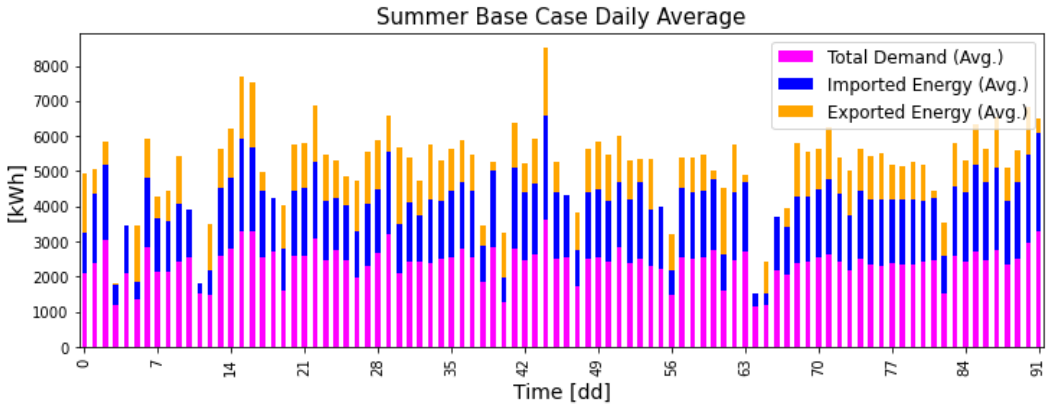

Figure A-3: Exchange of power and total demand for the Base Case summer.

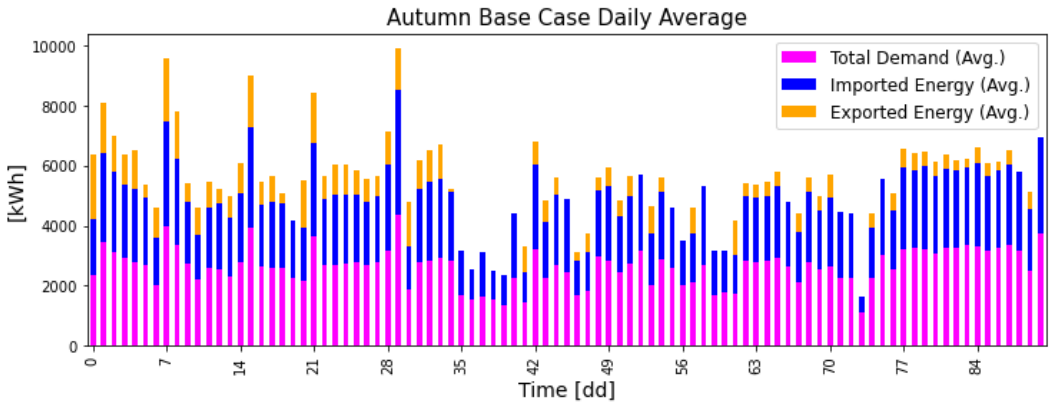

Figure A-4: Exchange of power and total demand for the Base Case autumn.

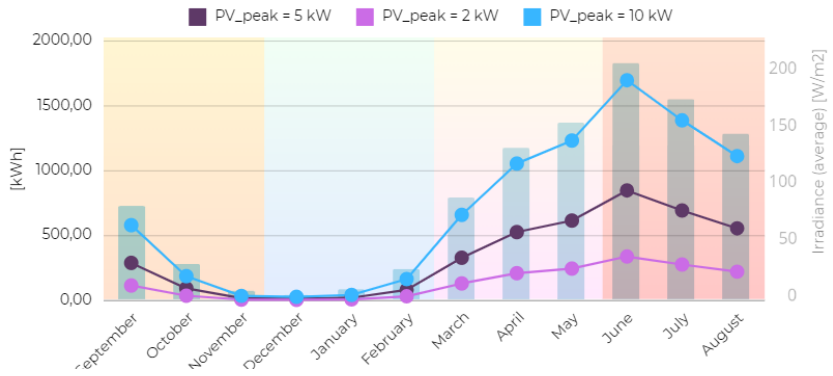

Figure A-5: Graph showing the average monthly irradiance and photovoltaic production for different system sizes.

Appendix B

Table B-1: Cumulative Costs for different configurations.

Initial Investment [€]						
Year 2021	0	26650	6750	25650	12600	36900
Cumulative Costs [€]						
Year	**Cons.**	**Base Case**	**Case 1**	**Case 2**	**Case 3**	**Case 4**
2022	3117,94	27638,72	9233,52	26740,69	14564,28	37057,60
2023	6145,07	28598,64	11644,70	27799,61	16471,35	37210,61
2024	9084,02	29530,61	13985,66	28827,69	18322,87	37359,16
2025	11937,38	30435,42	16258,43	29825,83	20120,46	37503,39
2026	14707,63	31313,89	18465,01	30794,89	21865,70	37643,41
2027	17397,19	32166,77	20607,31	31735,73	23560,11	37779,36
2028	20008,42	32994,81	22687,22	32649,17	25205,16	37911,35
2029	22543,59	33798,73	24706,55	33536,00	26802,30	38039,49
2030	25004,92	34579,23	26667,07	34397,00	28352,92	38163,90
2031	27394,56	35337,00	28570,48	35232,92	29858,38	38284,69
2032	29714,60	36072,70	30418,45	36044,50	31319,99	38401,96
2033	31967,07	36786,97	32212,60	36832,43	32739,02	38515,81
2034	34153,93	37480,44	33954,49	37597,42	34116,73	38626,35
2035	36277,09	38153,71	35645,64	38340,13	35454,31	38733,67
2036	38338,42	38807,37	37287,54	39061,20	36752,93	38837,86
2037	40339,71	39442,00	38881,62	39761,28	38013,73	38939,02
2038	42282,70	40058,13	40429,27	40440,96	39237,80	39037,23
2039	44169,11	40656,32	41931,84	41100,84	40426,22	39132,58
2040	46000,57	41237,09	43390,64	41741,51	41580,03	39225,15
2041	47778,69	41800,95	44806,96	42363,51	42700,23	39315,03
2042	49505,01	42348,38	46182,03	42967,40	43787,81	39402,29

Table B-2: Results for the year 2022 with monthly resolution (Base Case).

Seasons	**Months**	**Imported Energy** $[kWh]$	**Exported Energy** $[kWh]$	**Total cost of Imported Energy [€]**	**Total revenue from Exported Energy [€]**	**Net Cost for the user [€]**	DA_p **average** $[€/kWh]$	**PV prod. average** $[kWh]$	**LMI** [%]	**LMI** [%]
Base Case										
AUTUMN	September	1721,27	758,16	289,26	282,05	7,21	0,215	290,58	51,00	
	October	1406,36	313,20	166,18	85,30	80,88	0,114	94,17	43,00	48,65
	November	1641,54	287,00	321,45	80,50	240,94	0,195	18,25	44,00	
WINTER	December	1912,12	284,48	460,85	116,00	344,85	0,247	14,51	41,00	
	January	1875,00	235,97	235,88	42,36	193,52	0,106	21,87	38,00	44,18
	February	1663,25	265,98	171,18	37,85	133,33	0,081	82,77	47,00	
SPRING	March	1565,22	308,99	173,76	70,62	103,15	0,086	330,34	48,00	
	April	1207,04	273,46	123,60	53,74	69,85	0,079	527,93	56,00	60,14
	May	1539,52	771,53	182,04	175,63	6,42	0,133	616,70	64,00	
SUMMER	June	1155,37	736,99	123,10	172,74	-49,64	0,140	849,04	70,00	
	July	1310,34	781,51	180,37	212,91	-32,53	0,184	694,55	70,00	68,17
	August	1340,04	741,45	223,24	332,50	-109,26	0,261	556,66	58,00	

Table B-3: Results for the year 2022 with monthly resolution (Case 1. 2).

Seasons	**Months**	**Imported Energy** $[kWh]$	**Exported Energy** $[kWh]$	**Total cost of Imported Energy [€]**	**Total revenue from Exported Energy [€]**	**Net Cost for the user [€]**	DA_p **average** $[€/kWh]$	**PV prod. average** $[kWh]$	**LMI** [%]	**LMI** [%]
Case 1										
AUTUMN	September	855,13	18,51	236,51	6,84	229,67	0,215	290,58	22,00	
	October	1037,01	0,00	191,32	0,00	191,32	0,114	94,17	8,00	15,21
	November	1242,64	0,00	335,42	0,00	335,42	0,195	18,25	2,00	
WINTER	December	1530,65	0,00	268,95	0,00	268,95	0,247	14,51	1,00	
	January	1506,30	0,00	463,61	0,00	463,61	0,106	21,87	1,00	3,21
	February	1292,54	0,00	188,18	0,00	188,18	0,081	82,77	5,00	
SPRING	March	790,69	132,81	150,87	23,80	127,07	0,086	330,34	34,00	
	April	965,22	65,39	130,31	6,62	123,69	0,079	527,93	29,00	26,01
	May	790,69	132,81	150,87	23,80	127,07	0,133	616,70	34,00	
SUMMER	June	532,57	227,75	107,05	39,19	67,86	0,140	849,04	46,00	
	July	571,32	168,02	141,40	33,80	107,60	0,184	694,55	42,00	40,69
	August	608,71	129,35	205,66	36,58	169,08	0,261	556,66	36,00	
Case 2										
AUTUMN	September	1696,17	708,89	292,70	263,74	28,95	0,215	290,58	50,00	
	October	1409,64	285,10	172,87	77,03	95,84	0,114	94,17	41,00	47,24
	November	1625,68	274,34	322,95	75,63	247,32	0,195	18,25	41,00	
WINTER	December	1891,50	265,54	463,19	106,46	356,73	0,247	14,51	39,00	
	January	1855,07	216,24	238,92	37,56	201,36	0,106	21,87	36,00	42,86
	February	1645,50	248,21	172,32	33,70	138,62	0,081	82,77	45,00	
SPRING	March	1537,37	281,34	173,28	62,99	110,29	0,086	330,34	47,00	
	April	1188,48	252,17	122,99	48,83	74,16	0,079	527,93	56,00	59,37
	May	1508,15	740,96	180,55	168,02	12,53	0,133	616,70	63,00	
SUMMER	June	1140,04	722,79	123,12	168,72	-45,60	0,140	849,04	70,00	
	July	1293,08	766,97	179,63	208,36	-28,73	0,184	694,55	69,00	67,24
	August	1329,73	732,93	226,96	327,74	-100,78	0,261	556,66	58,00	

Table B-4: Results for the year 2022 with monthly resolution (Case 3. 4).

Seasons	**Months**	**Imported Energy** $[kWh]$	**Exported Energy** $[kWh]$	**Total cost of Imported Energy [€]**	**Total revenue from Exported Energy [€]**	**Net Cost for the user [€]**	DA_p **average** $[€/kWh]$	**PV prod. average** $[kWh]$	**LMI** [%]	**LMI** [%]
Case 3										
AUTUMN	September	1648,99	556,55	329,25	206,57	122,68	0,215	116,232	41,00	
	October	1385,14	260,82	206,20	69,73	136,47	0,114	37,668	34,00	44,81
	November	1601,05	253,86	359,30	69,17	290,13	0,195	7,3	35,00	
WINTER	December	1823,57	254,14	495,04	102,08	392,96	0,247	5,804	33,00	
	January	1785,18	207,13	265,30	36,14	229,16	0,106	8,748	32,00	35,62
	February	1617,55	239,65	205,49	33,06	172,43	0,081	33,108	40,00	
SPRING	March	1584,14	234,12	214,78	50,84	163,94	0,086	132,136	38,00	
	April	1320,70	168,09	175,02	31,75	143,27	0,079	211,172	43,00	51,28
	May	1540,11	519,23	226,77	117,66	109,11	0,133	246,68	54,00	
SUMMER	June	1182,60	422,00	169,21	98,57	70,64	0,140	339,616	61,00	
	July	1308,04	487,09	225,98	134,73	91,25	0,184	277,82	61,00	58,71
	August	1311,64	483,87	260,13	217,89	42,24	0,261	222,664	50,00	
Case 4										
AUTUMN	September	1887,44	941,07	277,52	347,03	-69,51	0,215	581,16	55,00	
	October	1591,48	374,08	162,21	102,85	59,36	0,114	188,34	46,00	56,72
	November	1816,19	316,26	313,28	90,23	223,05	0,195	36,5	46,00	
WINTER	December	2055,93	330,83	443,44	135,86	307,58	0,247	29,02	45,00	
	January	2011,69	279,00	217,58	50,80	166,78	0,106	43,74	42,00	46,21
	February	1781,24	325,98	152,47	47,00	105,47	0,081	165,54	52,00	
SPRING	March	1595,80	424,80	147,53	93,69	53,84	0,086	660,68	56,00	
	April	1160,32	443,18	92,87	83,78	9,09	0,079	1055,86	67,00	62,05
	May	1624,17	1146,60	160,65	254,63	-93,98	0,133	1233,4	69,00	
SUMMER	June	1253,27	1272,34	105,12	280,15	-175,03	0,140	1698,08	74,00	
	July	1429,08	1247,66	161,78	324,89	-163,11	0,184	1389,1	74,00	70,24
	August	1456,07	1100,95	200,74	466,68	-265,94	0,261	1113,32	66,00	

Acknowledgments

Italian Version

Desidero ringraziare il Politecnico di Torino per aver reso possibile la realizzazione di questo lavoro di Tesi Magistrale all'estero ed al Professor Enrico Pons per aver gentilmente accettato il ruolo di supervisore durante questo periodo, nonostante le sfide e le difficoltà connesse al lavoro a distanza.

Sono profondamente grato all'Aalto University per avermi accolto e per avermi fatto sentire immediatamente parte di un ambiente universitario così diverso da quello a cui ero abituato. Quest'esperienza mi ha inoltre permesso di collaborare con il Professor Matti Lehtonen e l'Ingegnere Verner Puvi, che hanno rispettivamente ricoperto i ruoli di supervisore e advisor. Ho sempre ricevuto il loro sostegno e apprezzamento, sono grato per la loro costante presenza. Grazie al loro supporto ed alla loro pazienza, ho acquisito maggiore fiducia nelle mie capacità e ho sviluppato un profondo rispetto nei loro confronti. Desidero ringraziare tutte le difficoltà che ho incontrato durante il mio percorso, sia quando ho deciso di trasferirmi a Torino che durante il mio anno in Finlandia. Queste sfide non solo mi hanno fatto crescere, ma mi hanno anche permesso di scoprire quanto amo mettermi alla prova. Mi hanno insegnato che posso superare i limiti che mi impongo e raggiungere traguardi che mai avrei pensato possibili.

Il mio più profondo grazie, tuttavia, va principalmente alle persone che hanno reso possibile tutto questo: i miei genitori. So che questi due anni e mezzo sono stati particolarmente duri per loro, troppo spesso do per scontato il mio apprezzamento nei loro confronti, ma non dovrebbe essere così. Le parole da sole non possono esprimere quanto sia grato per ogni forma di sostegno che mi hanno da sempre offerto. È attraverso i miei traguardi passati e futuri che spero possano percepire quanto sia orgoglioso di ciò che mi hanno permesso di essere. Ogni successo raggiunto è stato e sarà anche il loro. Grazie, di cuore, per tutto.

Mi sento di ringraziare infinitamente una persona che dal mio primo anno a Torino ha rappresentato un punto di svolta per la mia vita: Alessia. Lei mi ha permesso di essere me stesso, mi ha fatto capire che cosa significa amare qualcuno per quello che è senza volere cambiamenti. Mi è sempre stata accanto in tutti i modi possibili, passando da essere una mia semplice vicina di casa a vicina di anima. Ha la capacità incredibile di interessarsi a me ed essere

presente sempre anche da lontano, condivide con me sogni e paure, è il mio esatto riflesso. È stata fondamentale in questo mio percorso, da lei ho imparato a mettere impegno in tutte le cose ed a non accontentarsi mai, la ammiro. Abbiamo dovuto affrontare periodi molto duri, spesso lontani da casa, ma l'abbiamo fatto con la consapevolezza di non essere mai da soli. Ci siamo resi felici facendo pazzie, cercando di aggrapparci a quel poco tempo che avevamo a disposizione questo anno, sono fiero di noi e di quello che siamo.

Un grande grazie va al mio amico e compagno di viaggio Michele che ha condiviso con me emozioni, avventure accompagnando tutto con le solite nostre stupide cose. Siamo sempre stati in sana competizione e sono sicuro che ci siamo spinti a migliorare insieme.

Grazie anche al mio amico Carmelo, che ha sempre condiviso i miei stessi pensieri ed è stato sempre pronto ad aiutarmi nei momenti di bisogno. Sin dal primo giorno in cui ci siamo conosciuti, siamo stati inseparabili e so che potrò sempre contare su di lui.

Un altro grande grazie va anche a Francesco, Tiffany e Maria Pia, loro sono stati la mia piccola nuova famiglia a Torino. Ognuno di loro ha un ruolo molto importante nel rendere Torino una seconda casa per me.

Devo ringraziare tutti i miei vecchi amici, tutti i nuovi amici che ho conosciuto a Torino ed in Finlandia e tutte le persone che ho incontrato da quando ho deciso di cambiare vita. Ognuno di loro mi ha donato tanto anche con piccoli gesti, ognuno ha arricchito la mia vita di ricordi fantastici che porterò sempre con me.

Infine, devo ringraziare me, ho voluto tanto ed ho ottenuto tanto, ho viaggiato, ho riso, ho amato, ho costruito il mio futuro fino ad oggi e continuerò a farlo. Grazie di essere sempre stato con la testa dura, di avere questa gentilezza che conquista le persone.

Grazie.

English Version

I would like to thank the Politecnico di Torino for making it possible to carry out this Master's thesis abroad, and Professor Enrico Pons for kindly accepting the role of supervisor during this period, despite the challenges and difficulties associated with remote work.

I am deeply grateful to Aalto University for welcoming me and making me feel immediately part of a university environment so different from what I was used to. This experience also allowed me to collaborate with Professor Matti Lehtonen and Engineer Verner Puvi, who respectively served as supervisor and advisor. I have always received their support and appreciation, and I am grateful for their constant presence. Thanks to their support and patience, I have gained greater confidence in my abilities and developed a profound respect for them.

I want to thank all the difficulties I encountered during my journey, both when I decided to move to Turin and during my year in Finland. These challenges not only helped me grow but also allowed me to discover how much I love testing myself. They taught me that I can overcome the limits I impose on myself and achieve goals I never thought possible.

However, my deepest thanks go primarily to the people who made all this possible: my parents. I know that these two and a half years have been particularly tough for them. Too often, I take my appreciation for granted, but it shouldn't be so. Words alone cannot express how grateful I am for every form of support they have always offered me. It is through my past and future achievements that I hope they can perceive how proud I am of what they have allowed me to become. Every success achieved has been and will be theirs. Thank you, from the bottom of my heart, for everything.

I feel infinitely grateful to a person who has been a turning point in my life since my first year in Turin: Alessia. She allowed me to be myself, made me understand what it means to love someone for who they are without wanting changes. She has always been there for me in every possible way, transitioning from being just a neighbor to a soul neighbor. She has the incredible ability to care about me and always be present even from afar, sharing dreams and fears with me, she is my exact reflection. She has been fundamental in this journey of mine; from her, I have learned to put effort into everything and never settle, I admire her. We had to face very tough times, often far from home, but we did it with the awareness of never being alone. We made ourselves happy by

doing crazy things, trying to hold onto the little time we had available this year, I am proud of us and what we are.

A big thank you goes to my friend and travel companion Michele, who shared emotions and adventures with me, always accompanied by our usual silly things. We've always been in healthy competition, and I'm sure we've pushed each other to improve together.

Thanks also to my friend Carmelo, who has always shared my thoughts and has been ready to help me whenever I needed it. Since the day we met, we have been inseparable, and I know I can always count on him.

An other big thank you also goes to Francesco, Tiffany, and Maria Pia; they have been my little new family in Turin. Each of them has a very important role in making Turin a second home for me.

I must thank all my old friends, all the new friends I met in Turin and in Finland, and all the people I have met since I decided to change my life. Each of them has given me so much even with small gestures, each has enriched my life with fantastic memories that I will always carry with me.

Finally, I must thank myself. I wanted so much and I obtained so much, I have traveled, laughed, loved, and built my future up to now, and I will continue to do so. Thank you for always being stubborn, for having this kindness that wins people over.

Thank you.